Barometric Effect in Extensive Air Showers with Energies of 10^{17}–10^{19} eV

E. S. Nikiforova

Institute of Cosmophysical Research and Aeronomy, Yakut Research Center, Siberian Division, Russian Academy of Sciences, pr. Lenina 31, Yakutsk, 677980 Russia
e-mail: nikiforova@ikfia.ysn.ru
Received April 28, 2005; in final form, May 16, 2005

Seasonal variations in extensive air showers (EASs) detected at the Yakutsk EAS array are analyzed. The atmospheric pressure dependence of variations is pronounced. As the pressure increases by 1 mm of mercury, the EAS intensity decreases by 2%. No temperature dependence is revealed. © 2005 Pleiades Publishing, Inc.

PACS numbers: 96.40.Pq, 96.85.Ry

The ground stations of the Yakutsk EAS array are arranged in the form of a mesh of right triangles with sides of 500 m (small master) and 1000 m (large master). Showers are detected by the array when signals from three stations forming a master triangle coincide with each other. The array does not usually operate in summer. In this work, we analyze showers that have axes located within the perimeter of the array, zenith angles $\theta < 60°$, and charged-particle densities $\rho > 0.8$ particles/m^2 in the master stations.

Figure 1 shows the maximum and minimum diurnal temperatures, average diurnal pressure, and the number of showers per day (a) from October 18, 1999, to June 14, 2000, and (b) from September 12, 2000, to June 14, 2001. First, when the array begins to operate after a summer pause, the number of showers per day increases gradually. Then, correlation between local pressure extrema and the number of showers is observed. The number of showers increases as the pressure decreases.

Fluctuations in the number of showers are partially attributed to the inevitable failures and repair of individual detectors. Such a pronounced barometric dependence is not observed in earlier detection periods. The last modernization of the master stations of the array was performed in 1990, and the number of detected showers increases continuously since that time: it has tripled in ten years. It is evident that the detection periods have not tripled, and an increase in the statistics could be achieved due to an increase in the reliability and stability of the array operation. The atmospheric pressure dependence of variations is manifested at stable operation.

In contrast with the pressure, the temperature varies in time with a much fewer number of pronounced extrema. No correlation between the number of showers and the temperature is seen in Fig. 1.

Figure 2 shows the average temperature, pressure, and number of showers for several years as varying throughout the years divided into 24 equal sections. The fall increase in the number of showers is attributed to the gradual beginning of the operation of the array
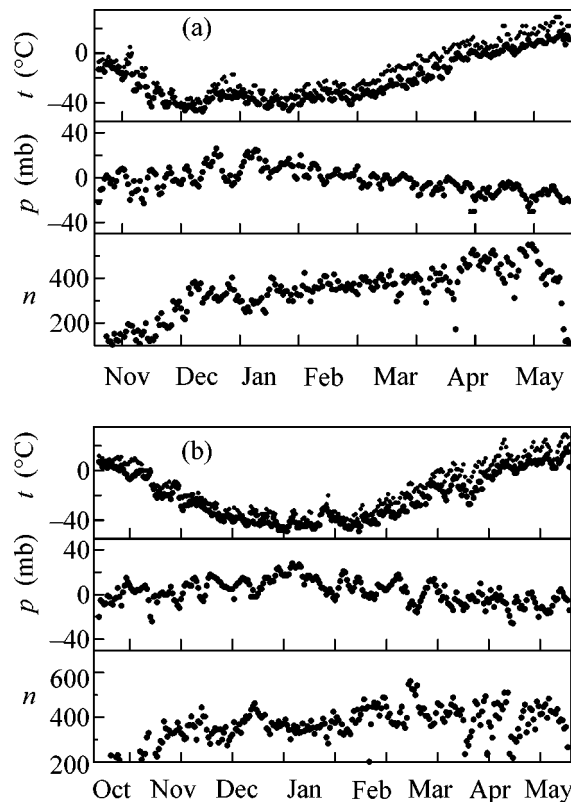
Fig. 1. ($\cdot$) Maximum and ($\bullet$) and minimum diurnal temperatures, average diurnal pressure, the number of showers per day (a) from October 18, 1999, to June 14, 2000, and (b) from September 12, 2000, to June 14, 2001.
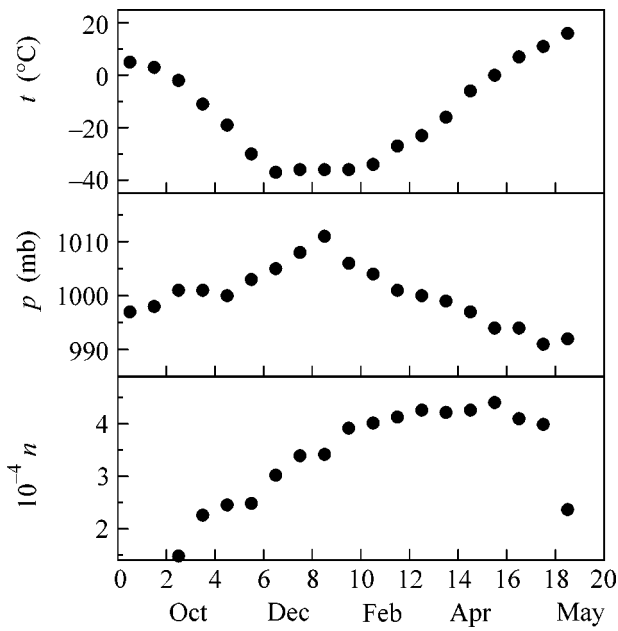
Fig. 2. Average temperature, pressure, and number of showers for several years vs. the time of the year divided into 24 sections.
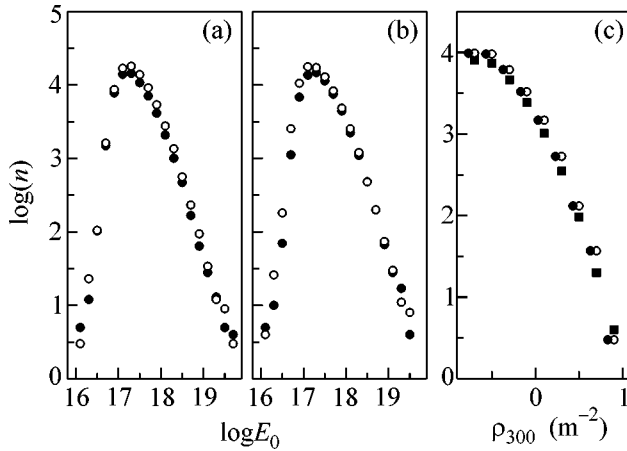
Fig. 3. Energy dependence of the number of showers detected in (●) January and (○) April (a) without and (b) with the recalculation of the Moliere radius (E_o is measured in electronvolts), and (c) the number of showers with $\cos\theta > 0.9$ that are detected by the small master vs. the charged-particle density ρ_{300} at a distance of 300 m from the axis in (■) January, (○) April, and (●) April as shifted to the left by 0.07 particles/m^2.

after the summer pause. A decrease in pressure and an increase in the number of showers are observed from cold to warm months. The number of showers increases with temperature, but these increases are different in different temperature ranges. Moreover, the number of the detected showers increases in January at constant

temperature, although the array is thought to regularly operate from December to May. Thus, an increase in the number of showers from cold to warm months is explained by a decrease in pressure rather than an increase in temperature. The same conclusion is valid for average characteristics, as well as for individual periods. According to the average characteristics from January to April, a decrease in pressure by 1 mbar and 1 mm of mercury leads to an increase in the number of showers by 1.5 and 2%, respectively.

Figure 3a shows the energy dependence of the number of showers detected in (closed symbols) January and (open symbols) April. It is seen that change in the number of showers is independent of energy in the range from 10^{17} to 10^{19} eV.

In order to eliminate the effect of atmospheric variations on the intensity of showers, the following procedure is applied at the Yakutsk EAS array. The lateral distribution function is described by the formula

$$\rho(R/R_i) \sim (R/R_i)^{-1}(1 + R/R_i)^{b-1}, \qquad (1)$$

where R is the distance from the axis and R_i is the Moliere radius of the electromagnetic cascade theory. It is thought that change in temperature and pressure leads to the redistribution of charged particles in a shower and the Moliere radius changes as

$$R_i = 75 \times \frac{1000}{p}\frac{T}{273}, \qquad (2)$$

where the temperature and pressure are measured in degrees Kelvin and millibars, respectively [4]. The total number of particles in a shower does not change. Taking into account this circumstance, the particle density at a distance of 300 and 600 m for the small and large masters is recalculated to the Moliere radius $R_o = 68$ m by the formula

$$\rho_*(R_o) = \rho_*(R_i)\left(\frac{R_o}{R_i}\right)^{b-2}\left(\frac{r + R_i}{r + R_o}\right)^{b-1}. \qquad (3)$$

Here, $r = 300$ and 600 m for ρ_{300} and ρ_{600}, respectively, and b is the parameter of the lateral distribution function.

The energy dependence of the number of showers that are recalculated by Eqs. (2) and (3) for January and April is shown in Fig. 3b. As is seen, the number of thus recalculated showers for energies $E_o > 10^{17}$ eV does not change with the seasons. Differences at energies below 10^{17} eV are associated with the effect of the detection threshold. The temperature dependence of the Moliere radius in Eq. (1) is stronger than the pressure dependence. From January to April, R_i changes by 14% as a function of temperature and by 2% as a function of pressure. As is seen in Fig. 2, seasonal variations in temperature and pressure correlate, or more exactly, anticorrelate with each other to a certain extent. Therefore, taking into account the primarily temperature

changes in Eqs. (1) and (2), we indirectly take into account the pressure variations.

Figure 3c shows the number of showers as a function of density ρ_{300} at a distance of 300 m from the axis for the small master and $\cos\theta > 0.9$. The closed and open symbols correspond to January and April, respectively. The latter symbols should be horizontally shifted by 0.07 particles/m^2 in order to superpose the data for January and April. The absorption path in the parameter λ upon a change in the atmospheric pressure can be estimated using two pressure values by the formula

$$\rho_{300}(\text{Apr}) = \rho_{300}(\text{Jan})\exp\left(\frac{1.02(p_{\text{Jan}} - p_{\text{Apr}})}{\lambda}\right). \quad (4)$$

The absorption path obtained in this way is $\lambda = 110$ g/cm^2, whereas the absorption path of the parameter ρ_{300} that is obtained at fixed values of the integral intensity for showers with various zenith angles is equal to $\lambda_{300} = (310 \pm 20)$ g/cm^2 [2] or, more accurately, $\lambda_{300} = (434 \pm 15) - (62 \pm 9)\log(\rho_{300}(0°))$ g/cm^2 [3]. The resulting λ and λ_{300} values differ from each other by a factor of about 3. The value $\lambda = 110$ g/cm^2 is probably determined by EAS-composing electron–photon cascades that almost do not overlap with each other and are not added to each other.

REFERENCES

1. I. V. Vasil'ev, O. S. Diminshteĭn, T. A. Egorov, *et al.*, *Cosmic Rays with Energy Above 10^{17} eV* (Yad. Fiz. Sib. Otd. Akad. Nauk SSSR, Yakutsk, 1983), p. 19 [in Russian].

2. *Extensive Air Showers with Energy Above 10^{17} eV* (Yad. Fiz. Sib. Otd. Akad. Nauk SSSR, Yakutsk, 1987), p. 3 [in Russian].

3. A. V. Glushkov, A. A. Ivanov, S. P. Knurenko, *et al.*, in *Proceedings of 28th ICRC* (Tsukuba, 2003), p. 393.

Translated by R. Tyapaev

Infrared Renormalons and the Relations between the Gross–Llewellyn Smith and the Bjorken Polarized and Unpolarized Sum Rules¶

A. L. Kataev

Institute for Nuclear Research, Russian Academy of Sciences, Moscow, 117312 Russia
e-mail: kataev@ms2.inr.ac.ru
Received May 13, 2005

It is demonstrated that the infrared renormalon calculus indicates that the QCD theoretical expressions for the Gross–Llewellyn Smith sum rule and for the Bjorken polarized and unpolarized ones contain an identical negative twist-4 $1/Q^2$ correction. This observation is supported by the consideration of the results of calculations of the corresponding twist-4 matrix elements. Together with the indication of the similarity of the perturbative QCD contributions to these three sum rules, this observation leads to simple new theoretical relations between the Gross–Llewellyn Smith and Bjorken polarized and unpolarized sum rules in the energy region $Q^2 \geq 1$ GeV^2. The validity of this relation is checked using concrete experimental data for the Gross–Llewellyn Smith and Bjorken polarized sum rules. © 2005 Pleiades Publishing, Inc.

PACS numbers: 12.38.–t, 13.85.Hd

It is known that, in the traditionally used $\overline{\text{MS}}$ scheme, the Borel image of the physical quantities in QCD contain infrared renormalons (IRR), namely, the singularities on the positive axis of integration of this image in the complex plane of the Borel variable δ (for reviews, see [1–3]). This related Borel integral can be defined as

$$D(a_s) = \int_0^\infty \exp(-\delta/\beta_0 a_s) B[D](\delta) d\delta, \qquad (1)$$

where $a_s = \alpha_s/4\pi$; α_s is the QCD coupling constant in the $\overline{\text{MS}}$ scheme; $\beta_0 = (11/3)C_A - (4/3)T_f N_f$ is the first coefficient of the QCD β-function with $C_A = 3$, $T_f = 1/2$; and $B[D](\delta)$ is the Borel image of the physical quantity $D(a_s)$ under consideration.

From our point of view, the most important theoretical works, which pushed ahead the study of the applicability of the IRR calculus to the analysis of nonperturbative contributions to the characteristics of different processes are those of [4, 5]. In particular, it was shown in [5] that, since there exists a $1/Q^2$ nonperturbative correction of twist-4 in the characteristics of deep-inelastic scattering, the related Borel images should have the IRR pole at $\delta = 1$; this does not manifest itself in the expression for the Borel image of the Adler D function of the e^+e^--annihilation process [4]. This crucial remark is later generalized to the discussion of the Bjorken polarized sum rule in [6]. It should also be mentioned

in passing that ultraviolet renormalons (UVR), which are associated with sign-alternating asymptotic perturbative contributions to the QCD perturbative series, manifest themselves in the Borel images as the poles at $\delta = -k$, where k are integer numbers.

The next problem, which arises in the process of applying the renormalon calculus to the analysis of the structure of both asymptotic perturbative contributions and nonperturbative corrections to physical quantities is the calculation of the corresponding Borel images $B[D](\delta)$. These calculations are usually performed using large-N_f expansion (where N_f is the number of quark flavors). What is really calculated is the so-called one-renormalon-chain approximation to the Born expression for the physical quantity under consideration. Note that the renormalon chain is associated with the gluon propagator, which is dressed by a large number of quark bubble insertions labeled by N_f. The contributions of this chain into the theoretical expression for the physical quantities are gauge-invariant, but they do not reflect the whole picture of the renormalon effects in the QCD. The latter only begin to manifest themselves after the application of the naive non-Abelianization ansatz [7], namely, after the replacement $N_f \longrightarrow -(3/2)\beta_0 = N_f - 33/2$ in the leading terms of the large-N_f expansion. This procedure transforms a large-N_f expansion into a large-β_0 expansion, which is also considered in some recent works [8], where it was associated with a BLM-type expansion [9].

In this letter, definite new consequences of the relations between the Borel images calculated in [10, 11] for the Gross–Llewellyn Smith (GLS) sum rule of νN

_____
¶ This article was submitted by the author in English.

deep-inelastic scattering (DIS) [12], the Bjorken polarized (Bjp) sum rule [13] of polarized charged-lepton–nucleon DIS, and the Bjorken unpolarized (Bjunp) sum rule [14] of νN DIS are discussed. In particular, it is argued that the values of the matrix elements of the twist-4 $1/Q^2$ corrections to the Bjp, Bjunp, and GLS sum rule should have the same value. Together with the similarity in the behavior of the perturbative corrections of all three sum rules discussed in [11], this new observation allows us to write theoretical expressions to relate these a priori different physical quantities.

To be more precise, first consider the definitions of the sum rules we are interested in, taking into account the twist-4 operators evaluated in [15] in the case of GLS and Bjunp sum rules and in [16] for the Bjp sum rule

$$
\text{GLS}(Q^2) = \frac{1}{2}\int_0^1 dx[F_3^{\nu n}(x, Q^2) + F_3^{\nu p}(x, Q^2)]
$$
$$
= 3C_{\text{GLS}}(Q^2) - \frac{\langle\langle O_1 \rangle\rangle}{Q^2}, \tag{2}
$$

$$
\text{Bjp}(Q^2) = \int_0^1 dx[g_1^{lp}(x, Q^2) - g_1^{ln}(x, Q^2)]
$$
$$
= \frac{g_A}{6}C_{\text{Bjp}}(Q^2) - \frac{\langle\langle O_2 \rangle\rangle}{Q^2}, \tag{3}
$$

$$
\text{Bjunp}(Q^2) = \int_0^1 dx[F_1^{\nu p}(x, Q^2) - F_1^{\nu n}(x, Q^2)]
$$
$$
= C_{\text{Bjunp}}(Q^2) - \frac{\langle\langle O_3 \rangle\rangle}{Q^2}, \tag{4}
$$

where

$$
G_{\text{GLS}} = 1 - 4a_s - O(a_s^2), \tag{5}
$$

$$
G_{\text{Bjp}} = 1 - 4a_s - O(a_s^2), \tag{6}
$$

$$
G_{\text{Bjunp}} = 1 - \frac{8}{3}a_s - O(a_s^2). \tag{7}
$$

The explicit expressions of the numerators of twist-4 contributions are defined as in review [17], namely,

$$
\langle\langle O_1 \rangle\rangle = \frac{8}{27}\langle\langle O^s \rangle\rangle, \tag{8}
$$

$$
\langle\langle O_2 \rangle\rangle = \langle\langle O_{p-n}^{\text{NS}} \rangle\rangle, \tag{9}
$$

$$
\langle\langle O_3 \rangle\rangle = \frac{8}{9}\langle\langle O^{\text{NS}} \rangle\rangle, \tag{10}
$$

where the matrix elements on the right-hand side of Eqs. (8)–(10) are known explicitly. Indeed, the matrix

elements $\langle\langle O^s \rangle\rangle$ and $\langle\langle O^{\text{NS}} \rangle\rangle$ were calculated in [15], while the matrix element $\langle\langle O_{p-n}^{\text{NS}} \rangle\rangle$ is calculated in [16].

Let us return to renormalon calculus. It is known from [10] that the Borel images for the GLS and Bjp sum rules coincide and have the following form:

$$
B[C_{\text{GLS}}](\delta) = B[G_{\text{Bjp}}](\delta) = -\frac{(3+\delta)\exp(5\delta/3)}{(1-\delta^2)(1-\delta^2/4)}. \tag{11}
$$

It was shown in [11] that the Borel image $B[C_{\text{Bjunp}}](\delta)$ of the Bjunp sum rule is closely related to Eq. (11), namely,

$$
B[C_{\text{GLS}}](\delta) = \left(\frac{3+\delta}{2(1+\delta)}\right)B[C_{\text{Bjunp}}(\delta)], \tag{12}
$$

where

$$
B[C_{\text{Bjunp}}](\delta) = -\frac{2\exp(5\delta/3)}{(1-\delta)(1-\delta^2/4)}. \tag{13}
$$

The consideration of Eqs. (11)–(13) allow the following conclusions to be made [11]: in the $\overline{\text{MS}}$ scheme, the asymptote of the perturbative series for the GLS, Bjp, and Bjunp sum rules is dominated by the first $\delta = 1$ IRR. Indeed, in the case of the GLS and Bjp sum rules, the first UVR at $\delta = -1$ responsible for the sign-alternating perturbative QCD contribution to the asymptotic behavior of the perturbative QCD series (for a more detailed discussion, see [1, 2]) is suppressed by the factor $(1/2)\exp(-10/3) = 0.018$ with respect to the dominant IRR at $\delta = 1$ responsible for the sign-constant $n!$ growth of the perturbative coefficients for these two sum rules. Moreover, it is obvious from the results of [11] that, in the case of the Bjunp sum rule, the first UVR, created by the pole at $\delta = -1$, is absent and that the residues of the first IRR in the Borel images for the GLS, Bjunp, and Bjp sum rules are the same. Therefore, it is possible to reach the conclusion that the asymptotic perturbative QCD contributions will have an identical structure [11]. This fact is supported by the next-to-next-to-leading order studies of [18], which were performed with the help of the method of effective charges [19].

Now, I will state the new conclusion that follows from the results of Eqs. (11)–(13) and is related to twist-4 $O(1/Q^2)$ corrections. Since the IRR contribution of the first $\delta = 1$ IRR pole enter into the Borel images of the GLS, Bjp, and Bjunp sum rules with the same negative residue (see (11)–(13)), the normalized to unity $O(1/Q^2)$ power correction in the GLS, Bjp, and Bjunp sum rules, which are related to the $O(\Lambda^2/Q^2)$ ambiguities in the Borel integrals generated by the $\delta = 1$ IRR pole, should have the same sign and a similar numerical value. Indeed, the Λ^2/Q^2 IRR ambiguities may be coordinated with the definitions of the twist-4 contributions (see, e.g., the reviews [1, 2]), and, if they

are the same, the twist-4 $1/Q^2$ corrections should be the same also.

Let us check this statement using concrete results of the calculations of the numerical values of the matrix elements by means of the three-point function QCD sum rules, namely, $\langle\langle O^s \rangle\rangle = 0.33$ GeV^2, $\langle\langle O^{NS} \rangle\rangle = 0.15$ GeV^2 as obtained in [20]. As to the error bars, we propose to use 50% conservative uncertainty. This choice is in agreement with the error bar of the following value for the twist-4 matrix element for the Bjorken polarized sum rule, namely, $\langle\langle O^{NS}_{p-n} \rangle\rangle = 0.09 \pm 0.06$ GeV^2, which was obtained in [21]. Now, taking $g_A = 1.26$, we find the following numerical expressions for the sum rules of Eqs. (2)–(4):

$$\text{GLS}(Q^2) = 3\left[1 - 4a_s - O(a_s^2) - \frac{0.098 \text{ GeV}^2}{Q^2}\right], \quad (14)$$

$$\text{Bjp}(Q^2) = \frac{g_A}{6}\left[1 - 4a_s - O(a_s^2) - \frac{0.071 \text{ GeV}^2}{Q^2}\right], \quad (15)$$

$$\text{Bjunp}(Q^2) = \left[1 - \frac{8}{3}a_s - O(a_s^2) - \frac{0.133 \text{ GeV}^2}{Q^2}\right]. \quad (16)$$

One can see that, within the theoretical uncertainties typical of the application of three-point function QCD sum rules, the prediction of the IRR calculus is confirmed. So, indeed, the $O(1/Q^2)$ corrections normalized to unity have the same negative sign and very close values.

In view of the fact that the IRR calculus also indicates that the known and still unknown perturbative QCD corrections to all three sum rules have a comparable value as well [11], I now write the following relation between the three sum rules we are interested in, namely,

$$\text{Bjp}(Q^2) \approx (g_A/18)\text{GLS}(Q^2) \approx (g_A/6)\text{Bjunp}(Q^2). \quad (17)$$

These relations are valid in the energy region where it is possible to separate the twist-4 contribution from the twist-2 effects and the $1/Q^4$ contributions are smaller than the $1/Q^2$ effects. The above-mentioned features should hold at $Q^2 \geq 1$ GeV^2. Therefore, the theoretical comparisons [22] of the expressions for the Bjp sum rule [23] and the GLS sum rule [24] within the analytic approach [25] should possess the same feature.

Now, I will consider whether the left-hand side of the basic equation (17) is respected by experiment. I will use the values for the GLS sum rule extracted from [26] at the energy points $Q^2 = 1.26, 2, 3.16, 5.01, 7.94,$ and 12.59 GeV^2. The results presented in [26] for these six energy points are GLS$(Q^2) \approx 2.39, 2.49, 2.55, 2.78, 2.82,$ and 2.80, where, for simplicity, we neglected both the statistical and systematical uncertainties. The application of the left-hand side of Eq. (17) gives one the following experimentally moti-

vated values for the Bjp sum rule, namely, Bjp$(Q^2) \approx 0.167, 0.168, 0.178, 0.195, 0.197,$ and 0.196 for the same energy points, where, again, the contribution of the statistical and systematical uncertainties are not taken into account.

It is interesting that the value of the Bjp sum rule extracted in [27] from the SLAC and SMC data is Bjp$(Q^2 = 3 \text{ GeV}^2) = 0.177 \pm 0.018$ and, within the existing error bars, does not contradict the value Bjp$(Q^2 = 3 \text{ GeV}^2) = 0.164 \pm 0.011$ extracted from [28] on the basis of measurements at CERN and SLAC before 1997. It is rather inspiring that these results agree with the GLS sum rule value at $Q^2 = 3.16$ GeV^2.

At relatively high energies, the SMC Collaboration gives Bjp$(Q^2 = 10 \text{ GeV}^2) = 0.195 \pm 0.029$ [29], which is consistent with the high-energy results for the GLS sum rule GLS$(Q^2 = 12.59 \text{ GeV}^2) \approx 0.196$ [26]. However, at low Q^2, the result Bjp$(Q^2 = 1.10 \text{ GeV}^2) \approx 0.136$, which was extracted from the CEBAF data in [30], is not consistent with the estimate Bjp$(Q^2 = 1.26 \text{ GeV}^2) \approx 0.167$ extracted from the low-energy results GLS$(Q^2 = 1.26 \text{ GeV}^2) \approx 2.39$ [26] with the help of Eq. (17). It may be interesting to clarify the origin of this disagreement taking into account the experimental uncertainties of the two independent analyses of the νN DIS data and lN polarized DIS data. As the next step, one could check the consistency of the other experimental results for the GLS sum rule and the Bjp sum rule with the IRR motivated expression of Eq. (17) for the energy points in the region 1 GeV$^2 \leq Q^2 \leq 5$ GeV^2 using the NuTeV data for the xF_3 structure function of the νN DIS and rely on the appearance of the future Neutrino Factory, which may provide data for the Bjunp sum rule as well (for a discussion of this possibility, see [31, 32]).

REFERENCES

1. M. Beneke, Phys. Rep. **317**, 1 (1999); hep-ph/9807443.
2. M. Beneke and V. M. Braun, in *At the Frontier of Particle Physics: Handbook of QCD, Boris Ioffe Festschrift*, Ed. by M. Shifman (World Sci., Singapore, 2001), pp. 1719–1773; hep-ph/0010208.

3. G. Altarelli, in *Proceedings of International School of Subnuclear Physics: 33rd Course "Vacuum and Vacua: The Physics of Nothing,"* Ed. by A. Zichichi (1995), p. 221.

4. V. I. Zakharov, Nucl. Phys. B **385**, 452 (1992).

5. A. H. Mueller, Phys. Lett. B **308**, 355 (1993).

6. X. D. Ji, Nucl. Phys. B **448**, 51 (1995); hep-ph/9411312.

7. D. J. Broadhurst and A. G. Grozin, Phys. Rev. D **52**, 4082 (1995); hep-ph/9410240.

8. V. Aquila, P. Gambino, G. Ridolfi, and N. Uraltsev, hep-ph/0503083.

9. S. J. Brodsky, G. P. Lepage, and P. B. Mackenzie, Phys. Rev. D **28**, 228 (1983).

10. D. J. Broadhurst and A. L. Kataev, Phys. Lett. B **315**, 179 (1993); hep-ph/9308274.

11. D. J. Broadhurst and A. L. Kataev, Phys. Lett. B **544**, 154 (2002); hep-ph/0207261.

12. D. J. Gross and C. H. Llewellyn Smith, Nucl. Phys. B **14**, 337 (1969).

13. J. D. Bjorken, Phys. Rev. **148**, 1467 (1966).

14. J. D. Bjorken, Phys. Rev. **163**, 1767 (1967).

15. E. V. Shuryak and A. I. Vainshtein, Nucl. Phys. B **199**, 451 (1982).

16. E. V. Shuryak and A. I. Vainshtein, Nucl. Phys. B **201**, 141 (1982).

17. I. Hinchliffe and A. Kwiatkowski, Annu. Rev. Nucl. Part. Sci. **46**, 609 (1996); hep-ph/9604210.

18. E. Gardi and M. Karliner, Nucl. Phys. B **529**, 383 (1998); hep-ph/9802218.

19. G. Grunberg, Phys. Rev. D **29**, 2315 (1984).

20. V. M. Braun and A. V. Kolesnichenko, Nucl. Phys. B **283**, 723 (1987).

21. I. I. Balitsky, V. M. Braun, and A. V. Kolesnichenko, Phys. Lett. B **242**, 245 (1990); Phys. Lett. B **318**, 648(E) (1993); hep-ph/9310316.

22. D. V. Shirkov, Eur. Phys. J. C **22**, 331 (2001); hep-ph/0107282.

23. K. A. Milton, I. L. Solovtsov, and O. P. Solovtsova, Phys. Lett. B **439**, 421 (1998); hep-ph/9809510.

24. K. A. Milton, I. L. Solovtsov, and O. P. Solovtsova, Phys. Rev. D **60**, 016001 (1999); hep-ph/9809513.

25. D. V. Shirkov and I. L. Solovtsov, Phys. Rev. Lett. **79**, 1209 (1997); hep-ph/9704333.

26. J. H. Kim, D. A. Harris, C. G. Arroyo, *et al.*, Phys. Rev. Lett. **81**, 3595 (1998); hep-ex/9808015.

27. G. Altarelli, R. D. Ball, S. Forte, and G. Ridolfi, Nucl. Phys. B **496**, 337 (1997); hep-ph/9701289.

28. J. R. Ellis, E. Gardi, M. Karliner, and M. A. Samuel, Phys. Lett. B **366**, 268 (1996); hep-ph/9509312.

29. B. Adeva, E. Arik, A. Arvidson, *et al.*, Phys. Lett. B **412**, 414 (1997).

30. A. Deur, P. Bosted, V. Burkert, *et al.*, Phys. Rev. Lett. **93**, 212 001 (2004); hep-ex/0407007.

31. M. L. Mangano, S. I. Alekhin, M. Anselmino, *et al.*, CERN-TH/2001-131, hep-ph/0105155, in ECFA/CERN Studies of a European Neutrino Factory, CERN Report CERN 2004-002, Ed. by A. Blondel, G. Buchalla, M. Campanelli, *et al.* (2004).

32. S. I. Alekhin and A. L. Kataev, J. Phys. G **29**, 1993 (2003); hep-ph/0209165.

Curvilinear Motion of Laser Soliton Complexes

N. N. Rozanov, S. V. Fedorov, and A. N. Shatsev

Research Institute of Laser Physics, St. Petersburg, 199034 Russia
e-mail: nrosanov@yahoo.com

Conditions under which the center of inertia of stable complexes of dissipative optical solitons moves curvilinearly have been determined. Such a character of the motion of dissipative structures is caused by asymmetry in the distribution of the intensity and energy fluxes, and it is pronounced for laser solitons with strong interaction. The results of the numerical simulation of these complexes in the model of surface emitting lasers or laser amplifiers with saturated amplification and absorption are presented. Such complexes may be observed in various spatially distributed nonlinear dissipative systems, in particular, in the form of discrete solitons. © *2005 Pleiades Publishing, Inc.*

PACS numbers: 05.45.Yv, 42.55.Ah, 42.65.Tg

The law of the rectilinear motion of the center of inertia of mechanical systems, which follows from the uniformity of space, belongs to the basic laws of mechanics and relativity theory [1, 2]. This law is also valid for the center of inertia of fields, including electromagnetic fields, both in vacuum [2] and in homogeneous transparent media, including nonlinear media [3], where the existence of particle-like (localized) structures—conservative solitons—is possible. However, of considerable interest are also media or systems with dissipation, where inflow and outflow of energy occur and, as a result of the energy balance, the existence of especially stable dissipative solitons is possible [4]. In this work, we demonstrate the possibility of the curvilinear motion of stable soliton complexes in homogeneous systems with dissipation. Although the results are general, we consider only 2D optical solitons in surface emitting lasers with saturated absorption in view of recent advances in experiments with semiconductor microcavities [5–7].

We simultaneously consider two (2 + 1) dimensional schemes in which laser solitons were predicted and analyzed (see [4] and references therein). The first scheme is a surface emitting laser that is characterized by a large Fresnel number and whose cavity contains a saturated absorber. We also assume that the scheme includes an anisotropic element such that losses are quite small only for one of two polarized components. Under this assumption, the problem reduces to a scalar problem. The relaxation times for amplification and absorption are considered to be small compared to the field lifetime t_c in the empty cavity. This relation corresponds to class A lasers. In this case, in the paraxial approximation of the mean field (after the averaging of the envelope of the electric field strength E over the longitudinal coordinate z), the dynamics described by the generalized complex Ginzburg–Landau equation [4, 8]

$$\frac{\partial E}{\partial t} = (i + d)\nabla_\perp^2 E + Ef(|E|^2),$$

$$f(|E|^2) = -1 + \frac{g_0}{1 + |E|^2} + -\frac{a_0}{1 + b|E|^2}. \tag{1}$$

Here, t is the time divided by t_c; $\nabla_\perp^2 = \partial^2/\partial x^2 + \partial^2/\partial y^2$ is the transverse Laplacian, where $(x, y) = \mathbf{r}_\perp$ are transverse coordinates divided by the Fresnel band width; d is the effective diffusion coefficient, which is assumed to be small ($0 < d \ll 1$); and the nonlinear function $f(I)$ of the radiation intensity $I = |E|^2$ describes nonlinear resonant amplification and linear nonresonant absorption (losses). If frequency detuning is disregarded, the function $f(I)$ is real; g_0 and a_0 are real positive coefficients of unsaturated (linear) amplification and absorption, respectively; and b is the ratio of the saturation intensities for amplification and absorption. Nonresonant losses are normalized to unity due to the time scale.

The second scheme described by the same governing equation (1) is an optical indicator also with saturated amplification and absorption. In this cavity-free scheme, the evolution variable t has the meaning of the longitudinal coordinate z. Below, we will use the standard definitions $\mathbf{S}_\perp = \mathrm{Im}(E^*\nabla_\perp E)$ for the transverse energy flux vector averaged over the optical period (Poynting vector) and $\mathbf{R}_\perp = \int \mathbf{r}_\perp |E|^2 d\mathbf{r}_\perp / \int |E|^2 d\mathbf{r}_\perp$ for the transverse coordinates of the center of inertia of the field.

According to the field dynamical equations (1), if the transverse distributions of intensity and the Poynting vector have the axis of symmetry, the center of inertia can move only along this axis. If two such axes exist,

the center of inertia is at rest; therefore, asymmetry is a necessary condition for the motion of the structure [4]. Below, we will consider complexes generated by vortex solitons whose field envelope in the polar coordinates (r, φ) has the form $E(r, \varphi, t) = A(r)\exp(im\varphi - i\eta t)$. The spectral parameter v serves as an eigenvalue with a discrete spectrum and it is a nonlinear frequency shift for the laser scheme or propagation constant shift for the amplifier. The topological charge is taken as $m = \pm 1$. Analysis shows that asymmetry is most pronounced for the case of the strong coupling of solitons, and the structure of energy fluxes is a convenient quantitative (topological) criterion of the difference between weak and strong couplings [8]. The results below are obtained with the following typical values of the parameters: $a_0 = 2$, $b = 10$, $0.04 < d < 0.15$, and $g_0 = 2.108$ and 2.11. The simulation is based on the splitting method and fast Fourier transform algorithm [9].

Figure 1a shows the instantaneous distribution of the intensity of a strongly coupled pair of vortex solitons with opposite charges $m_1 = 1$ and $m_2 = -1$. Strongly coupled pairs with such charges are always symmetric and very stable and rotate with a period of $T = 410$ (for the indicated parameters). According to Fig. 1c, the center of inertia of this pair moves along a circle. The period of this motion and pair rotation period coincide with each other; i.e., these two motions are synchronized. The Poynting vector additionally averaged over the cross section, $\langle \mathbf{S}_\perp \rangle = \int \mathbf{S}_\perp \, d\mathbf{r}_\perp$, is directed along a tangent of the trajectory of the center of inertia.

A strongly coupled pair of vortex solitons with the same topological charges $m_1 = m_2 = -1$ has central symmetry. Correspondingly, its center of inertia is at rest, and the pair rotates with a period of $T \approx 840$. However, if such a structure (core) is supplemented with a soliton that is weakly coupled with the core and has the same topological charge (satellite), a stable complex is formed after a certain transient period. In this complex, the periods of the rotation of the core $T_{\mathrm{core}} \approx 840$ and satellite (around the core) $T_{\mathrm{sat}} \approx 4400$ significantly differ from each other (see Fig. 1b and [10]). This complex is stable and is recovered after introduction of small perturbations. Owing to the central symmetry of the core, the entire structure is reproduced with the rotation by the angle $\alpha = \pi/(T_{\mathrm{sat}}/T_{\mathrm{core}} - 1)$ (see Fig. 1d) after the time interval $T_1 = \frac{1}{2}(T_{\mathrm{core}}^{-1} - T_{\mathrm{sat}}^{-1})^{-1}$. In addition to rotation, the whole structure undergoes translational motion with very low velocity on the order of the calculation error, see Fig. 1d.

As a result of the nonlinear interaction between the two rotations indicated above and synchronization, the ratio of the rotation periods within the synchronization band is necessarily a rational number: $T_{\mathrm{core}}/T_{\mathrm{sat}} = n_{\mathrm{sat}}/n_{\mathrm{core}}$, where $T_{\mathrm{core}} = T_0/n_{\mathrm{core}}$, $T_{\mathrm{sat}} = T_0/n_{\mathrm{sat}}$, T_0 is the minimum period of the rotation of the whole structure
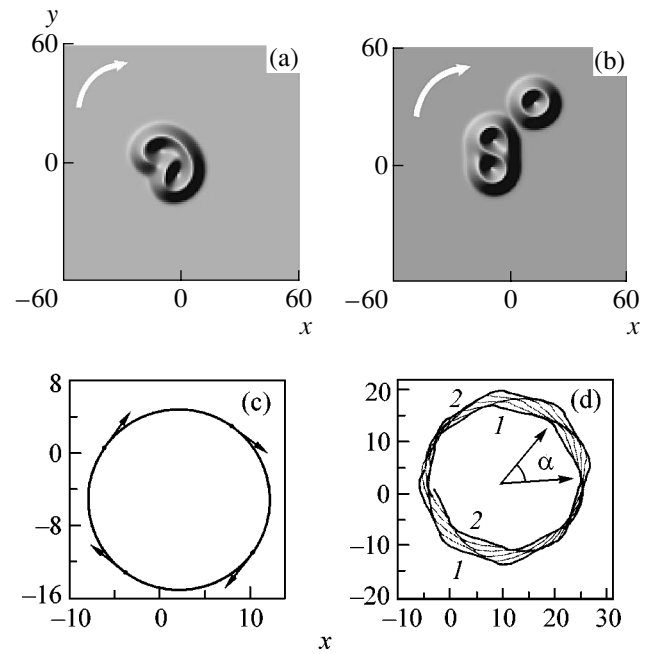
Fig. 1. (a, b) Instantaneous transverse distribution of intensity and (c, d) trajectories of the centers of mass for (a, c) a strongly coupled pair of vortex solitons with opposite charges at $d = 0.06$ and (b, d) a core-type structure with one weakly coupled satellite at $d = 0.12$; and *1* and *2* are the first [$t = (73710, 78110)$] and sixth [$t = (95310, 99710)$] rotations of the satellite. The arrows in (a, b) show the directions of the structure rotation, and the arrows in (c) show the direction of the average Poynting vector $\langle \mathbf{S}_\perp \rangle$ at various times, and $g_0 = 2.108$.
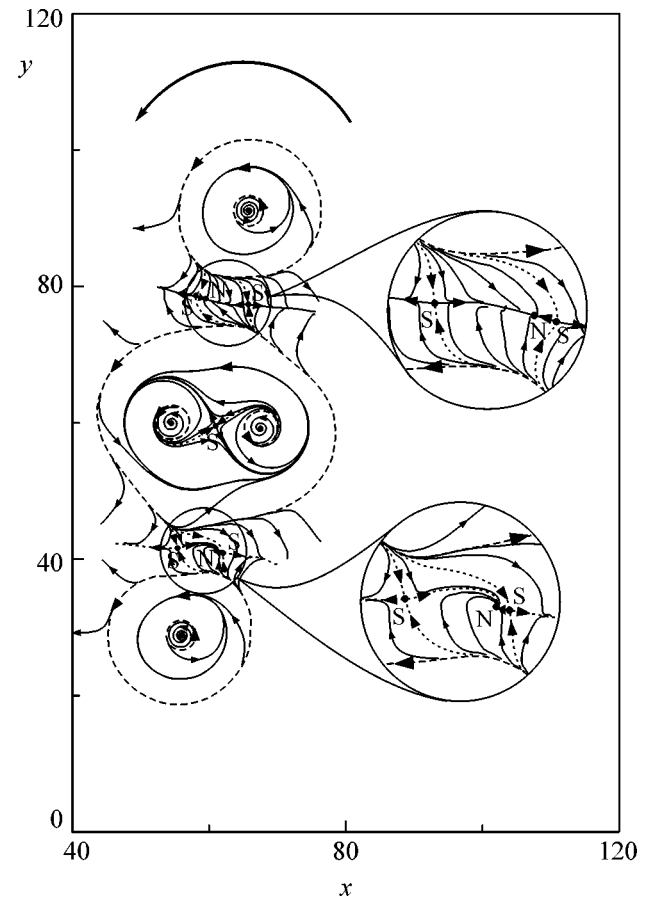
by an angle multiple to 2π, and n_{core} and n_{sat} are integers. Then, if the above negligibly slow translational motion is disregarded, the trajectory of the center of inertia is a closed curve consisting of a number of identical-shaped segments rotated by the angle α with respect to each other. For the case shown in Fig. 1d, $n_{\mathrm{core}} = 49$ and $n_{\mathrm{sat}} = 10$, and only half the entire period T_0 is presented. We note that the period $T_0 = 44\,000$ also characterizes the duration of the transient synchronization process, whereas the time of complex formation is close to $T_{\mathrm{core}} \ll T_0$. If the initial conditions are unfavorable, the satellite is not coupled with the core but, e.g., retires from it. Nevertheless, such a complex is very stable and exists over a wide parameter region ($0.036 < d < 0.15$, $2.097 < g_0 < 2.117$). Under our conditions, the integers n_{core} and n_{sat} for the formed complex are independent of the initial conditions but depend on the parameters of the system. In particular, when the diffusion coefficient d changes, complexes with $n_{\mathrm{sat}} = 1$ and n_{core} from 4 to 9 are formed.

Calculations indicate the existence of a new complex, where two satellites rotate around the same core with a period of $T_{\mathrm{sat}} = 11\,000$ (Fig. 2). In this case, the core rotation period is $T_{\mathrm{core}} \approx 1100$, the topological charges of four vortices are identical ($m = 1$), and the
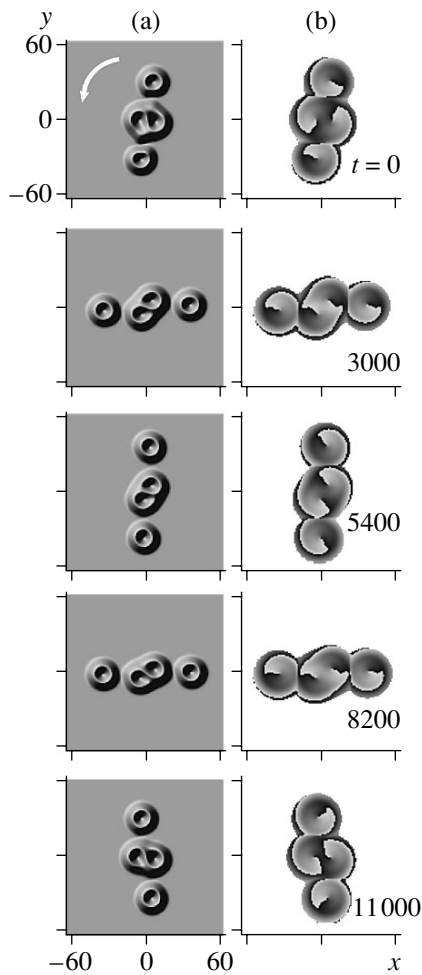
Fig. 2. Transverse distribution of the (a) intensity and (b) phase for the core–two satellite structure. The rotation period is equal to about 1100 and 11000 for the core and satellites, respectively. The arrows show the direction of the structure rotation. In the right panels, the phase varies from (dark color) $-\pi$ to (light color) π.

Fig. 3. Energy fluxes for the stable localized structure shown in Fig. 2 for $t = 0$. The closed trajectories correspond to limiting cycles. Two regions shown in a larger scale are the neighborhood of weak overlapping of the core and satellites and include nodes N and saddle points S with separatrices shown by the dotted lines. The large arrow shows the rotation direction.

rotation is counterclockwise. In order to demonstrate weak coupling of the satellites with the core, in Fig. 3, we represent the topological structure of energy fluxes that is obtained by the method described in [8]. It is seen that the core is enveloped with two common limiting cycles, which testifies to strong coupling of the vortices in the core. In contrast, each satellite holds three individual limiting cycles, which testifies to their weak coupling with the core. Thus, coupling of solitons in the complex is mixed. A large distance between solitons excludes their direct interaction. However, they interact with each other through the core. This means that a satellite perturbs the core and the other satellite interacts with the perturbed core. Therefore, the relative displacement of the satellites is not arbitrary. If one satellite is displaced, their opposite disposition with respect to the core is recovered after a certain time, as is shown in Fig. 4, which corroborates the stability of these struc-

tures. It is important that the center of inertia of these structures is nearly at rest due to symmetry.

The finite difference approximation of spatial derivatives in Eq. (1) corresponds to the two-dimensional system of single-mode waveguides, each of which is characterized by nonlinear (saturated) amplification and absorption, and both resonant and nonresonant variants of the scheme are allowed. Such one-dimensional schemes were studied recently [11]. A much richer variety of the dissipative discrete solitons exists in two-dimensional systems. For structures where the amplitudes and phases of modes vary slowly from waveguide to waveguide, the above results mean the existence of moving and rotating complexes of discrete solitons. The existence of structures with a sharp change in the amplitudes and phases of modes is possible. These structures have no analogs for continuous model (1).
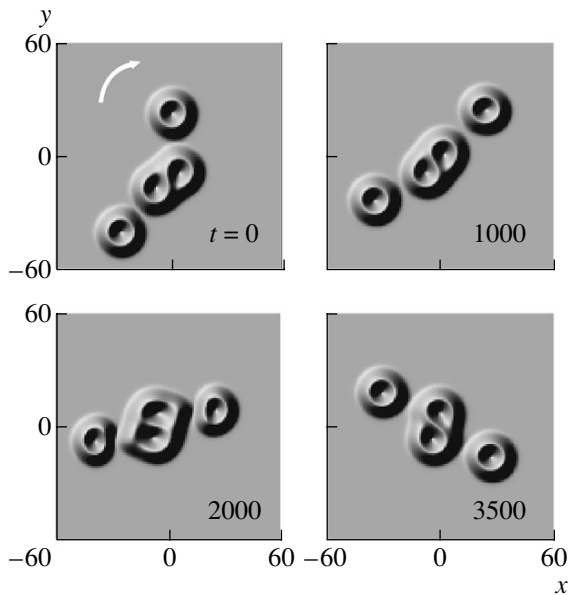
Fig. 4. Dynamics of the recovery of the opposite positions of two satellites after initial perturbation for the parameters $d = 0.15$ and $g_0 = 2.108$.

Thus, we likely present the first example of the steady curvilinear motion of the center of inertia of complexes of dissipative optical solitons. This property has been discovered for a wide class of axisymmetric vortex structures with strong interaction. The cause of the curvilinearity of the motion is the asymmetry of the sources and sinks of energy in the dissipative systems (in the absence of Galilean invariance). Curvilinear motion is generally possible not only upon strong interaction between solitons. In particular, Gaussian beams are exact solutions of Eq. (1) when the function f is a constant $f_0 = f(0)$, which corresponds to a linear dissipative system. For $d > 0$, their center moves along a hyperbola (curvilinearly); however, this motion is realized only at the transient stage that ends with the termination of the transverse motion. In the nonlinear case, the curvilinear motion of asymmetric complexes of weakly coupled dissipative systems is observed but, as previously, only in the transient process. A soliton complex with one axis of symmetry moves along with the axis if there is no symmetry with respect to its front and back parts in the direction of this axis. When axes of symmetry are absent, the complex rotates and its center of inertia moves curvilinearly. Although the position of the center of inertia is completely determined by the inten-

sity distribution, the curvature of the trajectory is associated with the "phase degree of freedom" of the field. We note that the complexes under consideration rotate as rigid bodies in the absence of the weak coupling between solitons composing a complex. For mixed coupling (a part of a soliton is coupled strongly, and the other part is coupled weakly), different parts of the complex rotate with different angular velocities. The nonlinearity of the system is manifested in the synchronization of the rotations and affects the shape of the trajectory of the center of inertia. The above type of the transverse motion of solitons can be promising in applications to the optical processing and storage of information, particularly in vertical-cavity surface-emitting lasers with saturated absorption, as well as in similar amplifiers, active waveguides, and nonlinear photon crystals.

REFERENCES

1. L. D. Landau and E. M. Lifshitz, *Course of Theoretical Physics*, Vol. 1: *Mechanics*, 2nd ed. (Nauka, Moscow, 1962; Pergamon, Oxford, 1965).
2. V. A. Fock, *The Theory of Space, Time and Gravitation* (Fizmatlit, Moscow, 1961; Pergamon, Oxford, 1964).
3. S. N. Vlasov and V. I. Talanov, *Self-Focusing of Waves* (Inst. Prikl. Fiz. Akad. Nauk SSSR, Gorki, 1970) [in Russian].
4. N. N. Rosanov, *Spatial Hysteresis and Optical Patterns* (Springer, Berlin, 2002).
5. S. Barland, J. R. Tredicce, M. Brambilla, *et al.*, Nature **419**, 699 (2002).
6. V. B. Taranenko, I. Ganne, R. J. Kuszelewicz, and C. O. Weiss, Phys. Rev. A **61**, 063818 (2000).
7. E. A. Ultanir, G. I. Stegeman, D. Michaelis, *et al.*, Phys. Rev. Lett. **90**, 253903 (2003).
8. N. N. Rozanov, S. F. Fedorov, and A. N. Shatsev, Zh. Éksp. Teor. Fiz. **125**, 486 (2004) [JETP **98**, 427 (2004)].
9. S. V. Fedorov, N. N. Rosanov, A. N. Shatsev, *et al.*, IEEE J. Quantum Electron. **39**, 197 (2003).
10. N. N. Rozanov, S. V. Fedorov, A. N. Shatsev, and N. A. Loĭko, Opt. Spektrosk. **97**, 96 (2004) [Opt. Spectrosc. **97**, 88 (2004)].
11. E. A. Ultanir, G. I. Stegeman, and D. N. Christodoulides, Opt. Lett. **29**, 845 (2004).

Translated by R. Tyapaev

Effective Temperature and the Directional Motion of Fast Ions in a Picosecond Laser Plasma

V. S. Belyaev[1], V. I. Vinogradov[1], A. P. Matafonov[1], V. P. Kraĭnov[2], V. S. Lisitsa[3], A. Ya. Faenov[4], T. A. Pikuz[4], I. Yu. Skobelev[4], A. I. Magunov[4, 5], S. A. Pikuz, Jr.[6], V. P. Andrianov[7], G. N. Ignat'ev[7], Yu. I. Kozhunov[7], O. B. Kozlov[7], and A. M. Chekmarev[8]

[1] *Central Research Institute for Machine Building (TsNIIMASH), ul. Pionerskaya 4, Korolev, Moscow region, 141070 Russia*

[2] *Moscow Institute of Physics and Technology, Institutskiĭ per. 9, Dolgoprudnyĭ, Moscow region, 141700 Russia*

[3] *Institute of Nuclear Fusion, Russian Research Centre Kurchatov Institute, pl. Akademika Kurchatova 1, Moscow, 123182 Russia*

[4] *Center of Data on Spectra of Multiply Charged Ions, All-Russia Research Institute of Physicotechnical and Radio Engineering Measurements, Mendeleevo, Moscow region, 141570 Russia*

[5] *Prokhorov General Physics Institute, Russian Academy of Sciences, ul. Vavilova 38, Moscow, 117942 Russia*

[6] *Joint Institute for High Temperatures, Russian Academy of Sciences, ul. Izhorskaya 13/19, Moscow, 127412 Russia*

[7] *Research Institute of Pulse Technique, ul. Luganskaya 9, Moscow, 115304 Russia*

[8] *Lebedev Physical Institute, Russian Academy of Sciences, Leninskiĭ pr. 53, Moscow, 117924 Russia*

Received May 11, 2005

Experimental data are reported on the generation of fast ions in a picosecond laser plasma at a laser-radiation intensity of 2×10^{18} W/cm^2. The results are obtained by measuring the Doppler spectra of hydrogen-like fluorine ions. An important feature of the energy distribution of fast ions is a slow decrease up to an energy of 1.4 MeV. In addition, the directional motion of fast ions deep into a target is found due to the redshift of the Doppler profile of the Ly_{α} line. The parameters of the energy distribution of the ions are theoretically estimated. © 2005 Pleiades Publishing, Inc.

PACS numbers: 32.30.Rj, 52.50.Jm, 52.70.La

1. INTRODUCTION

The generation of fast ions in a plasma produced due to the interaction of ultrashort laser pulses with solid targets is of considerable interest for the initiation of a number of nuclear reactions including fusion reactions with high thresholds. Most measurements of the energy spectra of ions in the laser plasma were carried out for light ions (hydrogen and deuterium). A series of measurements of the energy spectrum of heavier ions formed owing to the interaction of intense pico- or femtosecond laser radiation with solids or clusters was reported in [1–11]. In those measurements, for the flux densities of laser radiation beginning with 10^{18} W/cm^2, ion energies higher than 1 MeV were detected, and the energy increased linearly with the radiation intensity.

The standard mechanism of the acceleration of ions is the field of the space charge that is formed by electrons emitted from a target. However, various mechanisms of formation of this charge and the direction of the corresponding accelerating electric field are discussed. The situation is complicated by the presence of strong magnetic fields generated in the laser plasma irradiated by ultrashort laser pulses. The dominant directional motion of fast ions deeply into the target was recently found in [10] (see also [5, 12]). The mea-surement procedure is based on the detection of the spatial distribution of neutrons arising in the D–D reaction in deuterated targets.

In view of these circumstances, direct measurements of the energy spectra and direction of the motion of fast multiply charged ions using the Doppler contour of their spectral lines are of interest. This work is devoted to such measurements and their theoretical interpretation.

2. EXPERIMENTAL PROCEDURE

Experiments were carried out at the 10-TW "Neodim" laser facility [13]. This setup produces a laser pulse with an energy of 10 J, a wavelength of 1.055 μm, and a duration of 1.5 ps. The focusing system ensures the concentration of no less than 40% of the laser-beam energy onto a spot with a diameter of 15 μm and, correspondingly, the peak intensity 2×10^{18} W/cm^2 on the target.

The laser radiation of the Neodim setup is characterized by the presence of three prepulses. Two picosecond prepulses arising at 13 ns and 25 ps before the main laser pulse have the intensities 10^{-4} and 5×10^{-4} of the main-pulse intensity, respectively. The third prepulse is
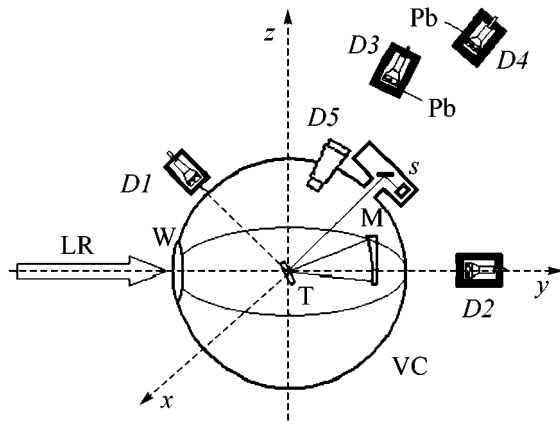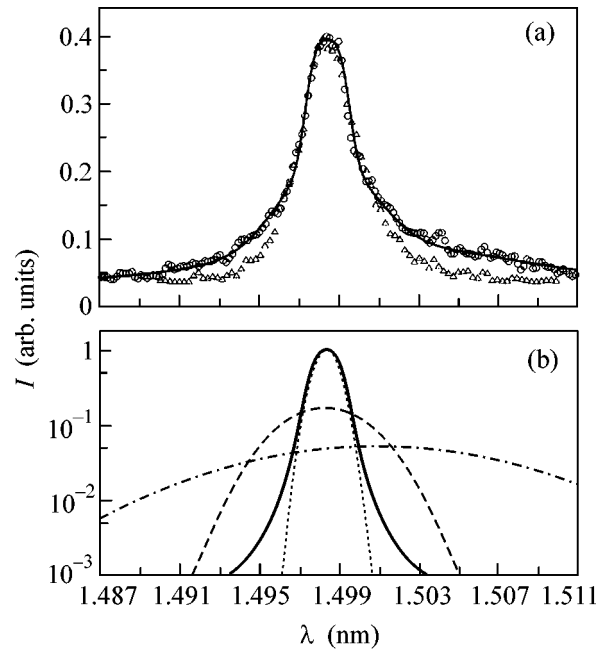
Fig. 1. Experimental scheme: (T) the target, (M) the off-axis parabolic mirror, (W) the window of the vacuum chamber, (LR) laser radiation, (VC) the vacuum chamber, (S) the spectrograph, (*D1–D4*) the scintillation detectors of γ radiation, and (*D5*) the camera obscura with a CCD matrix.

Fig. 2. (a) Experimental contour of the Ly_α line of the F IX ion in a plasma produced by a laser pulse with the duration $\tau_{las} = 1.5$ ps and energy E_{las} = (circles) 10 and (triangles) 1.5 J. The solid line is the calculation by Eq. (3) taking into account Doppler broadening for the ion temperature $T_i = 3$ keV and Stark broadening for the electron density $N_e = 10^{21}$ cm^{-3} and an optical thickness of 3.7 with additional inclusion of ions with $T_{int} = 35$ keV ($A = 0.17$) and $T_{fast} = 350$ keV ($B = 0.052$). (b) Relative contributions of various groups of ions to the total intensity of the Ly_α line given by Eq. (2). The solid line is the first term in Eq. (2), the dashed line is the contribution of ions with $T_{int} = 35$ keV (second term), and the dash–dotted line is the contribution of fast ions with $T_{fast} = 350$ keV (third term). The dotted line is the Doppler contour with $T_i = 3$ keV. For fast ions, the systematic redshift $\Delta\lambda_{sh} = 0.0025$ nm that is responsible for the asymmetry of the wings corresponds to $E_{ion} = 24.6$ keV.

the pulse of enhanced luminescence with a duration of about 4 ns and an intensity 10^{-8} of the main-pulse intensity.

Figure 1 shows the experimental scheme. A laser beam is focused by the off-axis parabolic mirror with a focal length of 20 cm on the surface of a solid target T at an angle of 40° with respect to the target normal. Flat fluoroplastic plates 200 μm in thickness were used as targets.

The x-ray radiation from the plasma produced due to the interaction of the laser pulse with the target was detected by the spectrograph S [14, 15] with spherically bent quartz or mica crystals (the curvature radius of the crystalline surface was equal to 150 mm). The observation angle for the spectrograph with respect to the target surface normal was equal to 20° in all the experiments, as was shown in Fig. 1. A Kodak-2492 x-ray film was used as a detector of the radiation reflected from the crystal. The input window of the cassette with the film was protected from visible light by two layers of a filter that was a polypropylene film 1 μm thick both of whose sides are coated by an Al layer with a total thickness of 0.2 μm. The emissive spectra of the plasma were analyzed in the spectral range containing the Ly_α line of the hydrogen-like F IX ion. Under the experimental conditions, the spectrograph ensured a spectral resolution $\lambda/\Delta\lambda$ no worse than 5000.

Hard x-ray radiation was detected by scintillation plastic and stilbene detectors *D1–D4* placed at distances from 20 cm to 4 m from the target. Lead filters with thicknesses from 2 to 13.5 cm were placed in front of the detectors. A camera obscura *D5* with a CCD matrix was used to control the size of the focusing spot of the x-ray radiation and to estimate its brightness in the range 1–5 keV.

3. EXPERIMENTAL RESULTS AND DISCUSSION

The spectral range of the laser-plasma radiation that corresponded to the Ly_α line of the hydrogen-like fluorine ion was detected in the experiment. Figure 2a shows (circles) the measurement results for a pulse duration of 1.5 ps and an energy of 10 J that correspond to the peak intensity above 10^{18} W/cm^2. For comparison, triangles show the previous measurements for the profile of the Ly_α line for a pulse energy of 1.5 J [11]. The new measurements indicate the presence of wider wings of the Ly_α line, which testifies to the more efficient generation of fast ions with energies 1 MeV and higher.

In order to interpret the measurements and to determine the energy parameters of the plasma, the observed line contour is simulated taking into account Doppler
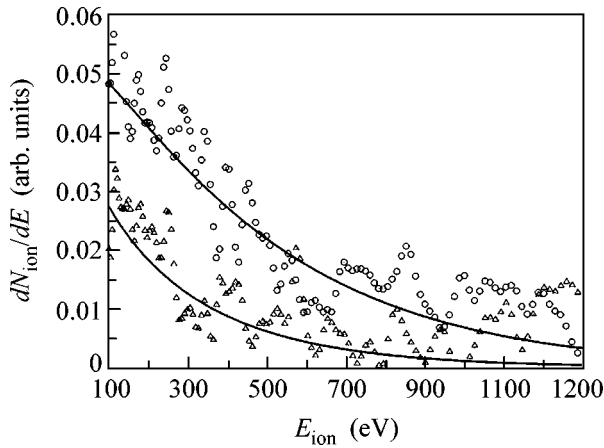
Fig. 3. Energy distribution of fast fluorine ions from measurements of the contour of the Ly_α line of the F IX ion. Circles correspond to ions moving towards the target (red wing of the line) and triangles are data for ions flying from the target (blue wing). The solid lines are the dependence $dN/dE = B\exp[-M(v - v_0)2/2T_{fast}]$, where v is the ion velocity in the observation direction, $Mv_0^2/2 = 25$ keV, and $T_{fast} = 350$ keV.

and Stark broadenings and the optical thickness of the plasma. The central part of the spectral line is calculated as in [11], taking into account Doppler and Stark broadening mechanisms for the plasma parameters $N_e = 10^{21}$ cm^{-3} (critical electron density) and $T_i = 3$ keV (thermal-ion temperature) by the formula (see, e.g., [16])

$$S(\lambda) = \sum_\alpha \int W(F, N_e) \exp[-(\lambda - \lambda_\alpha(F))^2/\Delta\lambda_T^2] dF. \ (1)$$

Here, $W(F, N_e)$ is the distribution function of the ion microfield F, $\lambda_\alpha(F)$ is the wavelength of the transition for the Stark component of the line, $\Delta\lambda_T = (2T_i/Mc^2)^{1/2}\lambda_0$ is the Doppler half-width of the line for thermal ions with mass M, and λ_0 is the transition wavelength. At the chosen electron density, the contribution from the collisional broadening in the wings of the Ly_α line of fluorine is small (i.e., the calculated curve differs slightly from the pure Doppler curve). To describe the observed wings of the line, the contributions from two groups of ions characterized by the temperatures T_{int} (intermediate ions) and T_{fast} (fast ions) are added to formula (1):

$$I(\lambda) = S(\lambda) + A\exp[-(\lambda - \lambda_0)^2/\Delta\lambda_{int}^2]$$
$$+ B\exp[-(\lambda - \lambda_0 - \Delta\lambda_s)^2/\Delta\lambda_{fas}^2], \quad (2)$$

where $\Delta\lambda_s$ is the systematic shift presenting the observed asymmetry of the line wings.

Expression (2) is valid for the optically thin plasma. The absorption is taken into account in the calculation in the homogeneous layer approximation

$$I'(\lambda) = C[1 - \exp(-\tau I(\lambda)/I(\lambda_0))], \quad (3)$$

where τ is the optical thickness of the plasma at the line center and C is the normalization constant.

The optical thickness $\tau = 3.7$ was taken from the previous calculations for the spectrum obtained at $E_{las} = 1.5$ J [11]. The relative contributions from ions of various groups to the radiation yield that are characterized by the constants A and B, as well as the parameters T_{int}, T_{fast}, and $\Delta\lambda_s$, are chosen by fitting the simulated line contour to the measurement data. Figure 2a shows the results of the approximation. They correspond to the parameters $T_{int} = 35$ keV, $T_{fast} = 350$ keV, $A = 0.17$, and $B = 0.052$. The shift $\Delta\lambda_s$ reproducing the observed asymmetry of the line corresponds to an ion energy of 25 keV. The line wings obtained in the measurements with a pulse energy of 1.5 J are almost completely determined by ions with $T_{int} = 35$ keV, whereas the far wing at a pulse energy of 10 J corresponds to a significant contribution from fast ions, including those with energies 1 MeV and higher.

Figure 2b shows the contributions from individual terms in Eq. (2). The results show that Stark wings (solid line) also do not make a significant contribution to the observed line contour.

The calculated energy distribution of fast ions is shown in Fig. 3 along with the values extracted from the experimental data by subtracting the symmetric contribution of thermal and intermediate ions [the first two terms in Eq. (2)] from the observed line contour. The calculated energy distribution of fast ions flying towards the target and from it is obtained from the third term in Eq. (2).

The observed asymmetry between the blue and red wings of the line is attributed to the spatial anisotropy of the scattering of fast ions from the picosecond plasma. The red wing possibly contains a contribution from dielectron satellites; however, their intensity for fluorine is not considerable.

Using the scintillation detectors *D1–D4* with the set of lead filters, we conducted the experiments for determining the maximum energy of γ photons in the laser plasma on the target. The weakening of the flux of γ photons was measured as a function of the thickness of a lead filter. Using the measured dependence, we estimated the maximum energy of γ photons as 3.5 MeV, and the number of such photons was on the order of 10^6.

The measurements with the camera obscura show that the focusing-spot size detected in the soft x-ray range of 1–5 keV is equal to ~15 µm.

4. THEORETICAL ESTIMATES OF THE PARAMETERS OF THE ENERGY DISTRIBUTION

The basic mechanisms of formation of multiply charged fluorine ions are field and collisional ionizations. When theoretically analyzing the above-barrier field ionization of fluorine atoms, it is necessary to take into account that, according to the Bethe rule (in atomic units), the field strength F of laser radiation is related to the ionization potential E_Z of the ion with the ionization degree Z as

$$F = E_Z^2/4Z. \qquad (4)$$

According to Eq. (4), the field ionization for a peak intensity of 2×10^{18} W/cm^2 ($F = 7.4$ au) can lead only to the appearance of fluorine ions with a charge of $+7$ that contain two electrons. Formation of the hydrogen-like fluorine ion containing one electron on the $1s$ shell requires an energy of 953 eV (for the separation of one of two electrons on the $1s$ shell). This process is possible only as a result of the collisional ionization of F^{7+} ions by hot electrons with energies above 1 keV. The number of such electrons is sufficiently large, because electrons undergoing the radial ponderomotive acceleration in the laser focus acquire relativistic kinetic energy up to the maximum value

$$E_e^{\max} = mc^2\left(\sqrt{1 + \frac{1}{2}\left(\frac{F}{\omega c}\right)^2} - 1\right). \qquad (5)$$

For the above parameters, this value is equal to 165 keV. Electrons with much lower energies are really responsible for collision ionization, because, according to the Lots theorem, the cross section for collisional ionization is inversely proportional to the kinetic energy of the incident electron. Moreover, the number of such electrons is much larger than the number of electrons with the maximum energy in view of fast time and spatial variation in the shape of the laser pulse.

The electric field created by radially scattered electrons due to the separation of charges entrains fluorine atomic ions. Their kinetic energy is larger than the energy of electrons by a factor of Z. Correspondingly, the maximum energy of ions with $Z = 8$ is estimated as 1.3 MeV. This value agrees with the experimental data shown in Fig. 3.

The energy spectrum of these ions can be compared with the following phenomenological formula for ion spectra that we derive using numerous recent experimental data [5, 6, 10, 17–19]:

$$dN(E) \propto \exp[-1.5E/ZI]dE. \qquad (6)$$

Here, the intensity is measured in the units of the atomic intensity $I_0 = 3 \times 10^{16}$ W cm^{-2} and ion energy E, in keV. According to this relation, the mean ion energy is equal to $ZI/1.5$ keV. For the above parameters, this expression yields 350 keV, which agrees with the
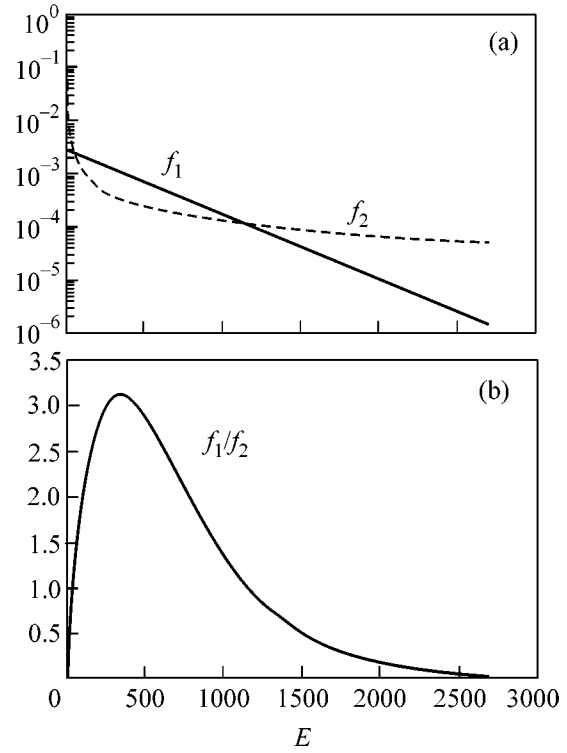
Fig. 4. (a) Normalized energy distributions of fast fluorine ions according to the theoretical estimates $f_1 = e^{-E/356}$ (6) and $f_2 = [10^{-3}E + 8]/E(10^{-3}E + 16)]$ (7) and (b) the ratio f_1/f_2.

experimental data discussed above and estimates of the contribution from fast ions by Eq. (2).

It is interesting to compare distribution (6) with the distribution obtained in [20], which has the following form for the fluorine ions with a charge of $+8$:

$$dN(E)/dE \sim [10^{-3}E + 8]/[E(10^{-3}E + 16)], \qquad (7)$$

where E is the ion energy in keV. In both cases, the maximum ion energies are estimated using Eq. (5), but the doubled value of this energy was used in [20]. Figure 4 shows both distributions (denoted as f_1 and f_2, respectively), which are normalized to unity, and their ratio. It is seen that these distributions differ from each other not too strongly.

5. CONCLUSIONS

The generation of fast ions in the picosecond laser plasma has been experimentally studied with laser radiation 2×10^{18} W/cm^2 in intensity. The comparison of the observed Doppler counters of spectral lines for various intensities of laser radiation indicates that, beginning with an intensity of 10^{18} W/cm^2, an intense tail corresponding to the generation of fast ions arises in the energy distribution of ions. Moreover, the directional motion of fast ions deeply into the target has been

detected by directly measuring the redshift of the Doppler profile of the Lyman line of the hydrogen-like fluorine ion. The energy of this motion (near 25 keV) agrees well with the data reported in [4] for intermediate energies of ions and the laser-radiation intensities under consideration. The theoretically estimated parameters of the energy distribution of ions are in reasonable agreement with the experimental data.

REFERENCES

1. S. Dobosz, M. Schmidt, M. Pedrix, *et al.*, JETP Lett. **68**, 454 (1998).

2. K. Krushelnik *et al.*, Phys. Rev. Lett. **83**, 737 (1999).

3. S. Dobosz, M. Schmidt, M. Pedrix, *et al.*, JETP **88**, 1122 (1999).

4. A. G. Zhidkov, A. Sasaki, T. Tajima, *et al.*, Phys. Rev. E **60**, 3273 (1999).

5. K. Krushelnick, E. L. Clark, M. Zepf, *et al.*, Phys. Plasmas **7**, 2055 (2000).

6. E. L. Clark, K. Krushelnick, M. Zepf, *et al.*, Phys. Rev. Lett. **85**, 1654 (2000).

7. A. G. Zhidkov, A. Sasaki, I. Fukumoto, *et al.*, Phys. Plasmas **8**, 3718 (2001).

8. T. Auguste, A. Ya. Faenov, I. Fukumoto, *et al.*, J. Quant. Spectrosc. Radiat. Transf. **71**, 147 (2001).

9. A. I. Magunov, A. Ya. Faenov, I. Yu. Skobelev, *et al.*, Laser Part. Beams **21**, 73 (2003).

10. H. Habara, R. Kodama, Y. Sentoku, *et al.*, Phys. Rev. E **69**, 036407 (2004).

11. V. S. Belyaev, V. I. Vinogradov, A. S. Kurilov, *et al.*, Zh. Éksp. Teor. Fiz. **125**, 1295 (2004) [JETP **98**, 1133 (2004)].

12. N. Izumi *et al.*, Phys. Rev. E **65**, 036413 (2002).

13. V. S. Belyaev, A. P. Matafonov, G. N. Ignat'ev, *et al.*, in *Proceedings of 31st EPS Conference on Plasma Physics* (ECA, London, 2004), Vol. 28G, p-2.039.

14. T. A. Pikuz, A. Ya. Faenov, S. A. Pikuz, *et al.*, J. X-Ray Sci. Technol. **5**, 323 (1995).

15. A. Ya. Faenov, S. A. Pikuz, A. I. Erko, *et al.*, Phys. Scr. **50**, 333 (1994).

16. H. R. Griem, *Spectral Line Broadening by Plasmas* (Academic, New York, 1974; Mir, Moscow, 1978).

17. S. C. Wilks, A. B. Langdon, W. E. Cowan, *et al.*, Phys. Plasmas **8**, 542 (2001).

18. I. Spencer, K. W. D. Ledingham, P. McKenna, *et al.*, Phys. Rev. E **67**, 046402 (2003).

19. S. Okihara, T. Zh. Esirkepov, K. Nagai, *et al.*, Phys. Rev. E **69**, 026401 (2004).

20. V. Yu. Bychenkov, V. T. Tikhonchuk, and S. V. Tolokonnikov, Zh. Éksp. Teor. Fiz. **115**, 2080 (1999) [JETP **88**, 1137 (1999)].

Translated by R. Tyapaev

New Branch of Intersubband Plasmons in a Nonequilibrium Two-Layer System

R. Z. Vitlina and A. V. Chaplik

Institute of Semiconductor Physics, Siberian Division, Russian Academy of Sciences, Novosibirsk, 630090 Russia
e-mail: chaplik@isp.nsc.ru
Received May 12, 2005

The plasma oscillation spectrum for 2D electrons in a double quantum well is calculated. It is shown that an additional branch of intersubband plasmons can exist without experiencing Landau damping in the case of nonequilibrium population of subbands. In an asymmetric structure, this branch is responsible for both the emergence of instabilities and the possibility of amplification of plasma waves. © *2005 Pleiades Publishing, Inc.*

PACS numbers: 73.20.Mf, 73.21.La

1. INTRODUCTION

Considerable advances in the technology of preparing multilayered structures (especially double quantum waves) in recent years have stimulated revived interest in collective oscillations of 2D multicomponent plasmas. The main theoretical results in this field were formulated at the beginning of the 1980s (see [1, 2]). The components of a 2D plasma are defined as groups of charge carriers differing in the quantum number of the third dimension, viz., the number of the transverse quantization level (subband number) or the number of the layer if tunneling between the layers is insignificant. It was proved that the plasma wave spectrum for multicomponent systems contains a number of branches including gapless plasmons (optical and acoustic branches), as well as finite-frequency plasmons for zero momentum. The latter are known as intersubband plasmons (ISP) since they correspond to electron transitions between different transverse quantization levels with simultaneous excitation of collective movements in the plasma. In this case, a depolarization shift plays a significant role. In this effect, the ISP frequency $\omega(0)$ for zero momentum differs from the frequency Ω of a single-particle vertical transition between corresponding subbands. In the simplest case of a two-component plasma, we have [2]

$$\omega^2(0) = \Omega^2 + \frac{e^2}{\varepsilon} L\Omega(N_1 - N_2) \qquad (1)$$

($\hbar = 1$ everywhere in the further analysis). Here, $N_{1,2}$ is the subband occupation numbers; ε is the background permittivity; and L is a constant with dimension of length, which is determined by the wave functions $\varphi_1(z)$ and $\varphi_2(z)$ of transverse motion at levels 1 and 2 (L is of the same order of magnitude as the quantum well width or the spacing between the layers). In equilibrium, the occupation numbers N_1 and N_2 are noticeably different;

in this case, only one ISP branch exists without experiencing attenuation in the collisionless approximation (i.e., without Landau damping). Surprisingly, many authors (unfortunately, including the authors of this publication) did not notice for more than 20 years that an additional undamped ISP branch appears in the case of deviation of subband occupation numbers from thermodynamic equilibrium; for $N_1 = N_2$, this branch begins right from zero momentum. The depolarization shift in this case vanishes (see Eq. (1)), and two branches in the limit $kL \longrightarrow 0$ satisfy the symmetric formulas

$$\omega_{\pm}(k) = \Omega \pm ku; \quad u = v_0 \frac{1+\gamma}{\sqrt{1+2\gamma}}, \qquad (2)$$

where k is the modulus of the 2D momentum, v_0 is the Fermi velocity in each subband, γ is equal to L/a^* in order of magnitude, a^* being the effective Bohr radius (the exact expression for γ will be given below). The lower sign in formula (2) corresponds to the new ISP branch.

This work is aimed at analysis of this branch and the ISP spectrum as a function of various parameters of the system but, primarily, occupation numbers N_1 and N_2. In addition, it will be shown that the nonequilibrium population of subbands in an asymmetric structure with mode coupling leads to instabilities of optical and acoustic plasma oscillations. The latter effect might be useful for generating terahertz radiation.

2. QUALITATIVE EXPLANATION OF THE NEW BRANCH ORIGIN

Plasma oscillations of the ISP type exist only when transition between different plasma components are possible. For example, in a two-layer system without tunneling between the layers, only the optical and acoustic branches exist, while the ISP is absent. Let us
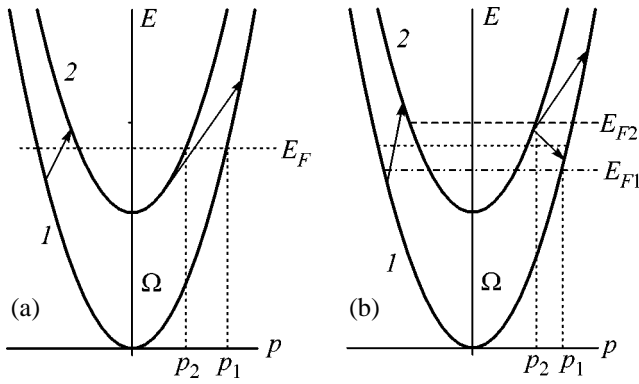
Fig. 1. (a) Thermodynamic equilibrium at $T = 0$; $p_{1,\,2}$ are the Fermi momenta of the subbands and E_F is the Fermi level. (b) Nonequilibrium population of subbands; the Fermi quasi-levels in the subbands are different.

now consider a quantum well with two populated subbands and with a standard energy–momentum relation $E = p^2/2m$. Figure 1a shows the populated states in the subbands at $T = 0$ in equilibrium. In this case, only upward transitions in energy shown by the arrows are possible. These transitions correspond to an ordinary intersubband plasmon. Figure 1b corresponds to overpopulation of the second subband and underpopulation of the first subband. It can be seen that each electron in the second subband with an energy lying between the Fermi quasi-levels E_{F1} and E_{F2} can now experience both upward and downward transitions on the energy scale. The maximal frequency of downward transitions is $\omega_{max} = \Omega + p_2^2/2m - p_1^2/2m$; the transferred momentum k is equal to $p_1 - p_2$ (we assume that the momentum distribution in each subband corresponds to $T = 0$ for a preset Fermi quasi-level). It is important to note that vertical (i.e., corresponding to $k = 0$) downward transitions are ruled out and the minimal admissible value of k is $p_1 - p_2$ (see the figure). If the occupation numbers of the subbands are equal ($p_1 = p_2$), we have $\omega_{max} = \Omega$, and the transferred momentum vanishes in accordance with Eq. (2). Figure 1b also shows that the frequency of such transitions decreases with increasing k (negative dispersion, the lower sign in Eq. (2)). We attribute these single-particle transitions to the new ISP branch; a quantitative theory of this effect will be constructed below.

3. ISP IN A SYMMETRIC STRUCTURE

To find the plasma wave spectrum, it is sufficient to employ the self-consistent field approximation. If we disregard retardation effects, this approximation is reduced to the Poisson equation for the induced potential $U(z, \mathbf{k})\exp\{i(\mathbf{k}\boldsymbol{\rho} - \omega t)\}$, where $\boldsymbol{\rho}$ and z are the coor-

dinates in the plane of the structure and along the normal to it, respectively:

$$\frac{d^2 U}{dz^2} - k^2 U = -\frac{4\pi e^2}{\varepsilon}\delta N(z, \mathbf{k}). \tag{3}$$

Here, the number density perturbation δN in the linear response theory can be expressed in terms of the polarization operator (see [2]),

$$\delta N = -\sum_{n,\,m} \Pi_{nm} U_{nm}(\mathbf{k})\varphi_n(z)\varphi_m(z), \tag{4a}$$

$$\Pi_{nm}(\mathbf{k}, \omega) = -\sum_q \frac{f_n(\mathbf{q}) - f_m(\mathbf{k} + \mathbf{q})}{W_n(\mathbf{q}) - W_m(\mathbf{k} + \mathbf{q}) + \omega + i\delta}, \tag{4b}$$

where $W_n(\mathbf{q}) = E_n + q^2/2m$, E_n are the bottoms of the subbands, and f_n are the Fermi occupation numbers. Expressing the formal solution to Eq. (3) in terms of its Green function $G(z, z_0) = \dfrac{1}{2k}\exp(-k|z - z_0|)$ and taking the matrix elements in transverse functions $\varphi_n(z)$, we arrive at the system of equations

$$U_{ij} + \frac{2\pi e^2}{\varepsilon k}\sum_{nm} I_{ij,\,nm}(k)\Pi_{nm}(k, \omega)U_{nm} = 0, \tag{5}$$
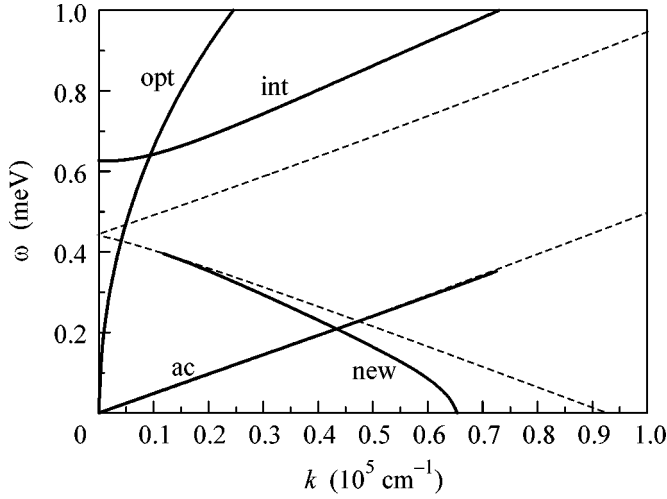
where

$$I_{ij,\,nm}(k)$$

$$= \int\limits_{-\infty}^{+\infty} \varphi_i(z)\varphi_j(z)\exp(-k|z - z_0|)\varphi_n(z_0)\varphi_m(z_0)\,dz\,dz_0. \tag{6}$$

In a structure symmetric about its middle plane, for the two lower subbands, we have $I_{11,\,12} = I_{22,\,21} = 0$ since $\varphi_1(z)$ and $\varphi_2(z)$ have different parities in z. Consequently, the characteristic equation of system (5) splits into the product of two factors. One of these factors contains Π_{11} and Π_{22} and leads to the energy–momentum relation for the optical and acoustic plasmons. The other factor is a function of Π_{12} and Π_{21} and corresponds to the ISP,

$$1 + \frac{2\pi e^2}{\varepsilon k}I(k)[\Pi_{12}(\omega, k) + \Pi_{21}(\omega, k)] = 0, \tag{7}$$

where $I(k) \equiv I_{12,\,12} = I_{12,\,21} = I_{21,\,12} = I_{21,\,21}$. Evaluating the integrals in Eq. (4b), we arrive at the final equation for the ISP,

$$1 + \frac{2e^2 m^2}{\varepsilon k^3}I(k)[(\omega_+ - \Omega)Q_2(\omega_+ - \Omega)$$

$$- (\omega_- - \Omega)Q_1(\omega_- - \Omega) + (\omega_+ + \Omega)Q_1(\omega_+ + \Omega)$$

$$- (\omega_- + \Omega)Q_2(\omega_- + \Omega)] = 0; \tag{8}$$

Fig. 2. Dispersion curves in a symmetric structure for the parameters $N = 6.4 \times 10^{10}$ cm^{-2}, $N_2/N_1 = 0.09$, $d = 2.5 \times 10^{-6}$ cm, and $mdV_0 = 0.7$. Coupling between oscillations is not observed.

Fig. 3. New intersubband plasmon branch for the parameters $N_2/N_1 = 0.81$, $d = 2.5 \times 10^{-6}$ cm, $mdV_0 = 0.7$, and $N = $ (1) 2×10^9, (2) 4×10^9, and (3) 6.4×10^{10} cm^{-2}.

$$Q_\alpha(\omega_\pm \pm \Omega) \equiv 1 - \sqrt{1 - k^2 v_\alpha^2/(\omega_\pm \pm \Omega)^2},$$

$$\omega_\pm = \omega \pm \frac{k^2}{2m},$$

where $\alpha = 1, 2$ and v_1 and v_2 are the Fermi velocities of subbands 1 and 2. The only analytically solvable limiting case that we managed to find for Eq. (8) corresponds to equal (or close) occupation numbers ($|v_1 - v_2|) \ll v_{1,2}$ and small values of k ($k \ll mv_{1,2}$). In the same limit, we can replace $I(k)/k$ by $L \equiv \lim_{k \to 0} I(k)/k$ since it follows from expression (6) that $I(k)$ tends to zero in accordance with a linear law for $k \longrightarrow 0$ in view of the orthogonality of $\varphi_1(z)$ and $\varphi_2(z)$. In this case, for positive frequencies ω, we can disregard the last two terms in the brackets of Eq. (8) and expand the radicals in the first two terms in $k^2/m(\omega - \Omega)$. For $v_1 = v_2 = v_0$, we obtain
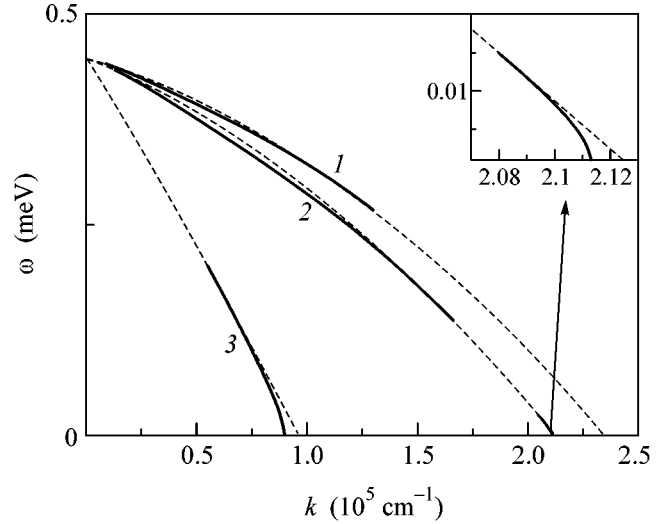
$$1 + \frac{2e^2 mL}{\varepsilon}\left(1 - \frac{|\omega - \Omega|}{\sqrt{(\omega - \Omega)^2 - k^2 v_0^2}}\right) = 0, \qquad (9)$$

which leads to the energy–momentum relation (2) with $\gamma = 2me^2L/\varepsilon$. For close but different occupation numbers, the expansion of Eq. (8) gives

$$|\omega - \Omega| + \text{sgn}(\omega - \Omega)m(v_1^2 - v_2^2)/2 \\ = (1 + 1/\gamma)\sqrt{(\omega - \Omega)^2 - k^2 v_0^2}. \qquad (10)$$

It follows from this relation that for $\omega > \Omega$, only one root exists for all values of k. It corresponds to the known ISP and determines the polarization shift for $k = 0$ in accordance with formula (1), in which $\omega^2(0) - \Omega^2$

may be replaced by $(\omega - \Omega)2\Omega$ in view of the closeness of N_1 and N_2. If, however, $\omega < \Omega$, no solution exists in the interval of k from zero to $k_c = (v_1^2 - v_2^2)m/2v_0$. The new branch exists for $k > k_c \approx m(v_1 - v_2)$ (this has already been concluded from qualitative considerations in Section 2).

In the case of arbitrary occupation numbers and not small values of the plasmon momentum, Eq. (8) was solved numerically. To calculate the form factor $I(k)$ explicitly, we must define functions φ_1 and φ_2. We used the exactly solvable model of a two-layer system, which was proposed by us earlier [3], where the potential of a double quantum well is defined as $V(z) = -V_1\delta(z - d/2) - V_2\delta(z + d/2)$. For a symmetric structure, we assume that $V_1 = V_2 = V_0$. Parameters V_0 and d were chosen so as to ensure the existence of two negative-energy levels in the system ($2mV_0d > 1$). Figure 2 illustrates a possible form of all four branches of the plasma spectrum in a symmetric structure. The dashed lines mark the boundaries of the continuum of single-particle excitations.

The details in the behavior of the new branch are determined to a considerable extent by the structure parameters. In equilibrium ($p_1^2 = p_2^2 + 2m\Omega$), only the ordinary branch of interband oscillations exists with $\omega \geq \Omega + \Delta_{\text{dep}}$, where Δ_{dep} is the depolarization shift. A new branch appears only for a noticeable deviation from equilibrium. For example, for the same parameters as in Fig. 2, N_2/N_1 must be greater than 0.68 (the equilibrium value of $N_2/N_1 = 0.63$). Various modes of behavior of the new branch are possible depending on the total concentration N (Fig. 3). Pay attention to
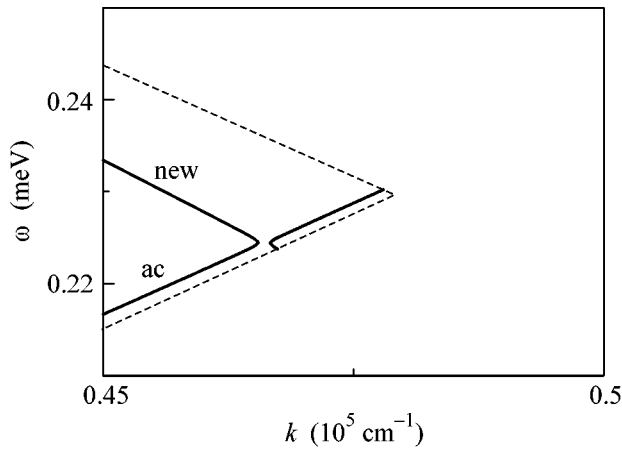
Fig. 4. Coupling between the new and acoustic branches for the parameters $N = 6.4 \times 10^{10}$ cm^{-2}. $N_2/N_1 = 0.9$, $d = 2.5 \times 10^{-6}$ cm, $mdV_1 = 0.703$, and $mdV_2 = 0.7$.

curve *2*, which demonstrates a possible discontinuity of the new ISP branch.

Finally, inverse population ($N_2 > N_1$) calculations show that the "int" and "new" branches in Fig. 2 change places: the frequency of a conventional ISP beginning from zero momentum now lies below Ω since the depolarization shift is negative for $N_2 > N_1$.

4. ASYMMETRIC STRUCTURE ($V_1 \neq V_2$)

In this situation, "skew" form factors $I_{11,\,12}$ and $I_{22,\,21}$ differ from zero, the interaction of branches becomes significant, and all crossings are replaced by anticrossings [3, 4]. The types of anticrossings of an ordinary ISP with the optical branch and of the new branch with the optical or acoustic branch are basically different. In accordance with the adopted classification of instabilities [5], the interaction of an ordinary ISP with an optical plasmon corresponds to case A: functions $\omega(k)$ and $k(\omega)$ are real-valued for all arguments. However, the interaction of the new branch with optical and acoustic plasmons leads to a bandgap in the spectrum along the k axis (i.e., to a complex frequency). Analysis of the signs of the coupling coefficients and the slopes of

branches at the crossing point shows that we have case D (absolute instability). Naturally, this is associated with the initially assumed nonequilibrium nature of the system. Figure 4 illustrates these arguments for the interaction between the new and acoustic branches as an example. Note that the degree of asymmetry in this case is rather small ($V_1/V_2 \approx 1.004$). For strong asymmetry, the right-hand side of the graph is expelled to the continuum region and only convergence of the new and acoustic branches is left. Analogous graphs can also be plotted for coupling between the new and optical branches. In the case of population inversion, instability emerges for coupling between the "opt" and "int" branches (ordinary ISP); i.e., the instability region always correspond to $\omega < \Omega$.

Thus, we have proved that an additional branch of plasma oscillations characterizes a nonequilibrium two-layer system. If, in addition, the structure is asymmetric, amplification plasma waves of both optical and acoustic types are possible.

REFERENCES

1. S. Das Sarma and A. Madhukar, Surf. Sci. **98**, 1 (1980).
2. R. Z. Vitlina and A. V. Chaplik, Zh. Éksp. Teor. Fiz. **81**, 1011 (1981) [Sov. Phys. JETP **54**, 536 (1981)].
3. A. V. Chaplik and R. Z. Vitlina, Superlattices Microstruct. **33**, 263 (2003).
4. C.-M. Hu, C. Schuller, and P. Heitmann, Phys. Rev. B **64**, 073303 (2001).
5. E. M. Lifshitz and L. P. Pitaevskiĭ, *Physical Kinetics* (Nauka, Moscow, 1979; Pergamon, Oxford, 1981), Sect. 64.

Translated by N. Wadhwa

Temperature Dependence of Aharonov–Bohm Oscillations in Small Quasi-Ballistic Interferometers

E. B. Olshanetsky[1],*, Z. D. Kvon[1], D. V. Sheglov[1], A. V. Latyshev[1],
A. I. Toropov[1], and J. C. Portal[2]

[1] *Institute of Semiconductor Physics, Siberian Division, Russian Academy of Sciences, Novosibirsk, 630090 Russia*
* e-mail: eolsh@thermo.isp.nsc.ru
[2] *GHML, MPI-FKF/CNRS, F-38042, Grenoble, France*
Received May 16, 2005

The temperature dependence of the Aharonov–Bohm oscillations of small quasi-ballistic ring interferometers (effective radius $R = 90$–110 nm) is studied in a wide temperature range of $(0.34$–$9)$ K. It is found that this dependence is determined not only by the size of the interferometer, but also by its microscopic state. It is shown that the effect may be associated with the influence of the fluctuation potential leading to different, but not completely stochastic, realizations of the scattering potential in conducting channels of the ring. © 2005 Pleiades Publishing, Inc.

PACS numbers: 73.23.–b, 73.63.–b

Theoretical and experimental studies of ring solid interferometers have been invariably attracting the attention of researchers over more than two decades [1–11]. This persistent interest in a ring prepared on the basis of a solid structure is due to the following reasons. First, the study of ring quantum interferometers provides a unique opportunity to observe fine and unexpected manifestations of the Aharonov–Bohm effect in mesoscopic systems. Second, advances in nanotechnology in the last decades have made it possible to produce ring interferometers of decreasingly small size, which raises hopes for realization of a Mach–Zehnder electron interferometer operating even at nitrogen temperatures. The development of lithography based on local anode oxidation of the surface of heterostructures with high-mobility electron gas by the probe of an atomic force microscope has made possible a qualitative advancement in this direction. Samples with a characteristic radius of approximately 100 nm can be prepared now without any difficulty [12]. This stimulates large-scale studies of small ring interferometers.

In this paper, we report on the results of analysis of the temperature dependence of the Aharonov–Bohm (AB) oscillations in small quasi-ballistic ring interferometers with an effective radius of $R = 90$–110 nm. These results show unambiguously that the temperature behavior of the same small ring depends to a considerable extent on the state of the ring realized for various cooling cycles. It is shown that such a behavior is due to the effect of the fluctuation potential, whose specific and different realization each time changes the energy spectrum of electrons and, accordingly, the temperature dependence of the AB oscillations in a quasi-ballistic interferometer.
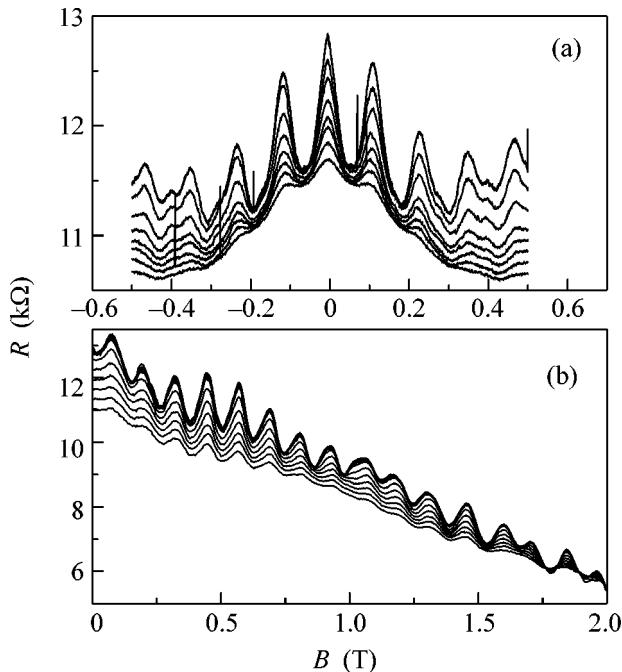
The ring interferometers with an effective radius of $R = 90$–110 nm studied here were prepared on the basis of an AlGaAs/GaAs heterostructure with a small (25 nm) distance between the plane of deposition of a 2D electron gas and the surface. The electron mobility in the initial heterostructure was $\mu = 10^5$ cm^2/V s for the 2D gas density $N_s = 5 \times 10^{11}$ cm^{-2}, which corresponded to an electron mean free path $l = 1.2$ μm. The ring interferometer was created by simultaneous local anode oxidation and mechanical action on the surface (TINE&MeMo technology [13]) by the probe of an atomic force microscope (Solver P-47H, NT-MDT) as described in [12]. Figure 1 shows the image of a ring formed with the help of this microscope. Magnetotransport measurements of rings were carried out according to the standard scheme using a phase-sensitive detector operating on small currents to avoid heating of the carriers. Measurements were made in magnetic fields up to 2 T and in the temperature range 0.34–15 K.

We measured the temperature dependence of the magnetoresistance for different states of the ring, which were obtained as a result of different cycles of sample cooling from room temperature to liquid helium temperature. Special attention was paid to obtain stable states and magnetoresistance curves reproducible in repeated measurements to a high degree of accuracy. The results of such measurements for two different states of the sample are shown in Fig. 2. It should be noted that, owing to the smallness of the interferometers in question, the AB oscillations were observed in a number of studied structures up to temperatures of 15 K, and saturation of the growth of their amplitude begins even at a temperature above 1 K, which is an order of magnitude higher than the saturation tempera-
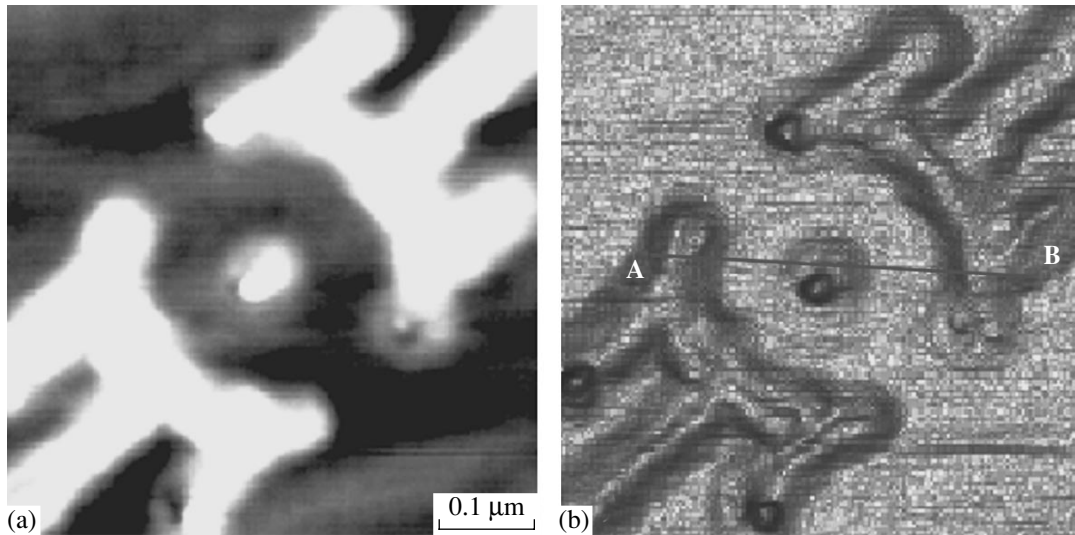
Fig. 1. Topographic (a) and phase (b) atomic force microscope images of a ring interferometer. The frame size of the images is 550×550 nm.

ture of the interferometers studied earlier. Large amplitudes of oscillations attaining 20% in the vicinity of the zero magnetic field is also worth noting. The magnetic-field dependences in Fig. 2 were processed using the rapid Fourier transformation technique. For each curve, a Fourier spectrum was obtained with a clearly mani-

fested main peak whose position corresponds to the effective mean radius of the ring (100 nm). Figures 3a and 3b show that the period of AB oscillations and, accordingly, the effective radius of the ring remain unchanged. Thus, the main parameter of the interferometer remains unchanged for different heating and cooling modes. The intensity of the AB oscillations at each temperature was estimated as the relative height of the peak in the Fourier spectrum corresponding to a given temperature. Figure 3c shows the temperature dependence of the amplitude of the AB oscillations, which were obtained in this way for the states of the sample depicted in Fig. 2. It can be seen that, in spite of the fact that the mean radius of the rings remains unchanged, the difference in the microscopic states of the ring emerging as a result of the sample heating/cooling is sufficient to noticeably change the temperature dependence of the AB oscillations. In the physics of mesoscopic systems, the microscopic state of the sample is determined by a set of parameters that depend on a specific realization of the random potential in the sample. In our case, such parameters include the variation of the electrostatic potential along the ring and, hence, the electron energy spectrum in the ring, as well as the transmittance, reflectance, effective width of the ring, and even insignificant variations of its shape [11].

Let us now find out how the microscopic state of the ring may affect the temperature dependence of AB oscillations. It was established earlier [7–10] that two independent processes determine this dependence: (i) averaging over the temperature and (ii) suppression of interference of electron waves over lengths exceeding the phase coherence length. The first process is the averaging of the transmittance $T(E, B)$ of the ring over an energy interval on the order of kT in the vicinity of

Fig. 2. Aharonov–Bohm oscillations corresponding to two different states of the same ring, obtained as a result of different cooling modes. The curves in the figure correspond to the following temperatures (from top to bottom): (a) 1.4, 2.0, 3.25, 4.2, 4.9, 5.7, 7.0, and 9.0 K and (b) 0.34, 0.4, 0.5, 0.7, 0.83, 1.1, 1.5, 2.0, 2.5, 3.0, 3.5, and 4.1 K.

the Fermi level. This averaging is described by the expression

$$G(E_F, B, T) = \frac{2e^2}{h}\int\left(-\frac{df(E, E_F, T)}{dE}\right)T(E, B)dE, \quad (1)$$

where $G(E_F, B, T)$ is the conductance of the ring and $f(E, E_F, T)$ is the Fermi–Dirac function.

The second process is associated with violation of coherence of electron waves due to inelastic collisions. As a result of the violation of coherence of electron waves on scales larger than the phase coherence length L_ϕ, the amplitude of AB oscillations must obey the law

$$\text{Amp}_{AB} \propto \exp\left(-\frac{\pi R}{L_\phi}\right), \quad (2)$$

where R is the ring radius. The exact temperature dependence of L_ϕ is determined by the type of electron transport in the ring and by the type of elastic scattering leading to coherence violation in the given system. A monotonic decrease in length L_ϕ with increasing temperature and, as a consequence, a decrease in the amplitude of AB oscillations is observed in all cases. Since such parameters as the mean radius, the type of electron transport, and the nature of inelastic scattering are independent of the specific microscopic state of the ring, these parameters should not affect the temperature dependence of AB oscillations, which is associated with suppression of coherence in the ring and is described by formula (2).

Let us consider in more detail the first mechanism, viz., temperature averaging. It can be seen from formula (1) that the quantity being averaged is the transmission coefficient $T(E, B)$, whose properties strongly depend on the nature of the electron transport in the ring. Experiment [8] and theory [7] show that temperature averaging of AB oscillations in the case of diffusion does not differ from temperature averaging of conventional mesoscopic fluctuations of conductance, is independent of the specific realization of the scattering potential in the image, and has a universal form $\text{Amp}_{AB} \propto (E_c/kT)^{1/2}$, where $E_c = hD/L^2$ is the correlation energy coinciding in order of magnitude with the mean distance between the energy levels in the system, D is the diffusion coefficient, and L is the size of the system. The above-mentioned universality of the temperature dependence is due to the fact that transmittance $T(E, B)$ in the diffusion-controlled sample is a stochastic function of the magnetic field and energy [7]. Upon a change in energy, the fluctuation pattern of function $T(B)_{E = \text{const}}$ varies smoothly till the correlation with the initial dependence for $\Delta E > E_c$ vanishes completely. Thus, for $kT > E_c$, the decrease in the amplitude of the fluctuations due to temperature averaging occurs as a result of a combination of uncorrelated fluctuation dependences. The change in the microscopic state of the sample in this case only changes the fluctuation pattern $T(B)_{E = \text{const}}$, while the statistical properties of the
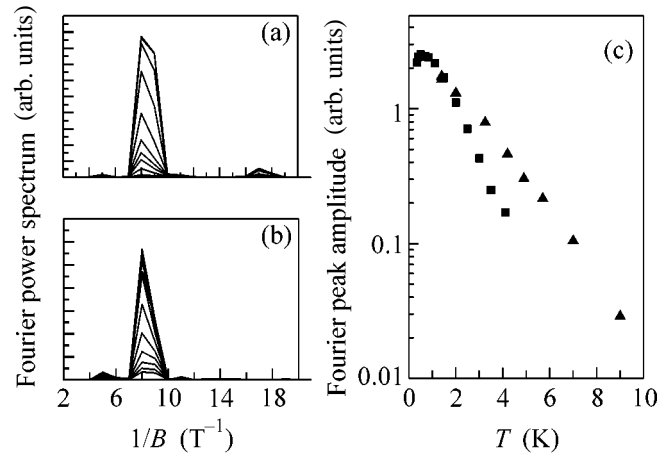
Fig. 3. (a, b) Fourier spectra of the dependences shown in Figs. 2a and 2b, respectively, and (c) temperature dependence of the amplitude of Aharonov–Bohm oscillations shown in (triangles) Fig. 2a and (squares) Fig. 2b.

function $T(E, B)$ described above remain unchanged; this imparts a universal nature to the temperature averaging in the case of diffusion.

Conversely, in an ideal ballistic ring, $T(E, B)$ is a regular periodic function of energy and magnetic field [1]. The period of function $T(E, B)$ in energy in the ideal model considered here is determined by the ring diameter. In accordance with expression (1), periodic dependences $T(B)$ with opposite phases are composed beginning from the instant when the temperature kT becomes larger than this period; this ultimately leads to a decrease in the amplitude of the conductance oscillations to zero in accordance with an exponential law.

In real interferometers prepared on the basis of a 2D electron gas with a high mobility, the role of the fluctuation impurity potential cannot be excluded completely and all such interferometers are quasi-ballistic. A specific realization of the fluctuation potential for different sample cooling cycles in these interferometers leads to different forms of $T(E, B)$, which do not differ from the form of $T(E, B)$ of an ideal ring, but are not completely stochastic as in diffusion-controlled rings. Consequently, such a fluctuation potential "individualizes" function $T(E, B)$, which leads to the experimentally observed nonuniversal temperature dependence of the amplitude of AB oscillations in a quasi-ballistic interferometer. This conclusion was not drawn earlier because analysis of the temperature dependence of AB oscillations in previous works was based on the diffusion approach [8] or on the model of an ideal ballistic ring [9, 10]; according to our results, this is not sufficient for real quasi-ballistic interferometers.

REFERENCES

1. M. Buttiker, Y. Imry, and R. Landauer, Phys. Lett. A **96**, 365 (1983).

2. G. Timp, A. M. Chang, J. E. Cunningham, *et al.*, Phys. Rev. Lett. **58**, 2814 (1987).

3. C. J. B. Ford, A. B. Fowler, J. M. Hong, *et al.*, Surf. Sci. **229**, 307 (1990).

4. A. A. Bykov, Z. D. Kvon, E. B. Olshanetsky, *et al.*, JETP Lett. **57**, 613 (1993).

5. J. Liu, W. X. Gao, K. Ismail, *et al.*, Phys. Rev. B **48**, 15148 (1993).

6. A. Yacoby, R. Schuster, and M. Heiblum, Phys. Rev. B **53**, 9583 (1996).

7. P. A. Lee, A. D. Stone, and H. Fukuyama, Phys. Rev. B **35**, 1039 (1987).

8. S. Washburn, C. P. Umbach, R. B. Laibowitz, *et al.*, Phys. Rev. B **32**, 4789 (1985).

9. M. Casse, Z. D. Kvon, G. M. Gusev, *et al.*, Phys. Rev. B **62**, 2624 (2000).

10. A. E. Hansen, A. Kristensen, S. Pedersen, *et al.*, Phys. Rev. B **64**, 045327 (2001).

11. O. A. Tkachenko, V. A. Tkachenko, D. G. Baksheev, *et al.*, Pis'ma Zh. Éksp. Teor. Fiz. **71**, 366 (2000) [JETP Lett. **71**, 255 (2000)].

12. V. A. Tkachenko, Z. D. Kvon, D. V. Sheglov, *et al.*, JETP Lett. **79**, 136 (2004).

13. D. V. Sheglov, A. V. Latyshev, and A. L. Aseev, Appl. Surf. Sci. **243**, 138 (2005).

Translated by N. Wadhwa

Critical Phenomena in the β-(2 × 4) ⟶ α-(2 × 4) Reconstruction Transition on the (001) GaAs Surface

Yu. G. Galitsyn, D. V. Dmitriev, V. G. Mansurov, S. P. Moshchenko*, and A. I. Toropov

Institute of Semiconductor Physics, Siberian Division, Russian Academy of Sciences, Novosibirsk, 630090 Russia
* e-mail: sergem@isp.nsc.ru
Received May 24, 2005

The critical exponents of the β-(2 × 4) ⟶ α-(2 × 4) reconstruction phase transition on the (001) GaAs surface are determined experimentally. It is found that the phase transition is analogous to a van der Waals transition. The critical parameters T_c, P_c, and Θ_c have been measured experimentally. The mean field theory is applied, and three-parameter isotherms are obtained that agree with the experimental results at the following values of the parameters: $E_{st} = 0.36$ eV, $\Delta E = 0.18$ eV, and $E_i = 0.134$ eV. Precision measurements of the critical exponents β and δ are carried out. Their values β = 1/8 and δ = 15 indicate that the phase transition is truly two-dimensional. © 2005 Pleiades Publishing, Inc.

PACS numbers: 64.60.–i, 68.35.Bs

Extensive literature is devoted to reconstruction phase transitions (PTs) on the (001)GaAs surface. This is not surprising, because this surface is a model for studying reconstructions and transitions between them for III–V semiconductors. In addition, arsenic-stabilized α(2 × 4) and β(2 × 4) surface reconstructions on (001)GaAs are widely used in the creation of various semiconductor structures by molecular beam epitaxy (MBE). At present, the composition of these surface phases is determined. Thus, the surface composition of the high-temperature disordered α(2 × 4) modification is 0.5 gallium atoms and 0.5 arsenic atoms, whereas that for the low-temperature β(2 × 4) modification is 0.25 gallium atoms and 0.75 arsenic atoms; that is, in the first case, four of eight surface atoms in the unit cell are arsenic atoms (in the form of two arsenic dimers), whereas there are six arsenic atoms (three dimers) on the surface in the second case. In this case, the α ⟶ β transition is formally associated with the adsorption of two arsenic atoms per unit cell of the α(2 × 4) phase in a flow of arsenic tetramers.

So far, there has been no consistent theory of reconstruction PTs on the GaAs surface in spite of available experimental data and significant advances in understanding the mechanism of particular reconstructions. However, the following main problems have still remained unsolved. The first problem concerns the type of the transition between the As-stabilized (2 × 4) reconstruction and the Ga-stabilized (4 × 2) reconstruction on GaAs(001). That is, the question is whether this transition is of the first or the second order. The next problem concerns the dimensionality of the transition; that is, whether the transition on the surface is true two-dimensional. Finally, this is the problem concerning the microscopic mechanisms and the driving force of the

transition. Thus, the authors of the review [1] argue that the (2 × 4) ⟶ (4 × 2) PT on (001)GaAs is a continuous second-order PT. At the same time, the authors of [2, 3] detected the coexistence of these phase by scanning tunneling microscopy (STM), which gave grounds to state that the PT is of the first order. Another controversial point is the suggestion that the lateral interaction between adsorbed arsenic atoms is of attractive character [1], whereas it is well known that lateral attraction exists between adsorbed atoms of the same type on the surface [4, 5].

In our papers [6, 7], we developed an approach to the consideration of PTs on (001) GaAs and InAs as phase transitions induced by arsenic adsorption on the (001) surface. Within this approach, we considered reconstruction transitions from the As-stabilized (2 × 4) surface to the Ga-stabilized (4 × 2) surface, as was assumed in most works. However, this transition in reality is more complicated and proceeds through a number of intermediate reconstructions. The analysis of such a transition requires a successive consideration of each elementary phase transition separately. This work is devoted to studying such a phase transition between the neighboring β(2 × 4) and α(2 × 4) reconstructions. Using reflection high-energy electron diffraction (RHEED), we performed precision measurements of the intensity of the fractional (0 2/4) reflection and its behavior in the β(2 × 4) and α(2 × 4) reconstruction phase transition in a wide range of surface temperatures and arsenic tetramer pressures in the MBE chamber. The point is that the intensity of the fractional (0 2/4) reflection in the ordered phase β(2 × 4) is comparable with the intensity I of the mirror reflection, but the reflection is completely quenched in the disordered high-temperature α(2 × 4) phase (see Fig. 1). Hence, it
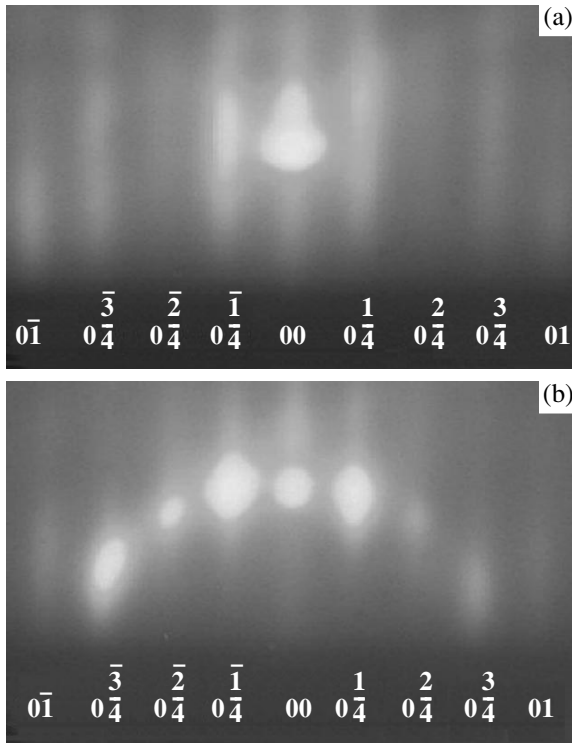
Fig. 1. Reflection high-energy electron diffraction pattern for (a) $\alpha(2 \times 4)$ and (b) $\beta(2 \times 4)$ phases. The designation of reflections are given below each photograph. The higher brightness corresponds to a higher intensity. It is evident that the (0 2/4) reflection and the (0 $\bar{2}$/4) reflection symmetrical to it in the $\beta(2 \times 4)$ phase have an intensity comparable with the (0 0) mirror reflection and are quenched in the $\alpha(2 \times 4)$ phase.
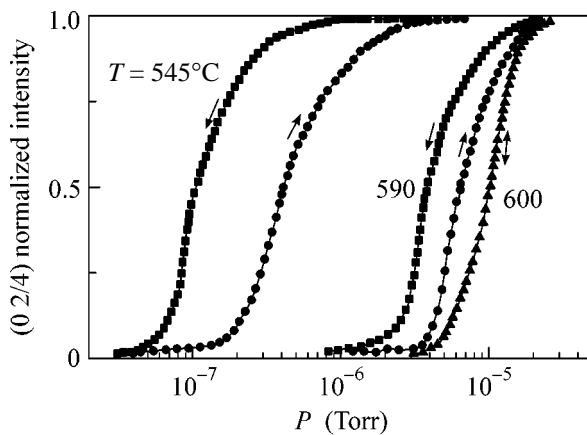
Fig. 2. Fractional (0 2/4) reflection intensity vs. the arsenic pressure at various temperatures. Arrows indicate the direct and reverse courses.

follows that the normalized intensity of the (0 2/4) reflection can be used for an experimental determination of the order parameter η ($\eta^2 = I/I_0$) in the indicated order–disorder reconstruction phase transition, and its

behavior upon varying the temperature and the As_4 pressure will assist in elucidating the nature of the PT.

All the experiments were carried out in the chamber of an MBE setup (Riber) equipped with a reflection high-energy electron diffractometer with a primary electron beam energy of 12 keV. The size of the gallium arsenide sample with the orientation (001) $\pm 0.5°$ was 3×3 mm^2. This provided sufficient uniformity of the surface both in temperature and in morphological perfection. All the measurements were performed after the growth of GaAs buffer layers 50 nm thick on the substrate. The results did not depend on the incident angle of the primary electron beam in the region of $1°$–$2°$. The evolution of the diffraction pattern was recorded by a digital video camera followed by computer processing of the reflection intensities.

The behavior of the fractional (0 2/4) reflection intensity in the $[\bar{1}10]$ azimuth is shown in Fig. 2 as a function of the arsenic tetramer pressure in the MBE chamber at various substrate temperatures. The (0 2/4) reflection intensity increases with increasing arsenic pressure and is saturated at a certain pressure depending on the sample temperature. Because the adsorption of arsenic on the surface increases with increasing pressure, arsenic dimers are accumulated and a transition occurs from the disordered $\alpha(2 \times 4)$ phase with two dimers per (2×4) unit cell to the ordered $\beta(2 \times 4)$ phase with three arsenic dimers. The direct and reverse courses of the intensity variation do not coincide for sample temperatures below 595°C; that is, an hysteresis typical for a first-order phase transition occurs. At the same time, no hysteresis is observed for temperatures above 595°C. Hence, we deal with a first-order PT at temperatures below 595°C and the $\beta(2 \times 4) \longrightarrow \alpha(2 \times 4)$ transition is a continuous second-order phase transition at temperatures above 595°C. The occurrence of both orders of PTs points to an analogy with a liquid–gas transition of the van der Waals type. From experimental data, we determined the critical temperature of the PT $T_c = 595 \pm 5°C$, the critical pressure of arsenic $P_c = 7 \times 10^{-6}$ Torr, and the critical surface coverage by arsenic $\Theta_i = 0.25$.

The van der Waals equation of state specifies a relation among the temperature, the pressure, and the density of the gas and liquid phases. In our case, the equation of state of the surface represents a relation among the As_4 pressure, the temperature, and the surface coverage by arsenic. The long-range order parameter for a classical van der Waals system is the difference between the densities of the liquid and gas phases. In our case, if we continue the analogy with the van der Waals equation, the long-range parameter (η) is related with the difference Θ of the number of surface dimers in the $\beta(2 \times 4)$ and $\alpha(2 \times 4)$ phases by the equation $\Theta = (1 - \eta)/2$ [5]. Measuring the behavior of the fractional (0 2/4) reflection intensity in diffraction at the $\beta(2 \times 4) \longrightarrow \alpha(2 \times 4)$ PT, we actually measure the

α(2 × 4) surface coverage by arsenic atoms as a function of the arsenic pressure in the growth chamber at a certain temperature.

Mean field theories are very useful for the analysis of microscopic mechanisms of PTs in particular systems and specific features of the given problem. In our case, to explain the experimental results, namely, the formation of the dense ordered β(2 × 4) phase upon arsenic adsorption on the α(2 × 4) phase, it is required to assume the existence of lateral attraction between the adsorbed arsenic dimers. In this case, the Langmuir isotherm (lateral interaction between adsorbate particles is absent) $P/P_0 = \Theta/(1 - \Theta)$, where P is the arsenic pressure and Θ is the surface coverage of the α(2 × 4) phase by arsenic, should be replaced by the Fowler–Guggenheim (FG) isotherm $P/P_0 = \Theta/(1 - \Theta)\exp(-4\Theta E_i/kT)$, where E_i is the lateral attraction energy between arsenic atoms. The FG isotherm describes both first- and second-order PTs. In our case, we will have a coincidence with the experiment at $E_i = 0.075$ eV, that is, $T_c = 595°C$. Such a one-parameter isotherm was already used in [1] in studying the (2 × 4) ⟶ (4 × 2) PT on (001)GaAs, where the authors obtained $E_i = 0.11$ eV, because this transition occurred at a higher temperature. However, such one-parameter approximations are possibly suitable for, say, PTs on the surface of single-component semiconductors, such as silicon, germanium, or a metal. In the case of two-component semiconductors such as gallium arsenide, arsenic and gallium sublattices are involved in the reconstruction transition. Moreover, as we mentioned already, the arsenic dimers adsorbed on the surface will repel each other. At least three physical parameters are required in the description of the PT on the (001) gallium arsenide surface. In our opinion, a three-parameter isotherm in the framework of the adsorbate-induced PT theory will represent the equation of state of the surface most correctly [4, 6, 7]

$$\frac{P}{P_0} = \frac{\Theta}{(1 - \Theta)}\exp\left(\frac{E_i\Theta}{kT} - \frac{E_{st}/kT}{1 + \exp\left[\frac{(\Delta E - E_{st}\Theta)}{kT}\right]}\right). \quad (1)$$

This equation also describes both first-order phase transitions and continuous phase transitions at temperatures above the critical temperature. Because, in our case, $T_c = 595°C$, the following values can be chosen for the parameters: $E_{st} = 0.36$ eV, $\Delta E = 0.18$ eV, and $E_i = 0.134$ eV. The stabilization energy E_{st} of the β(2 × 4) phase corresponds to the adsorption of one arsenic dimer per (2 × 4) unit cell of the α(2 × 4) phase. This value can be identified with the difference between the surface energies of the α(2 × 4) and β(2 × 4) phases. These values normalized to the (1 × 1) cell are presented in [8, 9]. Therefore, we obtain $E_{st} = 0.045 \times 8 = 0.360$ eV. The value of ΔE is the energy required for the transition of gallium atoms from the positions that they
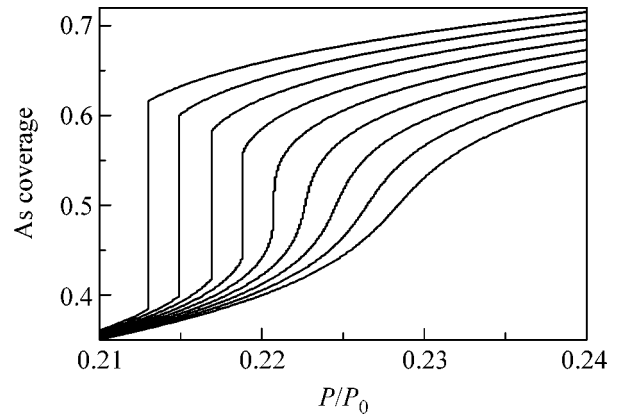
Fig. 3. Three-parameter isotherms calculated near the critical point for various temperatures (848–888 K) with the parameters $E_i = 0.134$ eV, $E_{st} = 0.36$ eV, $\Delta E = 0.18$ eV, and $T_c = 868$ K.

occupied in the α(2 × 4) phase to the positions of the β(2 × 4) phase. This value is more difficult to estimate, but it may be conventionally assumed that $\Delta E \approx 0.5E_{st}$ [4]. The repulsion energy E_i was varied so that the critical transition temperature coincided with the temperature measured experimentally. For $E_i = 0.134$ eV, $T_c = 868$ K, which coincides with the experimental value. The calculated three-parameter isotherms are shown in Fig. 3 in the vicinity of the critical region. In this region, Eq. (1) is simplified and we obtain

$$\Delta P = 3/2\Delta T + 5\Delta T\Delta\Theta + 15/4\Delta\Theta^3, \quad (2)$$

where $\Delta T = (T - T_c)/T_c$, $\Delta\Theta = (\Theta - \Theta_c)/\Theta_c$, and $\Delta P = (P - P_c)/P_c$. The expansion in Eq (2) satisfies the most general stability conditions for the α(2 × 4) and β(2 × 4) surface phases near the critical region. For the critical exponents in the critical isotherm, when $\Delta T = 0$, we obtain from Eq. (2) that $\Delta\theta = 4/15\Delta P^{1/3}$; that is, $\delta = 3$, and, under the condition $\Delta P = 3/2\Delta T$, that is, in the absence of an ordering external field, we obtain that $\Delta\theta = 4/3\Delta T^{1/2}$, that is, $\beta = 1/2$. As it must be for the mean field theory, the values of these exponents coincide with the exponents of the Landau PT theory.

Note that the E_{st}, ΔE, and E_i parameters can be replaced by one parameter E_{eff}, the effective attraction between arsenic dimers, which turned out to be equal to $E_{eff} = 0.075$ eV in our case. However, this parameter does not reflect the actual lateral interaction in the adsorbate, because chemisorbed particles of the same type repel each other [4, 5].

Note once again that the critical temperature of the phase transition T_c depends on the lateral interaction (in the case under consideration, on the E_{st}, ΔE, and E_i parameters, or on E_{eff}), but it is very important to emphasize that T_c does not depend on the binding energy of the adsorbate (arsenic atoms, in our case) with the surface. The characteristic energy of the lateral
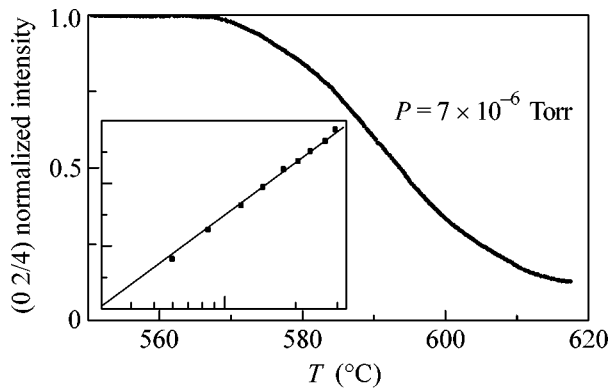
Fig. 4. Temperature dependence of the fractional (0 2/4) reflection intensity in the critical isobar. The dependence in the logarithmic scale is shown in the inset by points, through which a solid straight line corresponding to $\beta = 1/8$ is drawn.
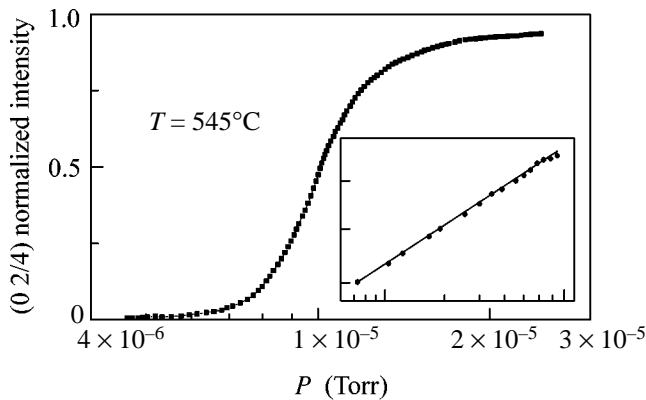
Fig. 5. Pressure dependence of the fractional (0 2/4) reflection intensity in the critical isotherm. The dependence in the logarithmic scale is shown in the inset by points through which a solid straight line corresponding to $\delta = 15$ is drawn.

interaction (E_{lat}) does not conventionally exceed 50–100 meV, which corresponds to PT temperatures of 400–600°C ($E_{\text{lat}} \sim kT_c$). However, the adsorption energy is, as a rule, higher than the lateral interaction energy. In our case, the arsenic binding energy with the surface is ~3 eV, which is almost two orders of magnitude higher than the scale of the lateral interactions! It was found in [10] that cesium adsorption on the (001) GaAs surface results in a decrease in the temperature of the $(2 \times 4) \longrightarrow (4 \times 2)$ PT by ~100°C. The authors of [10] related this decrease to the decrease in the binding energy of arsenic atoms with the surface (the strength of arsenic back bonds), that is, with the so-called vertical interaction, and completely disregarded the lateral interaction. This assumption is, in essence, based on the Langmuir model of adsorption. However, the notion of the transition temperature between various surface phases is absent in the Langmuir model because of the absence of the existence of different surface phases

such as in the framework of this model. Only the inclusion of the lateral interaction assigns a physical meaning to the PT temperature.

Let us briefly discuss the physical meaning of the P_0 parameter in Eq. (1). If the experiment was performed under equilibrium conditions of the gallium arsenide surface with the monatomic arsenic gas, then $P = P_0' \exp(-E_b/kT)$, where $P_0' = (2\pi mkT/h^2)^{3/2}kT$, and E_b would correspond to the true adsorption energy of monatomic arsenic. However, experiments are, as a rule, performed in a molecular beam of arsenic As$_4$ at pressures that are several orders of magnitude higher than the equilibrium pressure over the GaAs surface. Therefore, a steady-state adsorption–reaction equilibrium is attained on the surface under given conditions and the parameter P_0 has the meaning of an effective pressure. This was considered in more detail in our work [7]. For the region of relatively low temperatures (540–580°C), the following values were obtained from an Arrhenius approximation of the experimental data: $P_0' = 2 \times 10^{11}$ Torr and the effective binding energy of arsenic with the surface $E \approx 2.75$ eV.

According to current concepts, the order parameter exhibits a power dependence on the temperature and pressure in the vicinity of the critical region $\eta = \Delta T^\beta$ and $\eta = \Delta P^{1/\delta}$, where $\Delta T = (T - T_c)/T_c$ and $\Delta P = (P - P_c)/P_c$. The numerical values of the critical exponents β and δ depend on the dimensionality of the space in which the PT occurs. For a 3D transition, $\beta = 1/3$ and $\delta = 5$, whereas $\beta = 1/8$ and $\delta = 15$ for a true two-dimensional transition. The critical exponents of the PT do not coincide with the Landau exponents, because the significant contribution from the fluctuations of the order parameter in the vicinity of the critical point is neglected in the mean field theory. The behavior of adsorption phases on the surface of metals often exhibits two-dimensional features, see [5]. It is not evident a priori whether the reconstruction transitions on the (001) GaAs surface will have a two-dimensional character. The As-stabilized $\beta(2 \times 4)$ reconstruction on (001) GaAs spans three surface planes and is not equivalent at all to simple adsorption phases on the surface of metals. In the case of the $\beta(2 \times 4) \longrightarrow \alpha(2 \times 4)$ PT, three surface planes are involved in the rearrangement; therefore, the situation is not quite similar to the PT in an adsorption monolayer on the surface of metals.

We carried out precision measurements of the temperature and pressure dependences of the fractional (0 2/4) reflection in the vicinity of the critical point with the aim of determining the numerical values of the critical exponents. The temperature dependence of the (0 2/4) reflection intensity in the critical isobar ($P_c = 7 \times 10^{-7}$ Torr) is presented in Fig. 4. The dependence $I/I_0 = ((T_c - T)/T_c)^{2\beta}$ is presented on a double logarithmic scale in the inset, and the critical exponent $\beta = 1/7$–$1/8$ is determined from the line slope. The pressure depen-

dence of the intensity in the critical isotherm is shown in Fig. 5. Similarly, this dependence is presented on a double logarithmic scale in the inset and gives the critical exponent δ = 13–15. Thus, the obtained values of the critical exponents indicate that the β(2 × 4) ⟶ α(2 × 4) reconstruction phase transition is a true two-dimensional one.

It is interesting to compare our results with the results obtained by the research team from the University of Arkansas [11, 12]. The authors of these works studied the coalescence of 2D islands of the α(2 × 4) GaAs phase occurring on the β(2 × 4) surface and came to the conclusion that this process is two-dimensional. However, the critical exponent δ was not measured in these works but was estimated from the STM data ex situ. We believe that it is more correct to study a PT on a surface by a diffraction technique in situ, which has been demonstrated in this work.

Thus, we studied the α(2 × 4) ⟶ β(2 × 4) PT on the (001) GaAs surface. It was found that the PT is analogous to a van der Waals transition. The critical parameters T_c, P_c, and Θ_c were measured experimentally. The mean field theory of the α(2 × 4) ⟶ β(2 × 4) PT was used, and three-parameter isotherms were obtained with the parameters E_{st} = 0.36 eV, ΔE = 0.18 eV, and E_i = 0.134 eV in agreement with the experimental results. Precision measurements of the critical exponents β and δ were performed. Their values β = 1/8 and δ = 15 indicate that the PT is a true two-dimensional transition.

REFERENCES

1. H. Yamaguchi and Y. Horikoshi, Phys. Rev. B **51**, 9836 (1995).

2. J. Behrend, M. Wassermeier, L. Daweritz, and K. H. Ploog, Surf. Sci. **342**, 63 (1995).

3. J. Behrend, M. Wassermeier, and K. H. Ploog, Surf. Sci. **372**, 307 (1997).

4. V. P. Zhdanov and B. Kasemo, Surf. Sci. Rep. **20**, 113 (1994); V. P. Zhdanov, *Elementery Physico-chemical Processes on Solid Surfaces* (Nauka, Novosibirsk, 1988; Plenum, New York, 1991).

5. A. Zangwill, *Physics at Surfaces* (Cambridge Univ. Press, Cambridge, 1988; Mir, Moscow, 1990).

6. Yu. G. Galitsyn, S. P. Moshchenko, and A. S. Suranov, Fiz. Tekh. Poluprovodn. (St. Petersburg) **34**, 180 (2000) [Semiconductors **34**, 174 (2000)].

7. Yu. G. Galitsyn, V. G. Mansurov, S. P. Moshchenko, and A. I. Toropov, Fiz. Tekh. Poluprovodn. (St. Petersburg) **34**, 978 (2000) [Semiconductors **34**, 939 (2000)].

8. M. Itoh, Prog. Surf. Sci. **66**, 53 (2001).

9. J. E. Northrup and S. Frooyen, Phys. Rev. B **50**, 2015 (1994).

10. O. E. Tereshchenko, V. L. Al'perovich, and A. S. Terekhov, Pis'ma Zh. Éksp. Teor. Fiz. **79**, 163 (2004) [JETP Lett. **79**, 131 (2004)].

11. V. P. LaBella, Z. Ding, D. W. Bullock, *et al.*, Int. J. Mod. Phys. B **15**, 2301 (2001).

12. Z. Ding, D. W. Bullock, P. M. Thibado, *et al.*, Surf. Sci. **540**, 491 (2003).

Kelvin–Helmholtz Instability in Anisotropic Superfluids[¶]

T. Ruokola and J. Kopu

Low-Temperature Laboratory, Helsinki University of Technology, FIN-02015 HUT, Finland
e-mail: jkopu@boojum.hut.fi
Received May 25, 2005

Motivated by recent theoretical and experimental interest in the subject, we derive the condition of interfacial Kelvin–Helmholtz instability for a system of two flowing superfluids (one sliding on the other). The tensor structure of superfluid densities in anisotropic superfluids, such as ^{3}He-A and also ^{3}He-B under an external magnetic field, is properly taken into account. The consequences relevant to experiments on the A–B phase boundary in superfluid ^{3}He are discussed. © 2005 Pleiades Publishing, Inc.

PACS numbers: 47.20.Ma, 67.57.Np, 68.05.–n

1. INTRODUCTION

The Kelvin–Helmholtz (KH) instability of an interface separating two flowing fluids manifests itself in various everyday phenomena in nature, such as wave generation by wind blowing on water surfaces surface and flapping of flags and sails. A direct experimental verification of the theoretical prediction for the instability criterion, originally studied by Lord Kelvin [1], has nevertheless proven difficult with classical fluids. This is because viscous effects neglected by the theory affect the instability in an essential manner. However, as proven by experimental studies on the interface between the A and B phases of superfluid ^{3}He [2], in superfluid systems (where viscosity does not play a role), a well-defined instability can be observed and the original theoretical ideas tested in detail.

At the instability of the A–B interface, when a situation with shear flow is set up by rotating the sample, a small amount of quantized vorticity is transferred from the A phase to the B phase. Therefore, as a controllable vortex-injection mechanism, the KH instability has recently proven itself a valuable tool in various experimental studies concerning superfluid turbulence and the dynamics of quantized vortices in general [3]. Also, the dispersion relation for surface waves (ripplons) excited on the A–B interface has been shown to be closely related to relativistic dynamics in the Schwarzschild metric [4]; in this work, the idea of using superfluid ^{3}He as a laboratory model system for testing some aspects of black-hole physics has been raised (see also [5]). Furthermore, the superfluid KH instability has been discussed in connection with multicomponent Bose–Einstein condensates [6], phase-separated ^{3}He–^{4}He mixtures [7], and even as a possible source for pulsar glitches [8].

Motivated by these recent developments, we derive the condition for the superfluid KH instability. Since both ^{3}He-A and ^{3}He-B in applied magnetic fields are anisotropic, we take into account their anisotropic superfluid densities. Also, fluid layers of arbitrary thickness are considered. The resulting instability criterion involves a different combination of density-tensor elements than suggested previously [9].

2. KH INSTABILITY—MAIN FEATURES

The problem of the KH instability in classical hydrodynamics considers an interface separating two immiscible ideal fluids in relative motion (one fluid sliding on the other, both of infinite extent), i.e., a tangential discontinuity. Such shear flow becomes unstable if the velocity difference exceeds a critical value determined by (see, e.g., [11] for the derivation)

$$\frac{1}{2}\frac{\rho_1\rho_2}{\rho_1 + \rho_2}|\mathbf{v}_1 - \mathbf{v}_2|^2 = \sqrt{\sigma F}, \tag{1}$$

where ρ_1 and ρ_2 ($\mathbf{v}_1$ and $\mathbf{v}_2$) are the densities (velocities) of the two fluids, σ is the surface tension of the separating interface, and F is a force (per unit volume) due to an external field stabilizing the position of the interface. Usually, this force is provided by the gravitational field, $F = g(\rho_1 - \rho_2)$. The wave vector corresponding to the first unstable mode, which gets excited at the instability, is

$$k_0 = \sqrt{F/\sigma}. \tag{2}$$

The KH instability in the context of superfluids has been analyzed theoretically by Volovik [9]. As pointed out in this work, the most crucial modification as compared with the classical KH instability is the breakdown of the Galilean invariance originating from the two-fluid nature of superfluid hydrodynamics. A preferred

---

[¶] This article was submitted by the authors in English.

reference frame is provided by the frame of the container with respect to which the normal components of the two superfluids are stationary. In this frame, assuming that $\mathbf{v}_1 \parallel \mathbf{v}_2$ (which corresponds to the experimental situation in [2]), the instability criterion emerges as [9]

$$\frac{1}{2}\rho_1 v_1^2 + \frac{1}{2}\rho_2 v_2^2 = \sqrt{\sigma F}, \qquad (3)$$

with the same wave vector k_0, as in the classical case, given by Eq. (2). The densities and velocities in Eq. (3) refer to those of the superfluid components. Note that, here, the instability can also appear when $\mathbf{v}_1 = \mathbf{v}_2$ (cf., a flapping flag in the wind, where the flagpole breaks the Galilean invariance [10]).

Additionally, in the particular case of an A–B interface in superfluid ^{3}He, the position of the interface is stabilized by an external magnetic-field gradient, $F = \frac{1}{2}(\chi_A - \chi_B)|\nabla(H^2)|$, where χ_A and χ_B are the susceptibilities of the two superfluid phases ($\chi_A > \chi_B$). Therefore, a well-defined instability occurs even though the mass densities of the phases are equal to a high accuracy. The threshold determined by Eq. (3) is in remarkable agreement with the experimental observations [2].

## 3. KH INSTABILITY OF ANISOTROPIC SUPERFLUIDS

We now proceed to the derivation of the condition for superfluid KH instability allowing for mass anisotropy and finite thicknesses of the two liquid layers. As shown in [9], the instability criterion can be derived in various different ways. Here, we follow perhaps the most transparent of them, which considers the free energy connected with a perturbation of the interface between the two liquids. We take the unperturbed superfluid velocities $\mathbf{v}_{1(2)} = v_{1(2)}\,\hat{\mathbf{x}}$ of the liquids (in the rest frame of the container and the normal fractions) to be parallel to each other, and the coordinate z to be along the interface normal (see Fig. 1). Translational invariance in the y direction is assumed. We then write the superfluid velocities as $\mathbf{v}_{s1(2)} = \mathbf{v}_{1(2)} + \tilde{\mathbf{v}}_{1(2)}$, where $\tilde{\mathbf{v}}_{1(2)}$ are the modifications due to the perturbation of the interface.

The unperturbed interface is taken to be located at $z = 0$, and the outer walls bounding the liquid layers are situated at $z = -h_1$ and $z = h_2$. We consider small static interfacial perturbations uniform in the y direction, and of the form

$$\zeta = a\sin(kx). \qquad (4)$$

The perturbation parts of the superfluid velocities can be written as $\tilde{\mathbf{v}}_{1(2)} = \nabla\psi_{1(2)}$, where

$$\psi_1 = A_1\cosh[k_1^z(z + h_1)]\cos(kx),$$
$$\psi_2 = A_2\cosh[k_2^z(z - h_2)]\cos(kx), \qquad (5)$$
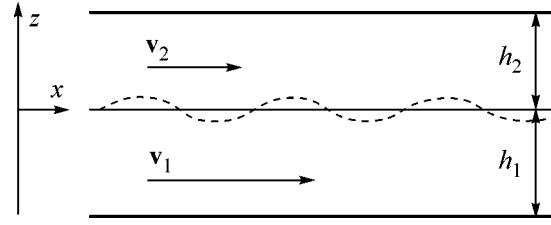
Fig. 1. Geometry of the problem. Small-amplitude static perturbations of an interface at $z = 0$ separating two superfluid layers of thicknesses h_1, h_2 and superfluid velocities $\mathbf{v}_1$, $\mathbf{v}_2$ ($\mathbf{v}_1 \parallel \mathbf{v}_2$) are investigated.

which satisfies $\tilde{v}_{1,z}(z = -h_1) = \tilde{v}_{2,z}(z = h_2) = 0$ at the solid outer boundaries. From the equations of continuity

$$\nabla \cdot (\bar{\boldsymbol{\rho}}_{s1} \cdot \mathbf{v}_{s1}) = 0, \quad \nabla \cdot (\bar{\boldsymbol{\rho}}_{s2} \cdot \mathbf{v}_{s2}) = 0, \qquad (6)$$

where $\bar{\boldsymbol{\rho}}_{s1(2)} = \rho_{1(2)}^x\hat{\mathbf{x}}\hat{\mathbf{x}} + \rho_{1(2)}^y\hat{\mathbf{y}}\hat{\mathbf{y}} + \rho_{1(2)}^z\hat{\mathbf{z}}\hat{\mathbf{z}}$ is the anisotropic superfluid density tensor, we obtain the conditions

$$\rho_1^x k^2 = \rho_1^z(k_1^z)^2, \quad \rho_2^x k^2 = \rho_2^z(k_2^z)^2. \qquad (7)$$

Additionally, we require that there be no mass flow through the interface,

$$\hat{\mathbf{s}} \cdot (\bar{\boldsymbol{\rho}}_{s1} \cdot \mathbf{v}_{s1}) = 0, \quad \hat{\mathbf{s}} \cdot (\bar{\boldsymbol{\rho}}_{s2} \cdot \mathbf{v}_{s2}) = 0, \qquad (8)$$

where $\hat{\mathbf{s}}$ is the unit normal of the interface, we find the further conditions (to the first order in the small perturbation)

$$\rho_1^z A_1 k_1^z \sinh(k_1^z h_1) - \rho_1^x a v_1 k = 0,$$
$$\rho_2^z A_2 k_2^z \sinh(k_2^z h_2) + \rho_2^x a v_2 k = 0. \qquad (9)$$

We return to the justification of Eq. (8) in more detail below.

The free-energy functional for the perturbed flow can be written in the form

$$\mathcal{F}[\zeta] = \frac{1}{2}\int dx\left[F\zeta^2 + \sigma\left(\frac{d\zeta}{dx}\right)^2 \right.$$
$$\left. + \int_{-h_1}^{\zeta} dz(\mathbf{v}_{s1} \cdot \bar{\boldsymbol{\rho}}_{s1} \cdot \mathbf{v}_{s1}) + \int_{\zeta}^{h_2} dz(\mathbf{v}_{s2} \cdot \bar{\boldsymbol{\rho}}_{s2} \cdot \mathbf{v}_{s2})\right].$$

The flow is unstable when the free energy of the perturbed flow is lower than that of the unperturbed flow, i.e., when $\mathcal{F}[\zeta] < \mathcal{F}_0 \equiv \mathcal{F}[\zeta = 0]$. Substituting Eqs. (4)–(9), we find that the first-order modification of the free energy vanishes and the second-order contribution reads

$$\mathcal{F}[\zeta] - \mathcal{F}_0 \propto a^2[F + \sigma k^2 - k(\rho_1^{\text{eff}} v_1^2 + \rho_2^{\text{eff}} v_2^2)], \quad (10)$$
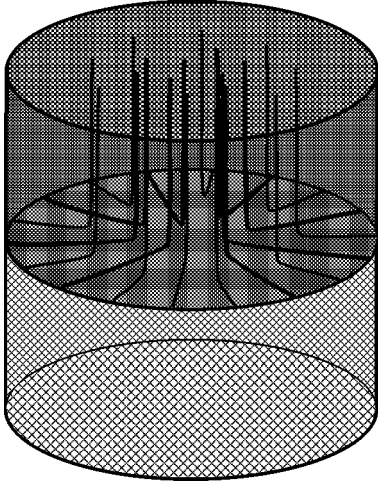
Fig. 2. Schematic representation of the A–B interface instability experiment in superfluid ^{3}He in a state of equilibrium. In a rotating cylindrical container, the A phase occupying the upper volume contains the equilibrium number of vortices and the lower B-phase volume remains vortex-free. The A-phase vortices bend to the container wall forming a vortex sheet on the interface.

with the definition

$$\rho_1^{\mathrm{eff}} \equiv \frac{\rho_1^x \sqrt{\rho_1^x/\rho_1^z}}{\tanh(kh_1\sqrt{\rho_1^x/\rho_1^z})}, \tag{11}$$

and similarly for ρ_2^{eff}. The criterion for the instability is now determined, so that the expression on the right-hand side of Eq. (10) first becomes negative for some wave vector k. In the limiting case of thick layers (appropriate for the experiments in [2]), $kh_1, kh_2 \gg 1$; this happens first for $k = k_0$, and the instability condition reads

$$\frac{1}{2}\left(\rho_1^x\sqrt{\frac{\rho_1^x}{\rho_1^z}}v_1^2 + \rho_2^x\sqrt{\frac{\rho_2^x}{\rho_2^z}}v_2^2\right) = \sqrt{\sigma F}. \tag{12}$$

In the isotropic limit, $\rho_{1(2)}^x = \rho_{1(2)}^z = \rho_{1(2)}$, the criterion in Eq. (3) is recovered. The full anisotropic result, however, differs from Eq. (21) in [9].

Another limiting case, which could be experimentally realized, as well as be interesting in view of [4], is that of one thin layer, say $kh_1 \ll 1$, and $v_2 = 0$. In this case, the parameters of fluid 2 (h_2, ρ_2^x, and ρ_2^z) do not enter the instability criterion. It then follows that the instability first develops with large wavelengths, $k \longrightarrow 0$, and the threshold velocity adopts the simple form

$$v_1 = \sqrt{Fh_1/\rho_1^x}. \tag{13}$$

4. BOUNDARY CONDITION

To give a physical motivation to the boundary condition in Eq. (8), we return again to the specific case of the A–B phase boundary in superfluid ^{3}He. Experimentally, a situation with shear flow can be accomplished by rotating a sample of superfluid ^{3}He where an A–B interface has initially been stabilized using an external magnetic field with a gradient along the axis of rotation (see Fig. 2). Because the critical velocity of vortex nucleation is much lower in ^{3}He-A than in ^{3}He-B, with moderate angular velocities of rotation, vortex lines appear in the A-phase volume, while the volume occupied by the B phase remains vortex-free. In this way, a relative flow between the superfluid components of these two quantum liquids is set up.

Since the vortices cannot terminate at the interface, they must bend to the container wall. Actually, the vortices form a surface sheet on the phase boundary [12]. In stable equilibrium, the net force on the vortex lines coating the interface must vanish when they are stationary in the container frame; i.e., $\mathbf{v}_L = \mathbf{v}_n$. In that case, there is no frictional force from the normal component and the equation of the force balance reads (see, e.g., [13])

$$\mathbf{F}_{\mathrm{tot}} = \mathbf{F}_M + \mathbf{F}_I + \mathbf{F}_{\mathrm{int}} = 0, \tag{14}$$

with the Magnus force from the local superfluid velocity field

$$\mathbf{F}_M = \rho\boldsymbol{\kappa}\times(\mathbf{v}_L - \mathbf{v}_s), \tag{15}$$

where ρ is the total mass density of the liquid and $\boldsymbol{\kappa}$ is the circulation vector, the Iordanskii force from the elementary excitations (quasiparticles in the system) is

$$\mathbf{F}_I = \boldsymbol{\kappa}\times[\bar{\boldsymbol{\rho}}_n\cdot(\mathbf{v}_s - \mathbf{v}_n)] \tag{16}$$

(with the normal-density tensor $\bar{\boldsymbol{\rho}}_n$) and the force from the interface is

$$\mathbf{F}_{\mathrm{int}} = f_{\mathrm{int}}\,\hat{\mathbf{s}}. \tag{17}$$

With these definitions, the vanishing of $\hat{\mathbf{s}}\times\mathbf{F}_{\mathrm{tot}}$ implies Eq. (8). Obviously, for the condition of local equilibrium to be valid, in the above derivation, we have assumed that the timescale characterizing the dynamics of the vortices is short compared with that determining the time evolution of the A–B interface.

5. CONSEQUENCES

Next, we discuss the implications of Eq. (12) regarding the A–B phase boundary experiments of the type reported in [2]. Since the A phase essentially contains the equilibrium number of vortices, $v_A \approx 0$, and the critical velocity of the KH instability is given by

$$v_B = \frac{(4\sigma_{AB}F)^{1/4}}{\sqrt{\rho_B^{\mathrm{eff}}}}, \tag{18}$$

where, now, $\rho_B^{\text{eff}} = \rho_B^x \sqrt{\rho_B^x / \rho_B^z}$. Despite the anisotropy inherent in the p-wave pairing of the superfluid ^{3}He, the unperturbed bulk B phase is isotropic in its physical properties. In the presence of an external magnetic field and superflow, however, a gap distortion induces an anisotropy to the superfluid density in ^{3}He-B [14]. The resulting density tensor is of uniaxial form with components given by

$$\rho_{B,ij} = \rho_B^{\parallel} \hat{l}_i \hat{l}_j + \rho_B^{\perp}(\delta_{ij} - \hat{l}_i \hat{l}_j), \qquad (19)$$

where the unit vector $\hat{\mathbf{l}} \equiv \hat{\mathbf{H}} \cdot \overline{\mathbf{R}}$ is the axis of orbital anisotropy ($\hat{\mathbf{H}}$ is a unit vector in the direction of the external magnetic field and $\overline{\mathbf{R}}$ is the rotation matrix defining the B-phase order parameter).

In the Ginzburg–Landau regime, the mass-density tensor components in the presence of an external field H can be written as [14]

$$\rho_B^{\parallel} \approx \left[1 - 3\frac{H^2}{H_0^2(1 - T/T_c)} \right] \rho_B^0,$$
$$\rho_B^{\perp} \approx \rho_B^0, \qquad (20)$$

where $H_0 = p_F/m^*\xi_0\gamma \approx 1.64$ T, and ρ_B^0 is the isotropic value corresponding to unperturbed bulk ^{3}He-B. In a first approximation, therefore, the tensor component along the direction of $\hat{\mathbf{l}}$ is suppressed, while the other components stay unaffected. We have neglected the small additional suppression due to counterflow, which is justified for the typical experimental velocities of $v_B \ll (2m^*\xi_0)^{-1} \approx 6.3$ cm/s.

To estimate the magnitude of the effect, we insert the values $H = 367$ mT and $T = 0.57T_c$ (one particular experiment was performed at a pressure of $p = 29$ bar; see [3] and reference [30] therein) in Eq. (20), thus, leading to $\rho_B^{\parallel} \approx 0.65\rho_B^0$. Although the extrapolation of the Ginzburg–Landau result to such low temperatures can certainly be questioned, we think it is safe to conclude that the anisotropy effects discussed here are large enough to have experimental significance.

Of course, the actual effect of the density anisotropy depends on the orientation of $\hat{\mathbf{l}}$ in our coordinate system, which is depicted in Fig. 1. This requires a careful analysis of several different mechanisms trying to orient the order parameter [15] originating, e.g., from the external magnetic field, counterflow, container surfaces (the instability is expected to occur near the surface where the counterflow is the highest), and the presence of the A–B interface. Because a detailed investigation of these effects is a fairly complicated problem, we list three possible orientations of $\hat{\mathbf{l}}$, which correspond to the preferred directions of different orienting influences.

(i) $\hat{\mathbf{l}} \parallel \hat{\mathbf{x}}$. This choice minimizes the kinetic energy of the flow; the axis of orbital anisotropy coincides with the flow direction, and we have

$$\rho_B^{\text{eff}}(\hat{\mathbf{l}} \parallel \hat{\mathbf{x}}) = \rho_B^{\parallel} \sqrt{\rho_B^{\parallel}/\rho_B^{\perp}}. \qquad (21)$$

According to Eq. (20), this results in a reduction of ρ_B^{eff} as compared to the isotropic value ρ_B^0, and an enhancement of the threshold velocity in Eq. (18).

(ii) $\hat{\mathbf{l}} \parallel \hat{\mathbf{y}}$. For this wall-dominated order-parameter orientation,

$$\rho_B^{\text{eff}}(\hat{\mathbf{l}} \parallel \hat{\mathbf{y}}) = \rho_B^{\perp}, \qquad (22)$$

and the main gap suppression is along the direction perpendicular to the plane of Fig. 1. In this case, therefore, no significant deviation from the isotropic result is to be expected.

(iii) $\hat{\mathbf{l}} \parallel \hat{\mathbf{z}}$. This orientation would follow in the absence of other effects than that of the axially oriented magnetic field. We obtain

$$\rho_B^{\text{eff}}(\hat{\mathbf{l}} \parallel \hat{\mathbf{z}}) = \rho_B^{\perp} \sqrt{\rho_B^{\perp}/\rho_B^{\parallel}}, \qquad (23)$$

resulting in an apparent enhancement of the effective superfluid density from the isotropic value, $\rho_B^{\text{eff}} > \rho_B^0$! With the values of H and T used in the earlier estimate above, we find $\rho_B^{\text{eff}} \approx 1.25\rho_B^0$. It is interesting to note that the authors of [3] state (reference [30] in the article) that a good fit to the experimental data of the instability threshold, using Eq. (3), was obtained by taking $\rho_B(H) \approx 1.15\rho_B(H = 0)$.

Even though the choice of $\hat{\mathbf{l}} \parallel \hat{\mathbf{z}}$ appears difficult to justify in the circumstances of the experiment (the A–B phase boundary has a strong tendency to orient to $\hat{\mathbf{l}} \perp \hat{\mathbf{s}}$ [16]), it is clear that any attempts aiming at a quantitative understanding of the A–B interface instability should take anisotropy effects into account.

REFERENCES

1. Lord Kelvin (Sir William Thomson), *Hydrodynamics and General Dynamics*, Mathematical and Physical Papers (Cambridge Univ. Press, Cambridge, 1910), Vol. 4.
2. R. Blaauwgeers, V. B. Eltsov, G. Eska, *et al.*, Phys. Rev. Lett. **89**, 155 301 (2002).
3. A. P. Finne, S. Boldarev, V. B. Eltsov, *et al.*, J. Low Temp. Phys. **136** (5/6), 249 (2004).

4. G. E. Volovik, Pis'ma Zh. Éksp. Teor. Fiz. **76**, 296 (2002) [JETP Lett. **76**, 240 (2002)].

5. G. E. Volovik, *The Universe in a Helium Droplet* (Clarendon, Oxford, 2003).

6. D. A. Abanin, Pis'ma Zh. Éksp. Teor. Fiz. **77**, 222 (2003) [JETP Lett. **77**, 191 (2003)].

7. S. N. Burmistrov, L. B. Dubovskii, and T. Satoh, J. Low Temp. Phys. **138**, 513 (2005).

8. N. Andersson, G. L. Comer, and R. Prix, Phys. Rev. Lett. **90**, 091 101 (2003).

9. G. E. Volovik, Pis'ma Zh. Éksp. Teor. Fiz. **75**, 491 (2002) [JETP Lett. **75**, 418 (2002)].

10. Lord Rayleigh (J. W. Strutt), *Scientific Papers* (Cambridge Univ. Press, Cambridge, 1899).

11. L. D. Landau and E. M. Lifshitz, *Course of Theoretical Physics*, Vol. 6: *Fluid Mechanics*, 4th ed. (Nauka, Moscow, 1986; Pergamon, New York, 1989), Sect. 62.

12. R. Hänninen, R. Blaauwgeers, V. B. Eltsov, *et al.*, Phys. Rev. Lett. **90**, 225 301 (2003).

13. G. E. Volovik, Pis'ma Zh. Éksp. Teor. Fiz. **62**, 58 (1995) [JETP Lett. **62**, 65 (1995)].

14. W. Janke and H. Kleinert, Phys. Lett. A **78**, 363 (1980).

15. H. Smith, W. F. Brinkman, and S. Engelsberg, Phys. Rev. B **15**, 199 (1977).

16. E. V. Thuneberg, Phys. Rev. B **44**, 9685 (1991).

Comment on the Surface Exponential for Tensor Fields¶

E. T. Akhmedov, V. Dolotin, and A. Morozov

Institute of Theoretical and Experimental Physics, Moscow, 117219 Russia
Joint Institute for Nuclear Research, Dubna, Moscow region, 141980 Russia
Received May 12, 2005

Starting from an essentially commutative exponential map $E(B|I)$ for generic tensor-valued 2-forms B, which were introduced in [10] as a direct generalization of the ordinary noncommutative P exponent for 1 forms with values in matrices (i.e., in tensors of rank 2), we suggest a nontrivial but multiparametric exponential $\mathcal{E}(B|I|t_\gamma)$, which can serve as an interesting multidirectional evolution operator in the case of higher ranks. To emphasize the most important aspects of the article, the construction is restricted to the backgrounds I_{ijk}, which are associated with the structure constants of the commutative associative algebras, which make it insensitive to the topology of the 2D surface. Boundary effects are also eliminated (straightforward generalization is needed to incorporate them). © 2005 Pleiades Publishing, Inc.

PACS numbers: 11.15.Tk

1. Motivations. Given a matrix-valued one-form $A_{ij}^\mu(x)dx_\mu$ on a line, one can introduce an ordered exponent, $P\exp(\int A_{ij}(x)dx)$, which can also be defined as a limit

$$
\begin{aligned}
z(\hat{I} + \hat{A}) &\equiv P\exp\left(\int A_{ij}(x)dx\right) \\
&= \lim_{N \to \infty} \prod_{n=1}^{N}\left(\hat{I} + \frac{1}{N}\hat{A}(n/N)\right),
\end{aligned}
\tag{1}
$$

with the unit matrix $I_{ij} = \delta_{ij}$ (the hats denote tensors with suppressed indices).

When a 1D line (real curve) is substituted by a 2D surface (complex curve) Σ, an appropriate generalization of a P exponent is badly needed for numerous string theory considerations. The problem is known under many names, from topological models [1, 2] to the Connes–Kreimer theory [3–5] and that of the 2 categories [6]. The role of a chain in (1) is now played by a "net"—a dual graph Γ describing a simplicial complex, which "triangulates"[1] Σ, and tensors $\hat{T}^{(m)}$ of rank

m stand as coupling constants at the vertices of valence m of this graph. To provide triangulation of a surface, the graph should have many vertices with valences $m \ge 3$, and essential generalization of (1) is unavoidable. Indices of $\hat{T}$'s at the vertices are contracted by special rank 2 tensors $\hat{g}$, which are called metric or propagator (it is assumed to have upper indices if all the $\hat{T}$ have lower ones). With such a graph, one associates a partition function [4] $\hat{Z}_\Gamma^{\hat{g}}\{\hat{T}\}$, which is a tensor of rank ext(Γ), equal to the number of external legs of the graph Γ (if Σ has no boundaries, ext(Γ) = 0).

2. Suggestion of [10]. In [10], a principally important step is made to bring the abstract constructions of [4, 11–13] closer to appropriate generalization of (1). The crucial additional structure used in (1) is decomposition of the rank-2 tensor $\hat{t} = \hat{I} + \hat{A}$ into "background" $\hat{I}$ and "dynamical" $\hat{A}$ parts. $z(\hat{I}) = 1$ is trivial, though $I_{ij} = \delta_{ij} \ne 0$ itself is not.

For complex curves, the background $\hat{I}$ should necessarily have rank greater than 2; for graphs of valence 3, it should have rank 3. It is well known [2] that there are nontrivial $\hat{I}$ and associated $\hat{g}$ that exist with trivial

$$
Z_\Gamma^{\hat{g}}(\hat{I}) = 1
$$

for *all* Γ without external legs[2] (they can be build from structure constants of any commutative associative algebra (see section below), but this does not exhaust all the possibilities), and the research [10] suggests to

---

¶ This article was submitted by the authors in English.

[1] In principle, to imitate surface integrals with arbitrary measures, one needs triangulations with lengths ascribed to the links [7]. However, as usual in the matrix-model realizations of string theory [8], one can ignore the lengths (consider "equilateral triangulations")—as is done in (1)—and the associated quantities will be quite informative (perhaps, even exhaustively informative: for example, it is believed—and confirmed by numerous calculations of particular quantities—that Polyakov's (sum over 2D metrics) and Migdal's (matrix-model sum over equilateral triangulations) descriptions of string correlators are equivalent). Still, the interrelation between arbitrary and equilateral triangulations remains an open problem, touching the fundamental questions of number theory [9]. The problem is also known as that of continuous limits in matrix models.

---

[2] Of course, for ext(Γ) $\ne$ 0, the $Z_\Gamma^{\hat{g}}(\hat{I})$ is an operator (has external indices) and cannot be unity. However, it can be made dependent only on ext(Γ) but not on Γ itself (see the section below).

make use of them exactly in the same way as in (1). Since, in this construction, $\hat{g}$ is rigidly linked to $\hat{I}$, we suppress the $\hat{g}$ labels in most formulas below.

According to the definition of $\hat{Z}_\Gamma$ for $\hat{T} = \hat{I} + \hat{B}$, we have [3]

$$\hat{Z}_\Gamma(\hat{I} + \hat{B}) \ = \ \sum_{\gamma \subset \Gamma} \hat{Z}_{\Gamma/\gamma}(\hat{I})\hat{Z}_\gamma(\hat{B}). \tag{2}$$

If we now take a limit of large $|\Gamma| \equiv$ (the number of vertices in Γ) with a graph growing in both dimensions to form a dense net and look at the terms with a given power of B, then statistically only graphs γ consisting of isolated points will survive after appropriate rescaling of B, and this logic leads to the following generalization of (1) [10]:

$$\hat{E}(\hat{B}|\hat{I}) \ = \ \lim_{|\Gamma| \to \infty} \hat{Z}_\Gamma \left(\hat{I} + \frac{1}{|\Gamma|} \hat{B} \right) \tag{3}$$

(the argument $\hat{I}$ in $\hat{E}$ will often be suppressed below). This is a very nice and interesting quantity, but it is essentially Abelian: as we shall see in (11), $\hat{E}(\hat{B}_1)\hat{E}(\hat{B}_2) = \hat{E}(\hat{B}_1 + \hat{B}_2)$ (for example, for a rank 3 2-form $\hat{B} = B_{ijk}^{\mu\nu} dx_\mu \wedge dx_\nu$ on Σ, we can define a surface integral as $E(\int_\Sigma \hat{B})$ and never encounter any ordering problems). This happens for the same reason that the homotopic groups π_k are commutative for $k > 1$: any two insertions of B at two remote points can be easily permuted by moving one around the another.

In what follows, we give a more formal description of the above construction, get rid of a subtle limiting procedure in (3), and introduce—with the help of $\hat{E}(\hat{B})$, just changing its argument—a less trivial exponential $\hat{\mathcal{E}}(\hat{B}|t)$. It should be useful in applications, it is well defined, but no "conceptual" limiting formula like (3) is immediately available for it.

---

[3] Note that the graph automatically picks up the tensors of appropriate rank from $\hat{B}$; if there is no match, $\hat{Z} = 0$. If we assume that $\hat{I}$ is exactly of rank 3 while $\hat{B}$ consists of tensors of various ranks (we will see below that it is useful not to restrict $\hat{B}$ to rank 3 only), then only subgraphs Γ/γ with vertices of valence 3 will contribute to the sum. The subgraph Γ/γ is defined by throwing away all the vertices of γ and all the links between them, $\text{ext}(\Gamma/\gamma) = \text{ext}(\Gamma) + \text{ext}(\gamma) - 2$ (the number of common external legs of Γ and γ). In other words, γ is treated as a "vertex-subgraph" of Γ. As explained in [4], the vertex-subgraphs (in variance with the "box-subgraphs") are related to a relatively simple set-theoretical aspect of quantum field theory (to the Shift $\mathcal{M}$ rather than Diff.$\mathcal{M}$ structure of the diagram technique). In the present context, this is the reason behind the oversimplicity (commutativity property (11)) of the exponential (3).

3. Backgrounds $\hat{I}$ from commutative associative algebras $\mathcal{A}$. Let $(\check{C}_i)_j^k = C_{ij}^k$ be structure constants of an associative algebra $\mathcal{A}$ ($\phi_i * \phi_j = C_{ij}^k \phi_k$):

$$[\check{C}_i, \check{C}_j] \ = \ 0. \tag{4}$$

Introduce a set of symmetric tensors $\hat{I}^{(n)}$:

$$I_{i_1 \ldots i_n} \equiv \text{Tr}(\check{C}_{i_1} \ldots \check{C}_{i_n}). \tag{5}$$

Among them will be the metric[4]

$$g_{ij} \ = \ I_{ij} \ = \ \text{Tr}(\check{C}_i \check{C}_j) \tag{6}$$

and the elementary vertex $I_{ijk} = \text{Tr}(\check{C}_i \check{C}_j \check{C}_k)$. The metric will be assumed to be nondegenerate, and its inverse g^{ij} will be used to raise the indices.

In what follows, we impose an additional commutativity condition on the structure constants:

$$C_{ij}^k \ = \ C_{ji}^k. \tag{7}$$

Then, tensors $\hat{I}$ are not just cyclic but totally symmetric.

Lemma. *For commutative associative algebra $\mathcal{A}$,*

$$I_{ijk} \ = \ g_{im} C_{jk}^m$$

or simply $I_{jk}^m = C_{jk}^m$. Indeed,

$$g_{im} C_{jk}^m \ = \ C_{il}^n C_{mn}^l C_{jk}^m \overset{(7)}{=} C_{il}^n C_{nm}^l C_{jk}^m$$

$$\overset{(4)}{=} C_{il}^n C_{jm}^l C_{nk}^m \ = \ I_{ikj} \overset{(7)}{=} I_{ijk}.$$

Lemma. *For commutative associative algebra $\mathcal{A}$,*

$$I_{i_1 \ldots i_m k_1 \ldots k_r} I_{j_1 \ldots j_n}^{k_1 \ldots k_r} \tag{8}$$
$$= \ I_{i_1 \ldots i_m k_1 \ldots k_r} I_{j_1 \ldots j_n \tilde{k}_1 \ldots \tilde{k}_r} g^{k_1 \tilde{k}_1} \ldots g^{k_r \tilde{k}_r} \ = \ I_{i_1 \ldots i_m j_1 \ldots j_n}$$

for any $r \neq 0$ and any m and n.

The proof follows from the observation that (4) and (6) provide the two transformations (the "flip" or "zigzag" transform and tadpole-eliminator), which generate a group with transitive action on the space of all connected triangulations (see [10] for the relevant illustrations).

Obviously, for any connected Γ, $\hat{Z}_\Gamma(\hat{I})$ is given by these tensors I:

$$(Z_\Gamma^{\hat{g}}(\hat{I}))_{i_1 \ldots i_{\text{ext}(\Gamma)}} \ = \ I_{i_1 \ldots i_{\text{ext}(\Gamma)}}. \tag{9}$$

---

[4] Note that this choice of metric is different from $G_{ij}^{(m)} = I_{ijm}^{(3)}$, used in the context of the generalized WDVV equations in [14].

In other words, in background theory, the connected diagram depends only on the number of external legs. One can, of course, associate additional factors with graphs, counting the numbers of vertices and loops, but they do not depend on $\mathcal{A}$ and are not of immediate interest for our consideration.

If Γ consists of disconnected parts, $\hat{Z}_\Gamma(\hat{I})$ will be a tensor product of $\hat{I}$ tensors.

If other traceless tensors $B^{(m)}$ of rank m are allowed in the vertices, we get a nontrivial B theory in the $\mathcal{A}$ background. The original $\hat{Z}(\hat{T})$ provides the unified background-independent formulation. Still, explicit transformation from one background to another remains an interesting open problem.

4. Commutative exponential. Introduce a $\hat{B}$-dependent tensor of rank n:

$$
E^{(n)}_{i_1\ldots i_n}(\hat{B}) = \sum_{m=1}^{\infty}\sum_{\{r_m\}}\sigma\{r_m\}
$$

$$
\times\left\{\left(B^{j_1^{(1)}}\ldots B^{j_{r_1}^{(1)}}\right)\left(B^{j_1^{(2)}j_2^{(2)}}\ldots B^{j_{2r_2-1}^{(2)}j_{2r_2}^{(2)}}\right)\right. \tag{10}
$$

$$
\left.\ldots\left(B^{j_1^{(m)}\ldots j_m^{(m)}}\ldots B^{j_{r_m-m+1}^{(m)}\ldots j_{r_m}^{(m)}}\right)\ldots\right\}_{i_1\ldots i_k j_1^{(1)}\ldots j_{r_m}^{(m)}\ldots}.
$$

Here, $\hat{B} = \{\hat{B}^{(1)},\hat{B}^{(2)},\ldots,\hat{B}^{(m)},\ldots\}$ is a direct sum of tensors of all possible ranks, and the sum in (11) is over all possible sets, including any number r_m of tensors of rank m.

Theorem. *For appropriate choice of the combinatorial factors* $\sigma\{r_m\}$*, the map* $\hat{E}(\hat{B})$ *satisfies the exponential property:*[5]

$$
E^{(m+r)}_{i_1\ldots i_m k_1\ldots k_r}(B_1)E^{(n+r)(k_1\ldots k_r)}_{j_1\ldots j_n}(B_2)
$$

$$
= E^{(m+n)}_{i_1\ldots i_m j_1\ldots j_n}(B_1 + B_2) \tag{11}
$$

for any $r \neq 0$ *and any* m *and* n *(no sum over* r *is taken). The relevant choice of* $\sigma\{r_m\}$ *is the usual Feynman-diagram factorial (see, for example, the generalized Wick theorem in [15])*

$$
\sigma\{r_m\} = \prod_{m=1}^{\infty}\frac{1}{r_m!(m!)^{r_m}}. \tag{12}
$$

---

[5] Note that, in terms of $\hat{T} = \hat{I} + \hat{B}$, this relation does not look homogeneous

$$
\hat{Z}_\Gamma(\hat{I} + \hat{B}_1 + \hat{B}_2) = \hat{Z}_\Gamma(\hat{I} + \hat{B}_1)\hat{Z}_\Gamma(\hat{I} + \hat{B}_2) + O(|\Gamma|^{-1}),
$$

and holds because of the Γ-independence property (9) of $\hat{Z}_\Gamma(\hat{I})$.

The factors $m!$ *can be eliminated by rescaling of* $B^{(m)}$*. As an immediate corollary of (11), the derivative of the exponent functor* $\hat{E}(\hat{B})$ *is* $\hat{E}(\hat{B})$ *itself:*

$$
\delta E^{(n)}_{i_1\ldots i_n}(B)
$$

$$
= \sum_{m=1}^{\infty} E^{(n+m)}_{i_1\ldots i_n j_1\ldots j_m}(B)\delta B^{j_1\ldots j_m}_{(m)} + O(\delta B^2). \tag{13}
$$

Thus, nothing such as the nontrivial Campbell–Hausdorff formula [16] (which describes the product of P exponents (1)) arises for $\hat{E}(\hat{B})$ the potential noncommutativity of the tensor product is completely eliminated by the naive continuum limit (3) as a corollary of relation (9) and the possibility to rely upon connected graphs.

5. Nontrivial exponential and directions of immediate generalization. The potential origin of the nontriviality of the exponential is twofold: there can be contributions from nontrivial (not totally disconnected) subgraphs γ to $\hat{Z}_\gamma(\hat{B})$ and from disconnected factor-graphs Γ/γ to $\hat{Z}_{\Gamma/\gamma}(\hat{I})$. The first origin (contribution from nontrivial γ) is eliminated by the naive continuum limit—both in the 1D formula (1) and in the 2D one (11). In 1D, property (9) perfectly holds for connected graphs, but disconnected Γ/γ also contribute to (1). What happens in 2D is that disconnected Γ/γ are statistically damped in the naive continuum limit, together with nontrivial γ, and direct generalization of the non-Abelian (1) from lines to surfaces is Abelian (commutative)!

In order to get a noncommutative exponential in 2D, one can, however, revive the contributions from the nontrivial γ simply by introducing a nontrivial multi-time evolution operator:

$$
\hat{\hat{\mathcal{E}}}(B|t) = \hat{E}\left(\sum_{\text{connected }\gamma} t_\gamma \hat{Z}_\gamma(B)\right) \tag{14}
$$

(of course, one can do—and often does—the same in 1D). Similarly, one can add contributions from disconnected Γ/γ by introducing certain nonlocal operators (involving contour integrals) in the exponent. Despite the fact that such quantities may seem less natural than (3), they naturally arise in physically relevant evolution operators and even in actions, bare and effective. Moreover, for special $\hat{B}$, for example, totally antisymmetric, the leading contribution with single-point γ vanishes in the symmetric background $\hat{I}$. Then, the next-to-leading contribution—from single-link (and two-point) γ—can be described by the appropriately modified limiting prescription (3).

$\hat{\hat{\mathcal{E}}}(\hat{B}|\hat{I}|t)$ is already a nontrivial (operator) special function, which deserves attention and investigation.

Note that, even if $\hat{B}$ was a rank-3 tensor and all the relevant graphs were of valence 3, the tensors $\hat{Z}_\gamma(\hat{B})$, which contribute to the argument of $\hat{E}$ in (14), have ranks ext(γ), which are not obligatorily equal to 3.

Despite the fact that nontrivial graphs γ are now incorporated in (14), they are still restricted to lie inside Σ, i.e., remain separated from the boundary of Σ by the requirement of the connectedness of Γ/γ (the external legs of Γ are not allowed to belong to γ). Additional corrections to (14) are needed to make it sensitive to boundary effects.

In this note, we restricted our consideration to the simplest possible case of commutative algebra $\mathcal{A}$, when tensors $\hat{I}$ are totally symmetric. Relaxing this requirement, one gets $\hat{I}$ with only cyclic symmetry, then (9) gets more complicated: universality classes are no longer enumerated by the ext(Γ) dependence on the number of handles that arise and the description in terms of wide graphs is needed [10] (see [5] for the corresponding generalization of [4]).

An interesting part of this story is exponentiation (the algebra $\longrightarrow$ group lifting) of associative algebras and higher-rank multiplications [12]. It involves limits like (3) along particular chains of graphs (obtained, for example, by iterative blowing up of triple vertices into triangles). In such situations, the B insertions have a higher probability to break the graph into disconnected components than in the case of generic net-graphs. Still, the enhancement is not sufficient and, as in (3), such contributions remain statistically damped in the naive continuum limit. Therefore, the transition from (3) to (14) should still be performed by hand.

A related open question concerns the generalization of the background $\hat{I}$ from the rank 3 case (related to associative algebras) to the generic situation and connection of this problem to the Batalin–Vilkovisky theory of Massis operations [17–19].

REFERENCES

1. A. Schwarz, Lett. Math. Phys. **2**, 247 (1978); E. Witten, Commun. Math. Phys. **117**, 353 (1988); Commun. Math. Phys. **118**, 411 (1988); Nucl. Phys. B **340**, 281 (1990); R. Dijkgraaf and E. Witten, Nucl. Phys. B **342**, 486 (1990); D. Birmingham, M. Blau, M. Rakowski, and G. Thompson, Phys. Rep. **209**, 129 (1991); R. Dijkgraaf, Nucl. Phys. B **342**, 486 (1990); Nucl. Phys. B **352**, 59 (1991); hep-th/9201003; T. Eguchi, K. Hori, and C.-S. Xiong, Int. J. Mod. Phys. A **12**, 1743 (1997); hep-th/9605225; A. Losev, hep-th/9801179; A. Gerasimov and S. Shatashvili, J. High Energy Phys. **0411**, 074 (2004); hep-th/0409238.

2. E. Verlinde, Nucl. Phys. B **300**, 360 (1988).

3. D. Kreimer, Adv. Theor. Math. Phys. **2**, 303 (1998); hep-th/9810022; A. Connes and D. Kreimer, Commun. Math. Phys. **199**, 203 (1998); Lett. Math. Phys. **48**, 85 (1999); hep-th/9904044; hep-th/9909024; hep-th/9909126; Commun. Math. Phys. **210**, 249 (2000); hep-th/9912092; hep-th/0003188; Ann. Inst. Henri Poincare **3**, 411 (2002); hep-th/0201157; A. Connes and M. Marcolli, math.NT/0409306; hep-th/0411114; hep-th/0504085.

4. A. Gerasimov, A. Morozov, and K. Selivanov, Int. J. Mod. Phys. A **16**, 1531 (2001); hep-th/0005053.

5. D. Malyshev, J. High Energy Phys. **0205**, 013 (2002); hep-th/0112146; hep-th/0408230.

6. See, for example, J. Baez, A. Crans, D. Stevenson, and U. Schreiber, math.QA/0504123; and discussions at http://math.ucr.edu/home/baez/.

7. E. Akhmedov, Pis'ma Zh. Éksp. Teor. Fiz. **80**, 247 (2004) [JETP Lett. **80**, 218 (2004)]; hep-th/0407018; hep-th/0502174.

8. A. Migdal, Phys. Rep. **102**, 199 (1990); A. Morozov, Usp. Fiz. Nauk **164**, 3 (1994) [Phys. Usp. **37**, 1 (1994)]; hep-th/9303139; hep-th/9502091; P. Di Francesco, P. Ginsparg, and J. Zinn-Justin, J. Phys. Rep. **254**, 1 (1995).

9. A. Levin and A. Morozov, Phys. Lett. B **243**, 207 (1990).

10. E. Akhmedov, Theor. Mat. Fiz. (in press); hep-th/0503234.

11. V. Dolotin, math.GT/9904026.

12. Yu. Chernyakov and V. Dolotin, math.RA/0501206.

13. Y. Kawamura, hep-th/0504017.

14. A. Marshakov, A. Mironov, and A. Morozov, Phys. Lett. B **389**, 43 (1996); hep-th/9607109; Mod. Phys. Lett. A **12**, 773 (1997); hep-th/9701014; Int. J. Mod. Phys. A **15**, 1157 (2000); hep-th/9701123; A. Mironov and A. Morozov, Phys. Lett. B **424**, 48 (1998); hep-th/9712177; A. Morozov, Phys. Lett. B **427**, 93 (1998); hep-th/9711194; G. Bonelli and M. Matone, Phys. Rev. D **58**, 045006 (1998); hep-th/9712025; G. Bertoldi and M. Matone, Phys. Lett. B **425**, 104 (1998); hep-th/9712039; Phys. Rev. D **57**, 6483 (1998); hep-th/9712109; H. W. Braden, A. Marshakov, A. Mironov, and A. Morozov, Phys. Lett. B **448**, 195 (1999); hep-th/9812078; Nucl. Phys. B **558**, 371 (1999); hep-th/9902205; J. Isidro, Nucl. Phys. B **539**, 379 (1999); hep-th/9805051; J. High Energy Phys. **0101**, 043 (2001); hep-th/0011253; A. Veselov, Phys. Lett. A **261**, 297 (1999); hep-th/9902142; hep-th/0105020; L. Hoevenaars, P. Kersten, and R. Martini, Phys. Lett. B **503**, 189 (2001); hep-th/0012133; H. Aratyn and J. van de Leur, hep-th/0111243.

15. A. Alexandrov, A. Mironov, and A. Morozov, Int. J. Mod. Phys. A **19**, 4127 (2004); hep-th/0310113; hep-th/0412099; hep-th/0412205; A. Morozov, hep-th/0502010.

16. See, for example, A. Morozov and L. Vinet, Int. J. Mod. Phys. A **13**, 1651 (1998); hep-th/9409093.

17. I. Batalin and G. Vilkovisky, Phys. Lett. B **102B**, 27 (1981); Phys. Lett. B **120B**, 166 (1983); Phys. Rev. D **28**, 2567 (1983); Nucl. Phys. B **234**, 106 (1984); J. Math. Phys. **26**, 172 (1985); I. Batalin, Phys. Rev. D **28**, 2567 (1983); J. Math. Phys. **26**, 172 (1985).

18. E. Witten, Phys. Rev. D **46**, 5467 (1992); hep-th/9208027; Phys. Rev. D **47**, 3405 (1993); hep-th/9210065; hep-th/9306122; E. Verlinde, Nucl. Phys. B **381**, 141 (1992); hep-th/9202021; M. Bershadsky, S. Cecotti, H. Ooguri, and C. Vafa, Commun. Math. Phys. **165**, 311 (1994); hep-th/9309140; Nucl. Phys. B **405**, 279 (1993); hep-th/9302103; W. Siegel, Phys. Lett. B **151B**, 391 (1984); hep-th/0107094; B. Zwiebach, Nucl. Phys. B **390**, 33 (1993); hep-th/9206084; N. Berkovits and W. Siegel, Nucl. Phys. B **505**, 139 (1997); hep-th/9703154; N. Berkovits, J. High Energy Phys. **0004**, 018 (2000); hep-th/0001035; J. High Energy Phys. **0409**, 047 (2004); hep-th/0406055; N. Berkovits and P. Howe, Nucl. Phys. B **635**, 75 (2002); hep-th/0112160.

19. A. Gorodentsev and A. Losev, *Lectures at ITEP-DIAS School* (2004).

New Experimental Results on the Interference of the States of the Hydrogen Atom Due to Long-Range Interaction with the Metal Surface

Yu. A. Kucheryaev[1], V. G. Pal'chikov[2], Yu. A. Pchelin[1],
Yu. L. Sokolov[1,*], and V. P. Yakovlev[3]

[1] *Russian Research Centre Kurchatov Institute, pl. Akademika Kurchatova 1, Moscow, 123182 Russia*
e-mail: lukich@nfi.kiae.ru
[2] *All-Russia Research Institute of Physicotechnical and Radio Engineering Measurements,*
Mendeleevo, Moscow region, 141570 Russia
[3] *Moscow Engineering Physics Institute (State University), Kashirskoe sh. 31, Moscow, 115409 Russia*
Received March 30, 2005; in final form, May 25, 2005

The interference of the $2P$ state of the hydrogen atom due to unknown long-range interaction with the metal surface (Sokolov effect) has been studied by an atomic interferometer. In contrast to previous experiments, where an atomic beam passed through slits in metal plates, a beam in the presented experiments passes at a given distance from the edges of the plates. It has been found that the interference is clearly observed if two plates are located on the same side of the beam. However, this interference disappears if one plate is displaced to the opposite side. This result cannot be explained in the framework of the available hypotheses on the nature of the effect under investigation. © 2005 Pleiades Publishing, Inc.

PACS numbers: 39.10.+j, 39.20.+q

In experiments on the interference of the $2P$ state of the hydrogen atom, it has been found that the metastable $2S_{1/2}$ atom flying over the metal surface interacts with this surface. This interaction is responsible for the appearance of a coherent addition of the $2P_{1/2}$ state to the initial pure $2S$ state, i.e., for the transition of the latter state to the $2S$–$2P$ superposition (Sokolov effect) [1, 2]. The existence of such an interaction is not surprising, but its observation to a distance of 0.6 mm between the metal surface and atom within the sensitivity limit of the instruments used in those experiments is surprising.

Figure 1a shows the scheme of an experiment, where unknown interaction is clearly observed [3]. A beam that is a mixture of the $1S$ and $2S$ hydrogen atoms with an energy of 20 keV passes through a system including the quenching field E (for removing $2S$ atoms from the beam in test measurements), the collimator C forming the beam in the form of a 0.05×2-mm strip, the slits S_1 and S_2 0.3-mm thick, and the detector D that detects L_α photons and is tightly connected with the slit S_2. The distance L between the slits S_1 and S_2 could smoothly vary in the range 0.2–15 mm. The slits are cut in bronze plates 0.8-mm thick that are coated with a 5-μm gold film and are properly grounded.

As the distance L varies, pronounced oscillations are observed in the intensity of the flux of $2P$ atoms; i.e., it is the interference of the components of this state that

arise in the perturbation regions near the slits S_1 and S_2 (see Fig. 1b).

More recently, an experimental procedure was developed where a beam of hydrogen atoms passed at a given distance from the edge of a slit rather than through it. This approach gave substantial results: a new aspect of the phenomenon is manifested.

Numerous such experiments were carried out in two variants: metallic plates with which atoms interact are located either on the same side of the beam or on opposite sides. Figure 2a shows one of experimental schemes. The plate P_2 and detector D of L_α radiation are at rest in the laboratory frame of reference. The plate P_1 and collimator C connected with it may be displaced at a given distance L. In order to measure the detector background associated with the main $1S$ component of the beam ($\approx 98\%$), one can create a quite strong electric field E quenching the $2S$ component ($\approx 2\%$). In this experiment, both plates are located on the same side of the beam at a distance of 0.15 mm from its axis. The detector signal obtained after the subtraction of the instrumental background and normalization to the beam monitor records is shown in Fig. 2b as a function of the distance L (interference pattern). Pronounced signal oscillations testify to the interference of two $2P$ components that are formed when $2S$ atoms fly over the

plates P_1 and P_2. The interference pattern is well approximated by the function [4]

$$F(L) = a_1 \exp\left(-\frac{L}{R}\right) + a_2 \exp\left(-\frac{L}{2R}\right)$$
$$\times \cos\left(\frac{2\pi L}{a_3} + a_4\right) + a_5, \quad (1)$$

where R is the mean free path of a $2P$ atom and $a_1, \ldots, a_5$ are the empirical parameters. The mean free path $R = 0.3276$ cm corresponds to an atom energy of 22.0 keV taken in this experiment (the lifetime of the $2P_{1/2}$ state is equal to 1.5962 ns). The measured period $a_3 = 0.188$ cm of spatial oscillations corresponds to a frequency of 1092 MHz. This value indicates that the $2S_{1/2}$–$2P_{1/2}$ transition occurs: the possible transition frequency lies in the range from 909.9 to 1147 MHz, because a mixture of the components of the hyperfine structure of the $2S$ state with the total angular momenta $F = 0$ and 1 is used in the experiment. The main part of the pedestal of the a_5 interference pattern (1305 units of 1412) is an additional background arising in the presence of the $2S$ component of the beam. On the whole, this experiment reproduces numerous observations of the Sokolov effect, including the structure of function (1), in previous experiments with slits.

Another picture is observed in an experiment whose scheme is shown in Fig. 3. The only difference of this experimental configuration from the above experiment is that the plates P_1 and P_2 are placed on opposite sides of the beam. As is seen in Fig. 3b, the interference pattern changes dramatically in this case: no regular oscillations are seen within the limit of the fluctuations. The exponential decay of the signal with a decrement of $1/R$ undoubtedly means that $2S$ atoms are subjected to perturbation from the plate P_1. It is difficult to think that perturbation from the plate P_2 that is clearly manifested in the interference pattern of the preceding experiment disappears in this experiment. However, two components of the $2P$ state that are produced in this experiment do not interfere with each other. The basic features of this situation are reproduced in other experiments, where the edges of the plates have the shape of sharp wedge.

It is reasonable to assume that the interaction of the atom with two *identically* located plates results in two phase-shifted contributions to the amplitude of the *same* $2P$ state and thereby in the interference effect. The absence of interference when the plates are placed on different sides of the atomic beam could be interpreted such that interaction with them excites *different* sublevels of the $2P$ state. From this point of view, the experiments discussed above provide certain new information on the structure of interaction whose mechanism is yet unknown.

Thus, the main result of the two above experiments is that the only change in the experimental conditions—
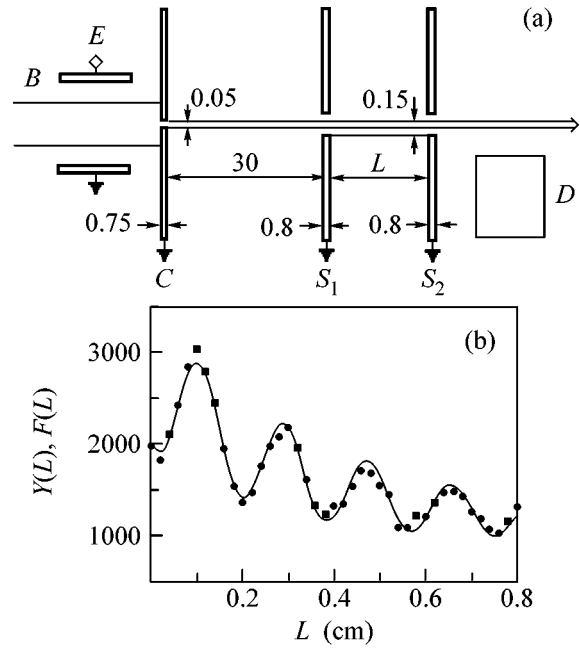
Fig. 1. (a) Experimental scheme: (B) the $H_{1S} + H_{2S}$ atomic beam, (E) the electric field quenching the H_{2S} component, (C) collimator, (S_1 and S_2) plates with slits for beam passage, and (D) the detector of L_α photons. (b) Interference pattern: points are measured $Y(L)$ values and the solid line is the approximation $F(L) = 1645\exp(-L/0.3276) + 732\exp(-L/0.6552)\cos((2\pi L)/0.184 + 2.64) + 1060$.
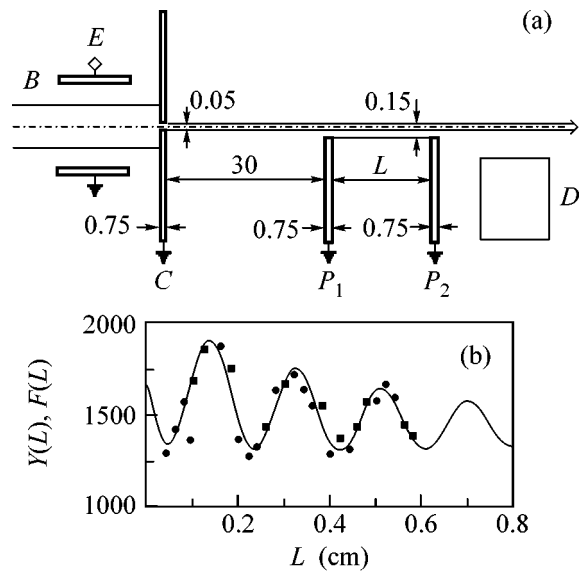
Fig. 2. (a) Experimental scheme: (B) the $H_{1S} + H_{2S}$ atomic beam, (E) the electric field quenching the H_{2S} component, (C) the collimator, (P_1) the movable plate, (P_2) the immovable plate, and (D) the detector of photons. (b) Interference pattern: points are measured $Y(L)$ values and the solid line is the approximation $F(L) = 308\exp(-L/0.3276) + 363\exp(-L/0.6552)\cos((2\pi L)/0.188 + 1.68) + 1412$.
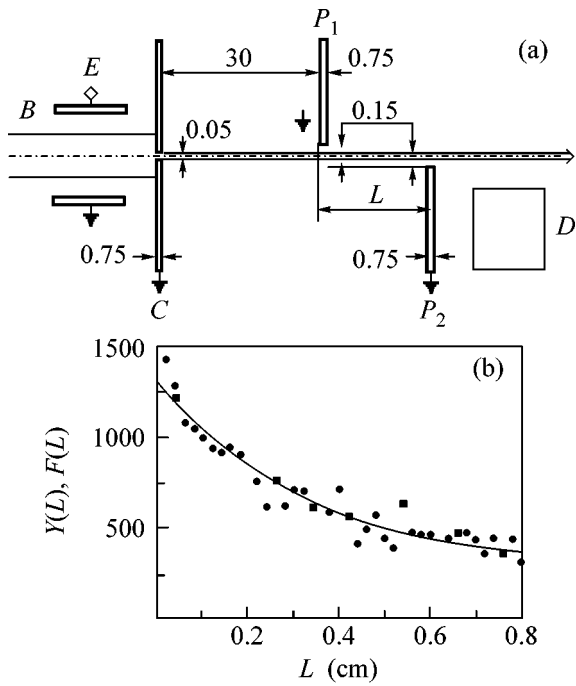
Fig. 3. Same as in Fig. 2, but the solid line is the approximation $F(L) = 1014\exp(-L/0.3276) + 284$.

displacement of the plate P_1 on the other side of the beam—leads to the disappearance of the interference between the $2P$ components of the superpositions. For several years, we experimentally verified various alternative theoretical explanations of the nature of the interaction found between excited hydrogen atoms and the metal surface in application to the problems discussed above.

In [3], we analyzed long-range atom–metal-surface interactions (classical van der Waals potential, Casimir effect, resonance radiation shift) that are treated as the interaction of the fluctuating dipole moment of the atom with its mirror image in the metal and (in the long range limit) as the Stark shift caused by changes in the boundary conditions (due to the presence of the conducting medium) for vacuum field fluctuations [5, 6]. The maximum shift of the $2P$ level at a distance of $r = 1$ μm is equal to 500 kHz, and the shift of the $2S$ level at this distance does not exceed a value of -2.3 kHz [7].

Among other recent publications on this theme, we point to [8–10], where theoretical and experimental aspects of investigations of long-range interactions for Rydberg atomic states were analyzed.

However, theoretical estimates of the interaction of the hydrogen atom with the metal surface at distances

$r = 200$–700 μm are negligibly small. The effect of long-range interaction that we observe in experiments at these distances is several orders of magnitude larger than the prediction following from the above works. The hypotheses proposed in [11–13] also cannot explain the experimental results discussed above.

We emphasize that experiments with metastable $2S_{1/2}$ hydrogen atoms are of considerable interest, because this state is separated from the short-lived $2P_{1/2}$ state by a Lamb shift of 4×10^{-6} eV. Therefore, very small perturbations of the $2S$ state may induce the $2S \longrightarrow 2P$ transition with the subsequent emission of an L_α photon that can be easily detected. Metastable $2S_{1/2}$ hydrogen atoms can be a fine tool for studying the discovered paradoxical phenomena.

REFERENCES

1. Yu. L. Sokolov, V. P. Yakovlev, and V. G. Pal'chikov, Phys. Scr. **49**, 86 (1994).
2. Yu. L. Sokolov, Usp. Fiz. Nauk **169**, 559 (1999) [Phys. Usp. **42**, 481 (1999)].
3. Yu. L. Sokolov, V. P. Yakovlev, V. G. Pal'chikov, and Yu. A. Pchelin, Eur. Phys. J. D **20**, 27 (2002).
4. Yu. A. Kucheryaev and Yu. A. Sokolov, physics/0304106.
5. E. M. Lifshitz, Zh. Éksp. Teor. Fiz. **29**, 94 (1955) [Sov. Phys. JETP **2**, 73 (1955)].
6. M. L. Levin and S. M. Rytov, *Theory of Equilibrium of Thermal Fluctuations in Electrodynamics* (Nauka, Moscow, 1967) [in Russian].
7. E. A. Hinds and V. Sandoghdar, Phys. Rev. A **43**, 398 (1991).
8. F. Hasselbach *et al.*, in *Decoherence: Theoretical, Experimental, and Conceptual Problems* (Springer, Berlin, 2001), pp. 201–212.
9. J. Tonomura, Int. J. Mod. Phys. A **15**, 3427 (2000).
10. Y. Levinson, J. Phys. A: Math. Gen. **37**, 3003 (2004).
11. B. B. Kadomtsev and M. B. Kadomtsev, Phys. Scr. **50**, 243 (1994).
12. B. B. Kadomtsev, *Dynamics and Information* (Uspekhi Fizicheskikh Nauk, 1997) [in Russian].
13. S. T. Beljaev, Eur. Phys. J. D **25**, 247 (2003).

Translated by R. Tyapaev

No Robust Phases in Aerogel: ^{3}He-*A* with Orientational Disorder in the Ginzburg–Landau Model (Comment on Papers by I.A. Fomin on Robust Phases)¶

G. E. Volovik

Low-Temperature Laboratory, Helsinki University of Technology, FIN-02015 HUT, Finland
Landau Institute for Theoretical Physics, Russian Academy of Sciences, Moscow, 117334 Russia
Received May 12, 2005

In series of papers [2, 7], Fomin introduced and discussed the so-called robust phases in a system with frozen orientational disorder (with application to superfluid ^{3}He in aerogel). We show that his consideration is based on the erroneous overestimation of the fluctuation energy, which comes from the interaction of the Goldstone modes with the frozen disorder. This interaction leads to the Imry–Ma effect, which destroys the orientational order but is unable to destroy the local structure of ^{3}He-*A*. There is no ground for the robust phases. © 2005 Pleiades Publishing, Inc.

PACS numbers: 67.57.Pq

Following Fomin, let us discuss the superfluid ^{3}He in aerogel using the Ginzburg–Landau (GL) model supplemented by the interaction with the frozen orientational disorder field η_{ij}:

$$F = F_0 + F_{grad} + F_\eta. \qquad (1)$$

Here, F_0 and F_{grad} are condensation and gradient energies, and

$$F_\eta = \int \eta_{ij}(\mathbf{r}) A_{\mu i}(\mathbf{r}) A_{\mu j}^*(\mathbf{r}) d^3 r, \qquad (2)$$

where $\langle \eta_{ij} \rangle = 0$, and we only consider the orientational anisotropy, i.e., the tensor η_{ij} is traceless: $\eta_{ii} = 0$.

We assume that the disorder is relatively small. Therefore, we can start with homogeneous states that have the spatially uniform order parameter $A_{\mu i} = A_{\mu i}^{(0)} = $ const. Since $\int \eta_{ij} d^3 r = 0$, the energy of such state only comes from F_0:

$$F(A_{\mu i}^{(0)}) = F_0(A_{\mu i}^{(0)}). \qquad (3)$$

We consider, here, the proper range of the parameters of the GL functional F_0 (the β-parameters of fourth-order terms in F_0 [1]), for which ^{3}He-*A* has minimum energy. The energy of the uniform ^{3}He-*A* is smaller than the energy of any other uniform phase by the magnitude $\sim F_0 \sim N_F \tau^2 T_c^2$, where N_F is the density of states in normal Fermi liquid, and $\tau = 1 - T/T_c$. The quasi-isotropic robust phase determined by the condition $\eta_{ij}(\mathbf{r}) A_{\mu i}^{(0)} (A_{\mu j}^{(0)})^* = 0$ [2] also has higher energy.

Let us consider now the second-order (η^2) correction to the energy F_0. The uniform ^{3}He-*A* is not the minimum of the total GL functional (1), that is why its energy can be reduced by adding the nonuniform corrections (fluctuations) $A_{\mu i} = A_{\mu i}^{(0)} + a_{\mu i}$, with $a \propto \eta$; thus, $\langle a \rangle = 0$. The η^2 terms contain the linear and quadratic terms in $a_{\mu i}$. In $\mathbf{k}$ representation after diagonalization of the a^2 terms, one obtains

$$F = F_0(A_{\mu i}^{(0)}) + F_{fl}, \qquad (4)$$

where the fluctuation energy

$$F_{fl} = \frac{1}{2} \sum_{n, \mathbf{k}} a_{n, \mathbf{k}}^2 \epsilon_n(\mathbf{k}) + \sum_{n, \mathbf{k}} \tilde{\eta}_{n, \mathbf{k}} a_{n, \mathbf{k}}. \qquad (5)$$

Here, $\tilde{\eta}_{n, \mathbf{k}}$ comes from the product of η and $A_{\mu i}^{(0)}$ matrices, and $\epsilon_n(\mathbf{k})$ is the spectrum of the nth mode. For Goldstone modes (GM),

$$\epsilon_G(\mathbf{k}) \sim N_F \xi_0^2 k^2, \qquad (6)$$

and for other modes with gaps,

$$\epsilon_{non-G}(\mathbf{k}) \sim N_F(\tau + k^2 \xi_0^2) = N_F \tau(1 + k^2 \xi^2), \qquad (7)$$

where $\xi = \xi_0 / \sqrt{\tau}$ is the GL coherence length.

After minimization over a, one obtains the contribution of fluctuations that reduce the ^{3}He-*A* energy:

$$F_{fl} = -\frac{1}{2} \sum_{n, \mathbf{k}} \tilde{\eta}_{n, \mathbf{k}}^2 \epsilon_n^{-1}(\mathbf{k}). \qquad (8)$$

¶ This article was submitted by the author in English.

There is no divergence at small k, and the integral is concentrated at large $k \gg 1/\xi$ if we assume that the frozen disorder is concentrated at $1/\xi_0 > k \gg 1/\xi$. It mainly gives the shift of the transition temperature T_c. Actually, the traceless orientational disorder increases the transition temperature. Subtracting from Eq. (8) the integral with $\tau = 0$ in the denominator, one obtains the integral $\propto \int d^3 k/k^2(1 + k^2\xi^2)$ concentrated at $k \sim \xi^{-1}$:

$$\Delta F_{\text{fl}} \sim (A^{(0)})^2 \frac{\eta_0^2}{\tau \xi^3 N_F^2} \sim \alpha F_0, \qquad (9)$$

where $\eta_0^2 = \int d^3 r \langle \eta(\mathbf{r})\eta(0)\rangle$ and α is the Larkin–Ovchinnikov parameter [3]:

$$\alpha = \frac{\eta_0^2}{\tau^{1/2}\xi_0^3 N_F^2} \ll 1. \qquad (10)$$

We can already stop at this point, since the fluctuation energy is small compared to the condensation energy, and, thus, ^{3}He-A remains the only possible phase. However, Fomin points out that the interaction of the frozen disorder with GM changes the situation, because, due to these modes, the amplitude of the fluctuations of the nonrobust states diverges at small k: $\langle a^2\rangle \propto \int d^3 k/k^4 \sim \int dk/k^2 \sim L$, where L^{-1} is the infrared cutoff parameter. This gives

$$\langle a^2\rangle \sim \frac{\alpha L}{\xi}(A^{(0)})^2. \qquad (11)$$

At $L \sim \xi$, fluctuations are small if $\alpha \ll 1$, and this is the condition for the applicability of the GL approach. But the fluctuations become comparable to $A^{(0)}$ at

$$L \sim \frac{\xi}{\alpha} \gg \xi, \qquad (12)$$

and this length scale L provides the infrared cutoff.

This consideration is certainly true, but it is the well-known Imry–Ma effect [4]: since Eq. (11) describes the fluctuations of the GM, it corresponds to the change in the orientation of the order parameter A without disturbing its structure. The scale L at which $\langle a^2\rangle \sim (A^{(0)})^2$ thus indicates the scale at which the orientation of A changes by an angle of the order $\pi/2$. This is just the Imry–Ma length scale. The state looses the orientational long-range order due to interaction of the GM with the frozen orientational disorder. The similar destruction of the long-range translational order in the mixed state of superconductors by inhomogeneities was found even earlier [5]. The Imry–Ma effect applied to ^{3}He-A in aerogel was discussed in [6].

Fomin claims that the GM also leads to the divergent contribution to the fluctuation energy, which is absent in the robust phases. Let us see. The contribution of the GM with wavelength L to the fluctuation energy F_{fl} in Eq. (8) is proportional to $\int_0^{1/L} k^2 dk /k^2 \sim 1/L$. The fluctuation energy in Eq. (9) comes from the scale ξ and is proportional to $\int k^2 dk /(k^2 + 1/\xi^2) \sim \int_0^{1/\xi} dk \sim 1/\xi$. Thus, the contribution of the GM with the wavelength L is by a factor of $\xi/L = \alpha$ smaller and gives the second-order in α correction to the GL energy. This is just the Imry–Ma energy gain due to the orientational disorder of the order parameter:

$$F_{\text{Imry–Ma}} \sim \alpha \Delta F_{\text{fl}} \sim \alpha^2 F_0 \ll F_0. \qquad (13)$$

At the Imry–Ma wavelength L, the interaction with the frozen disorder is on the order of the gradient energy [4]. Thus, the contribution of the GM with the wavelength $L \gg \xi$ to the energy is on the order of the gradient energy at this scale and thus contains the small factor ξ^2/L^2 compared to the condensation energy F_0. This is demonstrated in Eq. (13), since $\xi/L = \alpha \ll 1$.

Equation (13) contradicts the statement by Fomin [7], who erroneously concludes that the contribution of the GM contains the large factor $1/\alpha$ compared to the contribution of the non-Goldstone modes: $F_{\text{fl–G}} \sim \alpha^{-1}F_{\text{fl–non-G}}$, and, thus, due to the GM, the fluctuation energy is comparable to the condensation energy: $F_{\text{fl–G}} \sim F_0$. This provides the justification for the introduction of the robust phases where the disorder does not interact with the GM, and, thus, there is no divergence in the amplitude of the order parameter. This justification is wrong, and, thus, there is no basis for the robust phase. The same conclusion was made by Mineev and Zhitomirsky in their comment [8].

In conclusion, the Goldstone modes, i.e., the fluctuations in the direction of the degeneracy of the order parameter, do lead to the divergence of the amplitude of the order parameter. However, their contribution to the energy does not experience any divergence and is small compared to the condensation energy according to the parameter $\alpha^2 \ll 1$. This is nothing but the Imry–Ma effect. It leads to disorder in the orientation of the order parameter at large length $L = \xi/\alpha \gg \xi$ without changing the local structure of the order parameter. Since the condensation energy F_0 is dominating, the local order parameter must be in the ^{3}He-A state everywhere (at least within the GL model (1)). The robust phase is not the extremum of F_0 and, thus, is not the solution of the GL equations. Thus, within the GL model with the frozen orientational disorder, the Imry–Ma approach is valid and it does not leave any room for the robust phase.

REFERENCES

1. D. Vollhardt and P. Wölfle, *The Superfluid Phases of Helium 3* (Taylor and Francis, London, 1990).

2. I. A. Fomin, Pis'ma Zh. Éksp. Teor. Fiz. **75**, 220 (2002) [JETP Lett. **75**, 187 (2002)]; Pis'ma Zh. Éksp. Teor. Fiz. **77**, 285 (2003) [JETP Lett. **77**, 240 (2003)]; Zh. Éksp. Teor. Fiz. **125**, 1115 (2004) [JETP **98**, 974 (2004)]; J. Low Temp. Phys. **134**, 769 (2004); J. Low Temp. Phys. **138**, 97 (2005).

3. A. I. Larkin and Yu. N. Ovchinnikov, Sov. Phys. JETP **34**, 651 (1972).

4. Y. Imry and S. Ma, Phys. Rev. Lett. **35**, 1399 (1975).

5. A. I. Larkin, Sov. Phys. JETP **31**, 784 (1970).

6. G. E. Volovik, JETP Lett. **63**, 301 (1996).

7. I. A. Fomin, Pis'ma Zh. Éksp. Teor. Fiz. **81**, 362 (2005) [JETP Lett. **81**, 298 (2005)].

8. V. P. Mineev and M. E. Zhitomirsky, Pis'ma Zh. Éksp. Teor. Fiz. **81**, 360 (2005) [JETP Lett. **81**, 296 (2005)].

Reply to the Comment "No Robust Phases in Aerogel…"[¶]

I. A. Fomin

Kapitsa Institute for Physical Problems, Russian Academy of Sciences, Moscow, 119334 Russia
Received May 26, 2005

The arguments of Volovik are refuted. © *2005 Pleiades Publishing, Inc.*

PACS numbers: 67.57.–z

1. The estimations made in the comment are based on the assumption that the ABM order parameter (bulk *A*-phase) is the only relevant minimum of the Ginzburg and Landau (GL) free energy and its energy is smaller than that of other possible minima by the energy of the order of the full condensation energy. This situation is opposite to the situation considered in the criticized papers [C1], where competition of nearly degenerate states is assumed (in what follows, references to the comment are prefixed by a capital C). Free energy of bulk (without aerogel) superfluid ^{3}He has 18 extrema [1], and the situation assumed in the comment does not seem to be very realistic.

For the present discussion, the relative energies of the states corresponding to nonferromagnetic equal-spin pairing phases are of importance. Among the mentioned extrema, there are four minima meeting this requirement [2]. Two of them, the ABM and axiplanar state, are so close in energy that identification of the *A*-phase as an ABM state has been contested in the literature [3]. The Axiplanar state, unlike the ABM, contains in its vicinity robust states, as was discussed earlier [4]. These states are also close in energy to the ABM. For a crude estimation of the relative difference of energies of competing states (to be referred to as γ in what follows), weak coupling values of $\beta_1, \ldots, \beta_5$ parameters were used. With these values, the relative difference of energies of the robust state and the ABM corresponds to $\gamma \sim 1/20$. Strong coupling corrections to the parameters β will change the difference, still $\gamma \sim 1/10$ is a fair estimation. The contribution of the fluctuations to the energy has to be compared not with the full condensation energy F_0 but with the much smaller value γF_0. The regular part of this contribution, which comes from the gapped modes, is of the order of αF_0, which is in agreement with and in the notations of the comment. A value of the parameter $\alpha \sim (\eta^2/\sqrt{\tau})$ can be estimated from the measured width of the specific heat jump [5]. According to this data, $\alpha \sim 1$ when $\tau \sim 1/30$. Because of the weak dependence on τ everywhere in the GL region, the parameter $\alpha \approx 1/5$ is at least compa-

rable to or greater than γ, and even a regular contribution of fluctuations can mix-up the relative energies of the competing states in contrast to the statement of the comment.

2. The main object of the criticism in the comment is the contribution of the fluctuations of the Goldstone modes to the energy. According to the comment, this contribution is of the order of $\alpha^2 F_0$; thus, it is even smaller than the contribution of the gapped modes, so that the free energy is a regular function of α and the original free energy $F_0(A_{\mu j}^{(0)})$ is a good starting point for expansion on a small α. This assertion is in conflict with Imry and Ma's statement [C5] that the ordered state can be destroyed by an arbitrarily small random field. It indicates that new free energy $F(\bar{A}_{\mu j})$, which includes the contribution of fluctuations, has to be a singular function of α, and the argument based on the continuity has to be taken with great care.

The standard procedure [6] of finding of $F(\bar{A}_{\mu j})$ is based not on the direct averaging of the original free energy (or of its parts as is done in the comment) but on a derivation of the equation for the average order parameter, which, in the present case, has the following form:

$$\tau \bar{A}_{\mu j} + \frac{1}{2} \sum_{s=1}^{5} \beta_s \left[\frac{\partial I_s}{\partial A_{\mu j}^*} + \frac{1}{2} \left(\frac{\partial^3 I_s}{\partial A_{\mu j}^* \partial A_{\nu n} \partial A_{\beta l}} \langle a_{\nu n} a_{\beta l} \rangle \right. \right.$$
$$\left. \left. + 2 \frac{\partial^3 I_s}{\partial A_{\mu j}^* \partial A_{\nu n}^* \partial A_{\beta l}} \langle a_{\nu n}^* a_{\beta l} \rangle \right) \right] = -\langle a_{\mu l} \eta_{lj} \rangle. \tag{1}$$

The corresponding free energy, if necessary, has to be constructed so that it generates the derived equation. The averages of the fluctuations of the order parameter $\langle a_{\nu n} a_{\beta l} \rangle$ in "Goldstone" directions are proportional to a diverging integral, i.e., singular. It has been checked using a direct substitution that the coefficients in front of the singular averages are not identical zeros. This means that the GL equation contains singular terms. There is no reason for a cancellation of the singular terms in the expression for the free energy as well. It

---

[¶] This article was submitted by the author in English.

should be mentioned though that the free energy has not been used in the arguments of [C1].

Volovik, in construction of the free energy, followed the "physical" argument, which does not take into account important features of the problem. In particular, he overlooked the fact that the Goldstone directions depend on the average order parameter. As a result, the variation of his free energy will not contain terms that have to be present in equation (1).

The singular terms in Eq. (1), being proportional to the diverging integral, are much greater than the regular terms. That determines a procedure of its solution. As a first step, the principal terms are set equal to zero. This condition selects a degenerate class of robust order parameters. The remaining terms in the equation are treated as a perturbation lifting this degeneracy. They have to be considered on a class of robust order parameters. Consequently, robust order parameters are asymptotic solutions of the GL equation in a limit $\gamma \longrightarrow 0$, $\alpha \ll 1$, and the ABM order parameter is not a solution of this equation in the considered limit in contrast to the statement made in the comment. The energies of two states were not compared directly. The problem of comparison of different states does not arise here, because, in the considered limit, a family of robust phases is the only nontrivial extremum of the free energy.

Summing up, one can say that the declared in the comment error in the overestimation of the fluctuations does not exist. The diverging terms are present in the GL equation, and this is sufficient for selection of the robust phases. The robust phases are extrema of the proper free energy. The situation considered in the comment and the one discussed in [C1] correspond to different regions of the parameters $\gamma \sim 1$, $\alpha \ll 1$, so that $\gamma \gg \alpha$ (comment), $\gamma \leq \alpha \ll 1$ [C1]. For that reason, the criticism presented in the first part of the comment has no relevance to the problem discussed in the criticized papers.

About the situation in the real ^{3}He, it has to be mentioned that the present knowledge of the coefficients $\beta_1, \ldots, \beta_5$ is not sufficiently accurate for reliable reconstruction of the "topography" of the GL free energy. Even though the estimations given above show that the situation is favorable for the realization of robust phases, the competing situation [C7] cannot be ruled out, and it can be realized in its range of parameters, for example, when the aerogel is very dilute if a macroscopic description still applies.

REFERENCES

1. V. I. Marchenko, Zh. Éksp. Teor. Fiz. **93**, 141 (1987) [Sov. Phys. JETP **66**, 79 (1987)].

2. N. D. Mermin and G. Stare, *Materials Science Center* (Cornell Univ., 1974), Report No. 2186.

3. Y. H. Tang, Inseob Hahn, H. M. Bozler, and C. M. Gould, Phys. Rev. Lett. **67**, 1775 (1991).

4. I. A. Fomin, Pis'ma Zh. Éksp. Teor. Fiz. **77**, 285 (2003) [JETP Lett. **77**, 240 (2003)].

5. J. He, A. D. Corvin, J. M. Parpia, *et al.*, Phys. Rev. Lett. **89**, 115301 (2002).

6. A. I. Larkin and Yu. N. Ovchinnikov, Zh. Éksp. Teor. Fiz. **61**, 1221 (1971) [Sov. Phys. JETP **34**, 651 (1971)].